The Dissertation Committee for David Gregory Aristoff
certifies that this is the approved version of the following dissertation:

Ordering in Dense Packings

Committee:

_____
Charles Radin, Supervisor

_____
Hans Koch

_____
Rafael de la Llave

_____
Oscar Gonzalez

_____
Irene Gamba

_____
Mark Raizen

Ordering in Dense Packings

by

David Gregory Aristoff, B.A.

Dissertation

Presented to the Faculty of the Graduate School of

The University of Texas at Austin

in Partial Fulfillment

of the Requirements

for the Degree of

Doctor of Philosophy

The University of Texas at Austin

May 2011

Ordering in Dense Packings

David Gregory Aristoff, Ph.D.

The University of Texas at Austin, 2011

Supervisor: Charles Radin

We examine various models of soft matter, and one model of quasicrystals, focusing on abrupt changes as density is varied. We consider in detail two models, one of granular matter and another of confined wires, showing that the models become ordered as density is increased, with crystalline order observed in the former and nematic order observed in the latter. We associate the phenomenon of random close packing with the onset of crystalline order in our granular model, and we conjecture that crumpled wires should exhibit a nematic transition with increasing compaction. We also consider two other models of granular matter: one which describes dilatancy onset as a second order phase transition, and one which describes random loose packing as a precise, well-defined density. Finally, we examine an equilibrium model of quasicrystals with a first order phase transition to a solid phase without any crystalline order.

Table of Contents

I. INTRODUCTION

Equilibrium statistical mechanics has long been used to understand the collective behavior of large numbers of interacting particles. Though the theory has classically been associated with systems in thermal equilibrium, the ideas of statistical mechanics have more recently been used to understand, with varied success, a wide array of systems, including physical systems like granular matter [EO, Ra, AR2] and crumpled sheets [BK, AR1, AR3], as well as purely combinatorial systems like networks [PN]. P.G. de Gennes [dG1, dG2], S.F. Edwards [EO], and many others have advocated the broad applicability of statistical mechanics, adopting the hypothesis that, in principle at least, any many-body system can be described by the appropriate family of probability distributions, though the distributions may depend on the protocols used to prepare the system [SNRS, Ra].

The theory has been particularly successful in modeling phase transitions – abrupt changes in behavior corresponding to global restructuring of systems. In physical systems this restructuring often has a geometric nature, corresponding for example to molecules approximately aligning with a crystal lattice [An, LL]. To understand this concept it is worthwhile to consider the *hard sphere model* [Lo], a famous model of equilibrium statistical mechanics which has been used to explain the freezing and melting of real materials [TR, Bar].

Consider all the possible configurations of non-overlapping congruent spheres ("hard spheres") in a finite subset V of $\mathbb{R}^3$ at a fixed volume fraction ϕ. (Assume V is large and convex.) At low density, most configurations are disordered. At high density, however, computer simulations show that most configurations exhibit an ordered structure [HR, RH] close to that of the optimum-density configurations conjectured by Kepler (and recently proven by Hales [Ha]). Moreover, at certain intermediate densities, simulations show that most configurations are a mixture of these two types of structures, with both large disordered and large crystalline regions. This behavior is the hallmark of what is called a *first order phase transition*.

Now imagine simplifying the above model by replacing the spheres by congruent, parallel hexagons with edges and centers on a triangular lattice. Imagine further that the hexagons

are in a vertical plane and are subject to gravity and infinite friction, so that each hexagon must "sit" on another hexagon. In [AR2] we introduce such a model, which is in the style of the Edwards theory [EO] of granular matter, to understand the physical phenomenon of random close packing [Ra1]. Recent experimental work [ND] has shown that random close packing may correspond to the sudden appearance of "bulk" crystals in granular samples (see also [SCM]). Our model supports this experimental observation: we prove our model exhibits signs of crystallization at high density, and we show by Monte Carlo simulation that the model is disordered at low density. The boundary between these regimes in the model – to which we associate random close packing – corresponds to a phase transition, in support of a recent conjecture in [Ra1].

The geometric mechanism behind this high-density ordering is perhaps more apparent in the following model of *liquid crystals* [dGP, On]. Consider all possible configurations in $\mathbb{R}^2$ of nonoverlapping long, thin, congruent box-shaped rods of any orientation, at a fixed volume fraction ϕ. For ϕ near zero, the rods are mostly far apart from one another, and so in most configurations the orientations of the rods will be random. On the other hand, for $\phi \approx 1$ the rods will mostly be very close together, so that in most configurations neighboring rods must have nearly the same orientation. One might ask whether this orientation persists even for far away rods. Computer simulations suggest that this is the case: at high density, configurations have a long-range, preferred orientation, signaling a nematic phase [Fr].

Now consider modifying the above model of liquid crystals by connecting all the rods with tiny springs, so that a configuration can be thought of as one very long, thin (confined) string. Such "stiff" strings can be considered models of polymers [AR1, JK] or crumpled wires [AR3]. In [AR1] we introduce a lattice version of this model which is a generalization of the well-known Flory model [Fl] of polymer melting. We show the model behaves quite like the aforementioned model of liquid crystals, with a first order phase transition between a disordered, fluid-like phase and a nematic (orientationally ordered) phase. (For crumpled wires we do not know of any experimental evidence of such a transition.)

Crystalline and nematically ordered phases are easy to understand geometrically – one can think in terms of particles in the most probable configurations aligning with each other

(in a nematic phase) or with a lattice (in a crystalline phase). In [AR5, AR6], however, we consider models with transitions to "solid" phases in which the high-density ordering is unusual [AR6] or not apparent at all [AR5]. In [AR5] we consider a model of granular matter at dilatancy onset [Re, RN] which exhibits a kind of "solidification" without any obvious geometric ordering. We show that the model has a sharp change in volume response to an infinitesimal shear at dilatancy onset; this supports recent experimental evidence [SRNS, MSRSS] that dilatancy onset in sand corresponds to a phase transition. In [AR6] we introduce a lattice model of quasicrystals which is a generalization of the model of [KR]; the model exhibits a first order phase transition to a solid "quasicrystalline" [LS, GS] phase without any particle-type translational symmetry.

All of the work in this thesis is motivated by open, current physical problems which share a common characteristic – namely an abrupt change in the behavior of a physical system as a function of some parameter (like density). The models of [AR1, AR2], inspired by the possible phenomena of random close packing in granular matter and nematic ordering in crumpled wires, give a good picture of the main ideas underlying our work. In this thesis we examine in detail these models. Before describing results from [AR1, AR2], we examine the hard sphere model – a prototypical example of the theoretical pattern underying these results – in more detail in section II. In section III, we consider the model of granular matter from [AR2], proving it exhibits ordering at high density. In section IV we discuss Monte Carlo simulation and error analysis, following techniques of [AR4]. In section V we return to the model of [AR2], but focus on lower densities, using Monte Carlo techniques discussed in section IV. In section VI we examine the model of crumpled wires from [AR1]. In sections VII, VIII, and IX we include the full texts of (the preprint versions of) [AR5, AR6, AR4]. In section X we summarize all these results.

II. THE HARD SPHERE MODEL

In physics, the *hard-sphere model* is an old and famous model of equilibrium matter which has a close experimental realization in certain colloids [RDXRC]. The model consists of particles $x_1, ..., x_N$ in a volume $V \subset \mathbb{R}^3$ interacting with the pair potential

$$\Phi(x_i, x_j) = \begin{cases} \infty, & \text{if } |x_i - x_j| < \sigma \\ 0, & \text{otherwise} \end{cases}$$

where $\sigma > 0$. Consider a *microcanonical ensemble* with interaction Φ, where particle density and (kinetic) energy are fixed, with the latter at zero. The model then admits the following purely geometric description. Consider the set $X_{N,V}$ of all configurations of N non-overlapping unit-volume spheres centered inside a cube V. One obvious quantity of interest is the volume of $X_{N,V}$, namely

$$|X_{N,V}| = \frac{1}{N!} \int_{V'} d\mathbf{x} \tag{1}$$

where V' is the set of N-tuples $\mathbf{x} = (x_1, ..., x_N) \in V^N$ such that $|x_i - x_j| \geq \sigma := 2(\frac{3}{4\pi})^{1/3}$ for $i \neq j$. This is closely related to the *entropy density*

$$S_{N,V} := \frac{1}{N} \log |X_{N,V}|. \tag{2}$$

In order to see many interesting features of the model, one must consider how its behavior changes as the system size increases unboundedly. More precisely, one fixes a particular particle density $\phi := N/V$ (here the same as volume fraction) and takes the *infinite volume limit*, in which $N, V \to \infty$ and $N/V \to \phi$. A simple convexity argument implies that in the infinite volume limit there is a well-defined entropy density,

$$S(\phi) := \lim_{N,V \to \infty, N/V \to \phi} S_{N,V}. \tag{3}$$

It is generally accepted that the entropy density $S(\phi)$ has a flat portion, at the ends of

which are "kinks", so that $dS(\phi)/d\phi$ is discontinuous. The hard-sphere model then exhibits a *first order phase transition*, so called because the first derivative of $S(\phi)$ is discontinuous. (There are no proofs of this, however.) While this description of the transition is useful as a definition, it is not particularly illuminating; one may ask what a "typical" configuration looks like, and whether configurations look qualitatively different at low and high density.

In order to answer these questions, one puts a probability measure on the subsets of $X_{N,V}$, namely the uniform probability measure $\mu_{N,V}$ so that all configurations of spheres are equally probable. Then one takes a limit μ_ϕ of the measures $\mu_{N,V}$ as $N, V \to \infty$, $N/V \to \phi$. (One takes a weak-* limit of a subsequence, arguing existence of an accumulation point by showing that the measures live in a compact space [Ru1].)

One may employ the measures μ_ϕ to ask questions related to "most" configurations of a given density. (The measures may not be unique; different choices of boundary conditions in the infinite volume limit may give different limiting measures μ_ϕ.) It turns out that there are qualitative *geometric* differences between low and high density configurations; low density configurations are completely disordered and isotropic, while high density configurations have a crystalline geometric structure resembling the optimally dense configurations. Furthermore there is a region of intermediate densities in which large configurations are partly disordered and partly crystalline [Ra1].

More precisely, there exist $a \approx 0.49$ and $b \approx 0.54$ such that: for $\phi < a$, the measures μ_ϕ are supported on configurations which are completely disordered and isotropic (and furthermore for such ϕ there is a unique limiting measure μ_ϕ); for $\phi > b$ the μ_ϕ are supported on configurations which are *crystalline* and have approximately the same crystalline structure as the optimal configurations (for such ϕ the position and orientation of the crystalline configurations on which μ_ϕ is supported depend on the boundary conditions taken in the infinite volume limit); and for $\phi \in [a, b]$, μ_ϕ is a convex combination of μ_a and μ_b. It should be emphasized that none of this is proven, with the exception of μ_ϕ being unique and supported on disordered configurations at very low density $\phi << a$ [Ru1]. Most of the evidence for the claim comes from Monte Carlo and molecular dynamics simulations (see, for instance, [AF, ZHB]).

In simulations it is difficult to measure $S(\phi)$ for large ϕ (see [AF, HR, Sp] for some attempts). To show a transition through computer simulation, one generally uses ensembles which fix the average of ϕ instead of fixing ϕ at a precise value. One such ensemble is the *grand canonical ensemble*, which uses a parameter μ to control the average number of particles N in a fixed volume V. In the grand canonical ensemble, a first order phase transition can be seen in, for instance, a jump discontinuity (developing as $V \to \infty$) in the average of ϕ as a function of μ. (The average of ϕ, unlike the entropy $S(\phi)$, can easily be measured from simulations.) Here the jump discontinuity corresponds, via a Legendre transformation, to the flat portion of $S(\phi)$ [Gr]; at this precise μ, the disordered and crystalline phases coexist, and the average volume fraction ϕ does not have a well-defined value.

The first order phase transition, and corresponding geometric ordering, is a common feature of materials at high density. In the next section we explore its appearance in *granular matter*, a form of soft matter of which sand is a common example.

III. A MODEL OF GRANULAR MATTER

Granular matter can be loosely defined as a large collection of static, macroscopic noncohesive particles sedimented in a fluid (for instance air). Granular matter is a form of soft matter, the latter loosely defined as matter which can be macroscopically deformed with a small amount of energy compared with a typical equilibrium solid. A simple probabilistic model of granular matter, due to S.F. Edwards [EO], consists of a simple modification to the hard sphere model discussed above – the model is modified by restricting the space of configurations to those which are stable under gravity and friction. The Edwards model appears to be reasonably justified for granular samples which are prepared by the fluidization and sedimentation approach of [SNRS].

According to a conjecture of C. Radin [Ra1], the model behaves quite like the hard sphere model, as follows. Consider the measures μ_ϕ discussed above, except now the measures correspond to the new ensemble of configurations stable under gravity and (infinite) friction. There exist $d \approx 0.6$ and $e \approx 0.64$ such that: for $d < \phi < e$, the measures μ_ϕ are supported on geometrically disordered, isotropic configurations; for $\phi > f$ the μ_ϕ are supported on configurations which have the crystalline structure of optimally dense configurations; and for $e \leq \phi \leq f$ the measures μ_ϕ are convex combinations of μ_e and μ_f. Here $d \approx 0.6$ is the random loose packing density [AR4], the lowest density at which bulk random samples exist, and $e \approx 0.64$ is the random close packing density [Ra1], the lowest density at which large random samples exist without bulk-sized crystals. There is indirect experimental evidence for this conjecture in [SCM, ND]. In [AR2] an Edwards-style model is introduced to support the conjecture; we now discuss this model.

The model is a variant of the old equilibrium model of congruent hard hexagons on a triangular lattice [Bax, HP], with hexagonal edges a multiple of the lattice spacing. In analogy with S.F. Edwards' model of granular hard spheres [EO], we modify the model of [HP] by restricting phase space only to those configurations of hard-core parallel hexagons in a vertical plane which are stable under gravity and infinite friction. That is, the model consists of all configurations of hard-core parallel hexagons centered on the triangular lattice

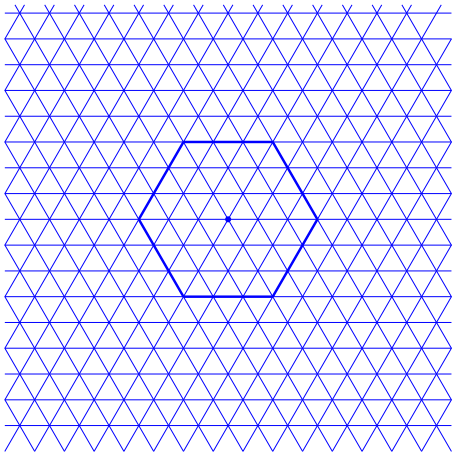

FIG. 1: A hexagon centered on the triangular lattice, with side length $s = 3$.

L, with side length s a fixed integer multiple of the lattice spacing, such that at least one of the lower edges of each hexagon intersects one of the upper edges of another hexagon. See Figs. 1-2. We use a fixed boundary consisting of a "shell" of hexagons which intersect their neighbors in full faces; see Fig. 2. The space enclosed by this boundary is called V. (Hexagons on the boundary are not considered part of the configuration.)

We use a *grand canonical ensemble*; that is, a probability measure m_V on the subsets of the set of all such configurations, such that the probability of seeing a configuration C with exactly n hexagons is equal to

$$m_V(C) = \exp(\mu n)/Z_V, \tag{4}$$

where μ is a variable parameter and Z_V is the appropriate normalization. Let m be any weak* limit point of the measures m_V, as $|V| \to \infty$. (Such limits exist by compactness. Clearly m_V and m depend on μ but we suppress this for ease of notation.)

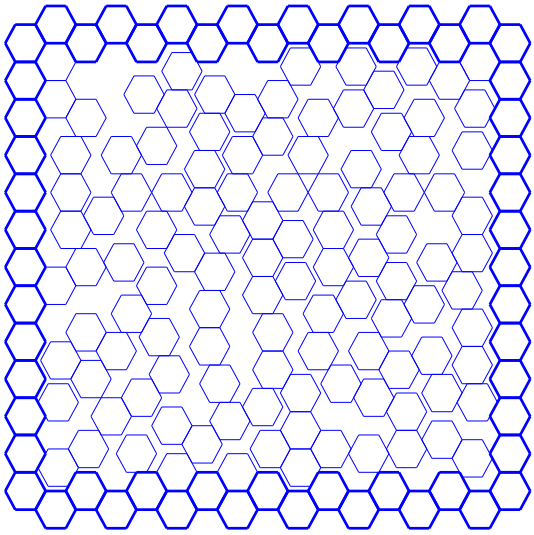

FIG. 2: A configuration (boundary is in boldface).

The model exhibits a phase transition from a disordered fluid phase to a crystalline solid phase, which we expect (but do not prove) to be first order. At large positive μ, the measure m depends on the precise boundary conditions chosen while taking the limit $|V| \to \infty$; for small positive μ, the measure m is unique. Thus for large μ, the center of a configuration will be sensitive to a distant boundary, while for small μ the system behaves like a disordered fluid. We first prove the former statement; we cite Monte Carlo simulation evidence to justify the latter.

Before giving a precise meaning to our result on sensitivity to the boundary we need a few definitions. Recall that L is the regular triangular lattice on which our hexagons are centered.

A *sublattice* is a subset of L consisting of the centers of a collection of hexagons which tile

the plane. (There are $3s^2$ distinct sublattices.) We say a collection H of hexagons is *on the boundary sublattice* if the centers of all the hexagons in H are in the sublattice defined by the hexagons on the boundary of the container V.

Given a point x in the boundary sublattice, we define the *neighborhood* N_x of x to be the set of all points in L inside a hexagon h centered at x, excluding those on the bottom three edges of h.

A *contour* is a connected component of the union of the following two sets: (the closure of) the set of all space inside V not covered by hexagons; and the set of all line segments of length at most $s-1$ which are intersections of neighboring hexagons. Given a contour C, the *region enclosed by* C is the simply-connected region of minimal area which contains C. We use the term *outer contour* for a contour which is not contained in any region enclosed by any other contour. See Fig. 3.

Let C be a contour of area k (in units of hexagon area), and let E be the region enclosed by C. The (closures of the) connected components of $E \setminus C$ will be called *C-interior regions*. Note that the hexagons which intersect the topological boundary of a C-interior region R are on the same sublattice. We say these hexagons are on the *outside* of R and we say the remaining hexagons in R are on the *inside* of R.

We will assume without loss of generality that the origin O is in the boundary sublattice. Our order parameter $p(\mu)$ is then defined as follows.

Definition 1. *Let $p_V(\mu)$ be the conditional m_V-probability that, given there is a hexagon h centered at a point in the neighborhood N_O of the origin, h is centered at the origin. We write $p(\mu)$ for the corresponding (infinite-volume) m-probability, $p(\mu) := \limsup_{V\to\infty} p_V(\mu)$.*

Note that if the influence of boundary conditions tends to disappear as $V \to \infty$, then $p(\mu)$ is identically equal to $(3s^2)^{-1}$ (the inverse of the number of distinct sublattices). In the following theorem, we prove this is not the case when μ is sufficiently large.

Theorem 1. *For sufficiently large μ, $p(\mu) > (3s^2)^{-1}$; that is, a hexagon centered in N_O will not be, in the infinite system, centered equiprobably on each of the $3s^2$ sublattices.*

Note that if there is no hexagon centered in N_O, or if there is a hexagon centered in N_O

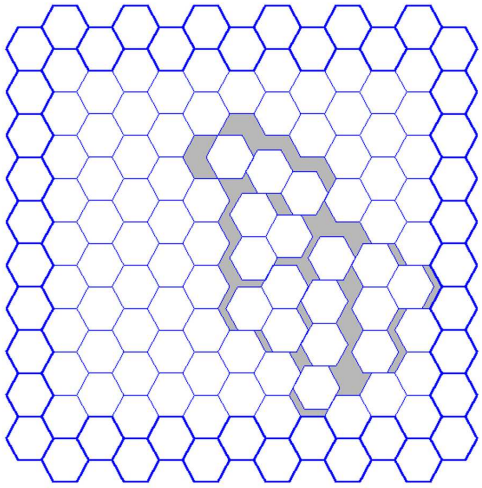

FIG. 3: An outer contour (shaded region).

but not at the origin itself, then there is an outer contour enclosing the origin. Our proof, which begins with this observation, relies on two main ingredients: First, we must show that the probability of seeing a fixed outer contour C becomes exponentially unlikely as the area of C increases; second, we put an exponential upper bound on the number of contours of fixed area enclosing the origin. The first estimate can be improved by taking μ large, and then by combining both ingredients one obtains the theorem.

Lemma 1. *Let C be an outer contour of area k (in units of hexagon area). The m_V-probability that a configuration has the contour C is at most* $\exp(-\mu k)$. *This estimate is independent of V.*

Proof. The main idea of the proof is to create a $1-1$ correspondence between configurations having the contour C, and configurations without C but with more hexagons, since for positive μ the latter will be exponentially more likely. Going in this direction, we define a $1-1$ correspondence $\mathcal{S} \to \mathcal{T}$, where

$$\mathcal{S} = \{\text{configurations in } V \text{ with the contour } C \text{ and } n \text{ hexagons}\},$$

$$\mathcal{T} = \{\text{configurations in } V \text{ with } n+k \text{ hexagons}\},$$

as follows. Let $A \in \mathcal{S}$. We define a map $A \to A'$ as follows. For each C-interior region R of A, pick a hexagon h on the outside of R, without loss of generality h is centered at $x \in N_y$, and translate R by $y - x$ while leaving the rest of A unchanged. This produces a unique arrangement A' of hexagons in V. We show that the hexagons in A' are non-overlapping, and furthermore that A' has a void C' which can be covered by k non-overlapping hexagons.

Suppose h_1 and h_2 are distinct hexagons in A, and let h_1' and h_2' be the images of these hexagons in A'. If h_1 and h_2 are in the same C-interior region then clearly their images in A' do not overlap, since translating the region does not change their positions relative to one another. Thus assume h_1 and h_2 are in different C-interior regions. If either hexagon is on the inside of the C-interior region to which it belongs, then the images of the two hexagons cannot overlap due to trivial distance considerations. (Any C-interior region is translated by a distance of at most s.) So assume both hexagons are on the outside of distinct C-interior regions, and write y_1 and y_2 for the centers of h_1 and h_2, respectively. Then $y_1 \in N_{x_1}$ and $y_2 \in N_{x_2}$ for some $x_1 \neq x_2$, since centers of distinct non-overlapping hexagons must be in distinct neighborhoods. By definition of the map $A \to A'$, the hexagons h_1' and h_2' are centered at x_1 and x_2, respectively. Since x_1 and x_2 are distinct points in the boundary sublattice, h_1' and h_2' do not overlap, as desired.

Now, consider the image H' in A' of the set H of hexagons on the outsides of the C-interior regions of A. By definition of the map $A \to A'$, the hexagons in H' are on the boundary sublattice. Notice also that all the hexagons in H' remain in the region enclosed by C. Since C is an outer contour, the hexagons on the outer border of C are also on the boundary sublattice, and these hexagons are fixed by the map $A \to A'$. It follows that there is a void C' in A', which can be thought of as the "image" of C, such that C' is bordered by hexagons which are all on the boundary sublattice. The void C' can be therefore be covered by k non-overlapping hexagons.

Let A'' be the image of A' under the map which fills C' with k non-overlapping hexagons and fixes the rest of A'. We claim that $A'' \in \mathcal{T}$. All that must be shown is that each hexagon in A'' intersects one of the three upper edges of another hexagon. If h'' is the image of a

hexagon on the inside of a C-interior region in A, then clearly this property holds true, since the relative local structures on the inside of C-interior regions do not change in the map $A \to A' \to A''$. On the other hand, if h'' is the image of a hexagon in the outside of a C-interior region, or if it is inside C', then this property also holds because C' is completely covered by nonoverlapping hexagons in A''.

Next we show that the correspondence $\mathcal{S} \to \mathcal{T}$ defined by $\mathcal{A} \to \mathcal{A}''$ is $1-1$. Suppose A_0 and A_1 are distinct configurations in $\mathcal{S}$. There is an obvious pairwise correspondence between the C-interior regions of A_0 and of A_1. The outsides of corresponding C-interior regions of A_0 and A_1 are identical, because the contour defines these outsides. So since A_0 and A_1 are distinct, either at least one of these pairs of corresponding C-interior regions, say R_0 and R_1, have distinct insides, or A_0 and A_1 must be different outside the region enclosed by C. In the latter case A_0'' and A_1'' must be distinct, because the map $A \to A''$ fixes everything outside the region enclosed by C. In the former case, the images of R_0 and R_1 are distinct and so A_0'' and A_1'' must also be distinct.

Using the correspondence $\mathcal{S} \to \mathcal{T}$ we can now put an exponential bound on the probability of seeing the outer contour C. Let $Z = Z_V$ be the normalization defined above, let H_n be the number of configurations A with the contour C and n hexagons, and let H_n'' be the number of configurations A'' with $n+k$ hexagons. By the above correspondence we have that $H_n'' \geq H_n$, and of course we also have that $\sum_{n=0}^{\infty} e^{(n+k)\mu} H_n'' \leq Z$. Thus, the probability of seeing the contour C is

$$\frac{1}{Z} \sum_{n=0}^{\infty} e^{n\mu} H_n \leq \frac{\sum_{n=0}^{\infty} e^{n\mu} H_n}{\sum_{n=0}^{\infty} e^{(n+k)\mu} H_n''} \leq e^{-k\mu}$$

as desired. □

Lemma 2. *The number of contours C of size k (in units of hexagon area) enclosing the origin is less than $a_k b^k$, where $a_k = O(k^2)$ and b is constant. (Both a_k and b depend on s.)*

Proof. Let C be a contour of area k (in units of hexagon area), such that C encloses the origin. Consider a graph with vertex set $L \cap C$ (recall L represents the underlying triangular

lattice). Join two vertices in the graph with an edge if they are nearest neighbors in L. Note that each connected component of this graph is at a distance of less than s from another component; join all the components by edges of length less than s.

Now we have a connected graph such that all its edges have length less than s. Consider a spanning tree for this graph, duplicate all the edges of the tree to get a graph G, and then choose a (directed) Eulerian path γ in G, that is, a path which traverses each edge in G exactly once. (It is a well-known fact of graph theory that Eulerian paths exists for such duplicate graphs.) Such a path covers all the points in $L \cap C$, so to upper-bound the number of possible contours C it suffices to upper-bound the number of such paths γ.

Since each hexagon contains $O(s^2)$ lattice points, the number of possible starting points for γ is $O(s^4k^2)$. Also, since all the edges of γ have length less than s, given a point on γ there are $O(s^2)$ possibilities for the next point on γ. Observing that γ traverses $O(s^2k)$ points, the result follows. □

Proof of Theorem 1. From Lemmas 1-2, we find that the probability of seeing an outer contour enclosing the origin is no greater than $\sum_{k>0} a_k(\exp(-\mu)b)^k$, and this sum can be made arbitrarily small for μ sufficiently large. Recall that if there is no hexagon centered at the origin, then there is an outer contour enclosing the origin. Since the latter event has arbitrarily small probability for μ sufficiently large, the former must also; one concludes, therefore, that the probability there is a hexagon centered at the origin is arbitrarily large for μ sufficiently large. This probability is smaller than the conditional probability $p(\mu)$, so we conclude that $p(\mu) > (3s^2)^{-1}$ for μ sufficiently large, as desired. □

Note that although the result of Theorem 1 holds for any fixed finite hexagon side length s, it does *not* apply in the "continuum" limit $s \to \infty$.

IV. MONTE CARLO SIMULATION AND ERROR ANALYSIS

Models in statistical mechanics are often analytically intractable. In particular key quantities like the free energy cannot be computed analytically; more generally, the probability measure describing the system is unknown, because the appropriate normalization – the partition function – cannot be calculated. In such cases it is often useful to consider Monte Carlo simulation, in which one takes advantage of the fact that many *relative* probabilities can be calculated.

The basic such technique, called the *Metropolis algorithm* [MRRTT], is as follows. (Here we focus on discrete models for simplicity; see e.g. [AR5] for a continuum example.) Consider a model given by a probability measure $Pr(\cdot)$ on the subsets of configurations in the model. Writing X for the (finite) set of all configurations, let

$$Pr(A) = f(A)/Z \tag{5}$$

be the probability of $A \in X$, where $f : X \to \mathbb{R}$ is a known function and $Z = \sum_{A \in X} f(A)$ is the appropriate normalization. (Assume all configurations have positive probability.) The Metropolis algorithm generates a sequence $A_0, A_1, ...$ of random configurations from the model, where A_n is the nth configuration selected.

The Monte Carlo step – which selects the next configuration, A_{n+1}, given the current configuration, A_n – is as follows. Suppose the nth configuration, A_n, has been selected. A trial configuration A'_n is then proposed according to some (usually simple) algorithm. The probability of A'_n relative to A_n is

$$Pr(A'_n)/Pr(A_n) = f(A'_n)/f(A_n) \tag{6}$$

Here the probability normalization Z, which is often impossible to analytically compute, has disappeared. Set $A_{n+1} = A'_n$ with probability p, and $A_{n+1} = A_n$ with probability $1-p$,

where

$$p := \min\{1, Pr(A'_n)/Pr(A_n)\} \tag{7}$$

is easily computed from $f(A_n)$ and $f(A'_n)$.

Consider now a sequence $A_0, A_1, ..., A_n$ of configurations obtained in this way, where A_0 is an initial configuration. (Note that the selection of each configuration depends only on the previous configuration; that is, the configurations are realizations of a Markov chain.) If

(1) for all $A, A' \in X$, the conditional probability of proposing a step $A \to A'$, given that the current configuration is A, is the same as that of proposing the reverse step $A' \to A$, given that the current configuration is A';

(2) any configuration in X can be reached, with positive probability, from A_0 by some sequence of steps; and

(3) f is not a constant function,

then it can be proven that in the limit $n \to \infty$, configurations will be selected according to equation (5), regardless of the initial configuration A_0. (The condition that f is nonconstant ensures that the underlying Markov chain is aperiodic.) More precisely: as $n \to \infty$, the conditional probability of selecting $A_{n+i} = A$ at the $(n+i)$th step, given that the ith selection was A_i, approaches $Pr(A)$.

Since sampling with the Metropolis algorithm is only proven to approach the distribution (5) in the limit as $n \to \infty$, it is important to consider how large n must be for the samples to be reasonably accurate. While in some cases one can prove rates of convergence [CD], it is common to use nonrigorous techniques to argue that the samples are accurate.

Many such techniques involve the (standard unbiased) *autocorrelation* R [Ge], given by

$$R(k) = \frac{\sum_{i=0}^{n-k} (\psi(A_i) - \lambda) \cdot (\psi(A_{i+k}) - \lambda)}{(n-k+1)\sigma^2}, \tag{8}$$

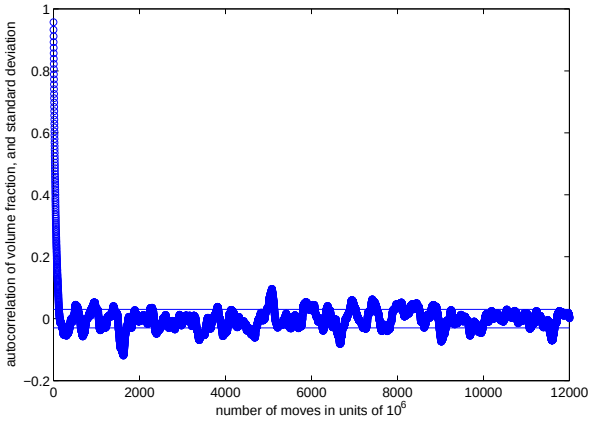

FIG. 4: A typical graph of autocorrelation $R(k)$ vs. number of Monte Carlo steps k, for $\psi =$ volume fraction (a typical measurement on configurations in a model).

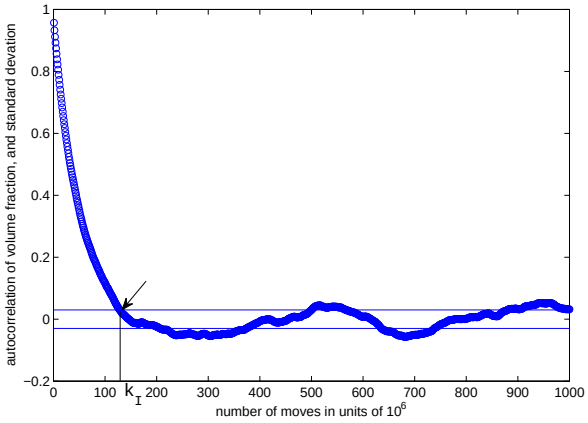

FIG. 5: A zoomed-in look at the graph from Fig. 4, with a definition of the initialization time k_I.

.

where $\psi : X \to \mathbb{R}$ is some relevant function on configuration space (for example, particle density), and λ and σ^2 are the sample average and variance of ψ over the sequence $A_0, ..., A_n$

of configurations; that is,

$$\lambda = \frac{\sum_{i=0}^{n} \psi(A_i)}{n+1}, \tag{9}$$

and

$$\sigma^2 = \frac{\sum_{i=0}^{n} (\psi(A_i) - \lambda)^2}{n}. \tag{10}$$

The value $R(k) = 1$ indicates perfect correlation, and $R(k) = -1$ indicates perfect anti-correlation. If $R(k) \approx 0$ for $k \geq k_0$, one suspects that the sampling, at least with respect to the function ψ, has converged to the appropriate distribution when at least k_0 Monte Carlo steps are made. (Of course it is always possible the sampling is stuck in a particular region in configuration space, and in practice one always tries to rule this out.) See Fig. 5 for typical graphs of autocorrelation. As k approaches n, the number of summands averaged in (8) becomes small, making the value $R(k)$ less reliable. For this reason the domain of $R(k)$ is often restricted to a smaller order of magnitude, for instance $k < T := 10^{-1}n$.

A simple benchmark for how many Monte Carlo steps are needed for the sampling to converge is the following. Let k_0 be the smallest positive integer with $R(k_0) < 0$, and define

$$\sigma_0^2 = \frac{1}{(T - k_0 - 1)} \sum_{k \in (k_0, T)} R(k)^2. \tag{11}$$

Then set k to be the smallest positive integer with $R(k) < \sigma_0^2$. The value $k = k_I$, called an *initialization time*, estimates the number of Monte Carlo steps necessary before the sampling loses dependence on the initial configuration A_0. (See Fig 5.)

Once sampling has converged, it is useful to have a measure of how many Monte Carlo steps are needed to produce a sample which is independent of an arbitrary past sample. A simple measurement of this is the following. Delete the first k_I configurations from the original chain $A_0, A_1, ..., A_n$ to obtain a new chain $A_{k_I}, A_{k_I+1}, ..., A_n$. Now recompute R and k from the new chain as above, and set $k_M = k$. The value k_M is called a *mixing time*. If the length, n, of the chain $A_0, ..., A_n$ is a large multiple of the mixing time, k_M, one

expects that the sample average

$$\bar{\psi} = \frac{1}{n+1} \sum_{i=0}^{n} \psi(A_i) \tag{12}$$

reasonably approximates the ensemble expected value

$$E(\psi) = \frac{1}{Z} \sum_{A \in X} \psi(A). \tag{13}$$

There remains the problem of quantifying the expected error in the estimate $\bar{\psi} \approx E(\psi)$. A common method is *batch means* [Ge], in which one divides the chain $A_0, ..., A_n$ into "batches" $A_0, ...A_{b-1}; A_b, ..., A_{2b-1}; ...; A_{(l-1)b-1}, ..., A_n$. Here b is the number of configurations in a batch, and $l = \lfloor n/b \rfloor$ is the total number of batches. "Batch averages" $\bar{\psi_j}$ are then computed,

$$\bar{\psi_j} = \frac{1}{b+1} \sum_{i=0}^{b-1} \psi(A_{jb-1+i}). \tag{14}$$

If the batch size b is a large multiple of the mixing time k_M, then an appropriate central limit theorem implies that the batch means should be approximately normally distributed [KV]. Furthermore, for large batch size b the batch means $\bar{\psi_j}$ should be approximately independent. For confidence intervals, one applies Student's t-distribution to the batch means [St]. (A p-confidence interval around $\bar{\psi_j}$ is, strictly speaking, the realization of a random interval which covers the true mean $E(\psi)$ with probability at least p.)

If the batch averages really were independent and normally distributed, such confidence intervals would be rigorous; of course in practice one can only argue that the batch averages are close to being independent and have distributions close to being normal. The assumption of normality seems more stringent, since relatively large numbers of independent samples are generally needed for normality. However, the t-distribution has been shown to be quite robust against deviations from normality [DL], and the method of batch means is often used even without batch size being large enough for the batch averages to be approximately normally distributed [AR4].

V. A MODEL OF GRANULAR MATTER AT LOW DENSITY

In this section we consider again the model of section III. (We use the notation of that section.) Recall that section III focuses on the behavior of the model at large positive μ. Here we discuss the behavior of the model at small positive μ, beginning with the following conjecture.

Conjecture 1. *For sufficiently small nonnegative μ, $p(\mu) \equiv (3s^2)^{-1}$; that is, a hexagon centered in N_O will be, in the infinite system, centered equiprobably on each of the $3s^2$ sublattices.*

For sufficiently negative μ, one can prove that average volume fraction ϕ approaches zero as $V \to \infty$. We are not interested in that regime; we consider only $\mu \geq 0$. (Although $\mu = 0$ should correspond to zero pressure, or random loose packing [AR4], we do not make this claim here.) Since for such μ configurations are still quite dense, one cannot understand them as arrangements of approximately independent particles, as is done in low-density virial expansions in classical equilibrium statistical mechanics.

We do not prove the above conjecture here. We instead produce simulation evidence that for small positive μ – we will focus somewhat arbitrarily on the interval $1 \leq \mu \leq 2$ – configurations are disordered, in the sense that our order parameter $p(\mu)$ (defined in Definition 1 of Section III) is identically equal to $(3s^2)^{-1}$. Assuming the conjecture is true, we have the following corollary.

Corollary 1. *The order parameter $p(\mu)$ is not analytic at some positive $\mu = \mu_c$. The model therefore has a phase transition at μ_c.*

The nonanalyticity occurs when $p(\mu)$ rises above $(3s^2)^{-1}$. At the transition, the sublattice determined by the boundary hexagons becomes probabilistically favored. The phase transition, therefore, corresponds to the model inheriting the crystalline structure of the boundary.

In our simulations we can only estimate the finite-system parameter $p_V(\mu)$. It is important to note that $p_V(\mu)$ is analytic for any finite V, so $p_V(\mu)$ cannot be precisely equal to $(3s^2)^{-1}$

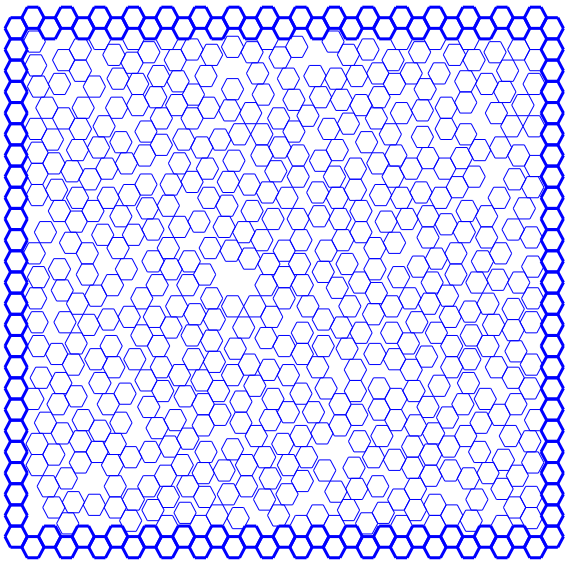

FIG. 6: A plot of a configuration in equilibrium at $\mu = 1$ and volume 729 (in units of hexagon volume)

.

at low μ; small fluctuations must be expected. In all of our simulations, however, we find the finite-size system parameter $p_V(\mu)$ to be within small confidence intervals of $(3s^2)^{-1}$ for $\mu \in [1, 2]$. We therefore expect the infinite-system parameter $p(\mu)$ to be identically equal to $(3s^2)^{-1}$ for $\mu \in [1, 2]$. Note that the burden is easier to show *independence* of the boundary, as we do, than it is to show *dependence* on the boundary, since the latter requires careful study of finite size effects as the system size grows. For the former, if small systems already are (mostly) boundary independent, one expects the same to be true for larger systems.

We simulated systems with volumes ranging from 276 to 1151 (in units of hexagon volume) using the Metropolis algorithm described in Section IV. We first checked that our simulations were not sensitive to the initial configuration; since simulations starting at low density tended

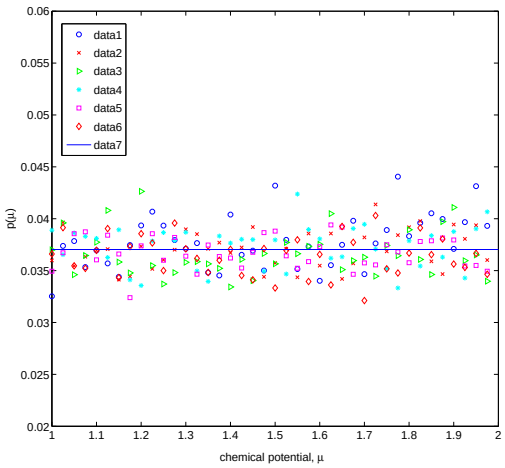

FIG. 7: Plot of $p(\mu)$ vs. μ for systems of volume $|V| = 276$ (data1) to $|V| = 1151$ (data6), for $s = 3$. Data7 is the line $p(\mu) = \frac{1}{3s^2} = \frac{1}{27}$.

to equilibrate faster, we started our main simulations with void configurations. To obtain numerical estimates of $p_V(\mu)$, we considered the following functions of our Monte Carlo configurations. For a configuration A we let $\delta(A) = 1$ if there is a hexagon in A centered at the origin; we let $\delta(A) = 0$ otherwise. We define $t(A) = 1$ if there is a hexagon in A centered at a point in the neighborhood N_O of the origin, and $t(A) = 0$ otherwise. Then for each system size V we compute the following statistic:

$$p_M := \frac{\delta(A_1) + \delta(A_2) + \cdots + \delta(A_M)}{t(A_1) + t(A_2) + \cdots + t(A_M)} \tag{15}$$

So the expected value of p_M is exactly $p_V(\mu)$. We obtain error bars for p_M as described in section IV, using batch means to obtain 95% confidence intervals from Student's t-distribution. (We used about 10 batches for each μ, with batch size at least 5 mixing times.) See Fig. 7 for the data from all system sizes, and Fig. 8 for the data on the largest system with confidence intervals. Notice that the confidence intervals cover the desired value $(3s^2)^{-1}$ about 95% of the time, as appropriate.

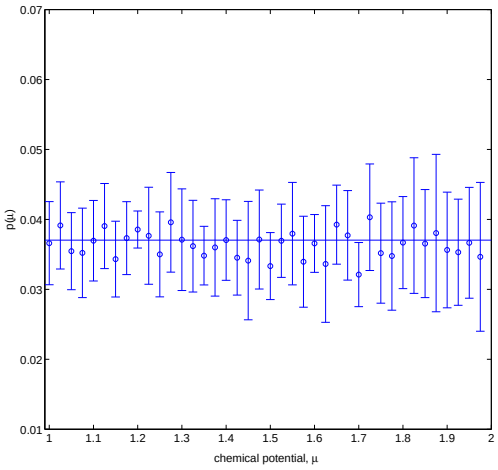

FIG. 8: Plot of $p(\mu)$ vs. μ for a system of volume 1151, with confidence intervals, for $s = 3$. The line is $p(\mu) = \frac{1}{3s^2} = \frac{1}{27}$.

In review, we have proven in section III that for sufficiently large positive μ, $p(\mu)$ is greater than $(3s^2)^{-1}$, and in fact $p(\mu)$ approaches 1 as $\mu \to \infty$. We also have evidence from Monte Carlo simulation that for $\mu \in [1, 2]$, $p(\mu)$ is identically equal to $(3s^2)^{-1}$, which is indicative of boundary insensitivity (which we associate with disorder). Since a constant function cannot be analytically extended to have different values, the order parameter $p(\mu)$ cannot be analytic, and so the model undergoes a phase transition at some $\mu > 2$. The transition, which corresponds to the sudden appearance of crystalline structure at a critical μ, is consistent with the conjecture of [Ra1].

VI. A MODEL OF CRUMPLED WIRE

Crumpled materials – for example crumpled sheets or wires – are, like granular matter, a form of soft matter. Imagine crumpling a sheet of paper into a compact ball. The sheet develops creases and folds. While the creases are "irreversible", the folds can be considered elastic. We introduce a model to study the geometric changes associated with the folds of a long, thin wire as it is compacted in a thin box.

Consider such a wire which has been compacted into a very high density state. Suppose that the wire does not crease, so that it has a minimum radius of curvature, and suppose further that there is a significant energy cost for elastic bending. The most probable very high density configurations are then "layered", consisting of parallel rows of wire, with few bends between the rows. On the other hand, at low density, configurations of wire are disordered, with many "wiggles" and no orientational order. One may ask whether the transition between these types of behavior is smooth or singular. In our model we show that the transition is singular, in the precise sense of a phase transition. Although there is not yet experimental evidence for a transition, statistical mechanics ensembles have been used to study crumpled materials in [BK, SB], with the authors of [BK] finding a second-order transition in a field-theoretic continuum model of crumpled wires.

We use a grand canonical statistical mechanics ensemble, with parameters to control the average density and energy of a walk. To understand the use of energy as an independent parameter, consider the following. Suppose that we have many identical wires with unit square cross-sections, and assume it costs energy E to bend a single such wire to a given curvature. Then it should cost energy nE to bend a row of n parallel such wires to the same curvature. Now consider a wire built of the same material but with circular cross sections of radius r, with $\pi r^2 = n$; one would expect it to cost energy greater than nE to bend such a wire to the same curvature. Furthermore if the circular cross section has radius cr, the energy cost should be greater than $c^2 nE$. Thus the bending energy is nonlinear in the thickness of the wire, so energy is justifiably an independent parameter in our modeling.

Our model consists of a single random self-avoiding walk (SAW) on a finite square lattice,

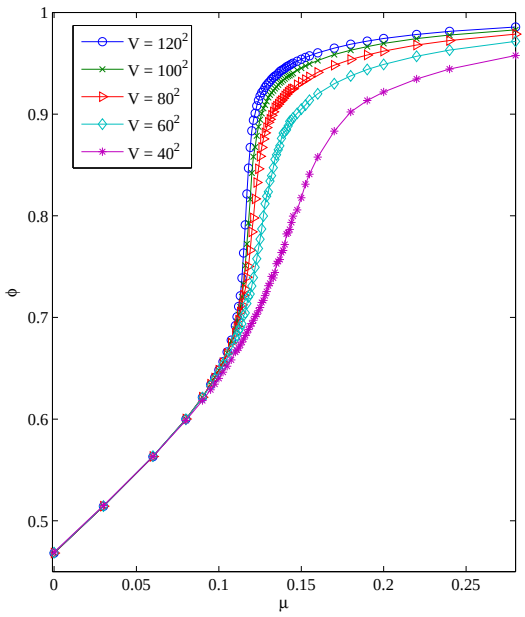

FIG. 9: (a) The graph of average density versus μ at $\beta = 1.5$, for system volumes $V = 40^2$ through $V = 120^2$.

with an energy cost for bends in the walk. The model is a generalization of the Flory model [Fl, JK] of polymer melting: the Flory model fixes density at its optimum value of 1, while we include density as a variable. (Here density is particle density, with the particles corresponding to the vertices of the walk.) While the Flory model has a second order phase transition between disordered and nematic states [JK], our model has a first order phase transition. (A useful history of the Flory model, and a prediction that the transition becomes first order at lower density, can be found in [JK].)

We now describe the model in detail. Consider the set $\mathcal{W}$ of all self-avoiding polygons (i.e., closed self-avoiding loops) on the square lattice with periodic boundary conditions, $L = (\mathbb{Z}/v\mathbb{Z})^2$, with v a fixed positive integer. The energy $E(w)$ of polygon w in $\mathcal{W}$ is defined as the number of right angles in w, and the length $N(w)$ of w is the number of unit line segments in w. Given an inverse temperature $\beta = 1/T$ and a chemical potential μ, the free

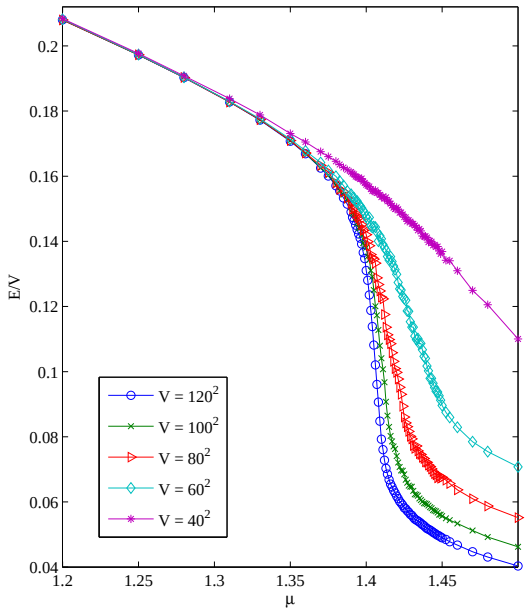

FIG. 10: The graph of average energy per volume vs. β at $\mu = 0.15$, for system volumes $V = 40^2$ through $V = 120^2$.

energy of the model is $\beta E - \beta\mu N - S(E, N)$ where $S(E, N)$ is the entropy, that is, the natural logarithm of the volume in phase space of self-avoiding polygons at fixed E and N.

As usual in a grand canonical ensemble this is optimized by the probability measure $m_{\beta,\mu}$ defined on the subsets of $\mathcal{W}$ by

$$m_{\beta,\mu}(w) = \frac{1}{Z_{\beta,\mu}} e^{-\beta(E(w)-\mu N(w))} \tag{16}$$

for $w \in \mathcal{W}$, where $Z_{\beta,\mu}$ is the appropriate normalization. In this notation we have suppressed the dependence of $m_{\beta,\mu}$ and $Z_{\beta,\mu}$ on the system volume $V = v^2$.

To simulate the model we fix either β or μ, and then slowly increase the other parameter, starting from well into the disordered regime. The basic Monte Carlo step is as follows (see pgs. 41-44 in [vR]). Given a polygon $w(t)$ at step t in the simulation, we introduce,

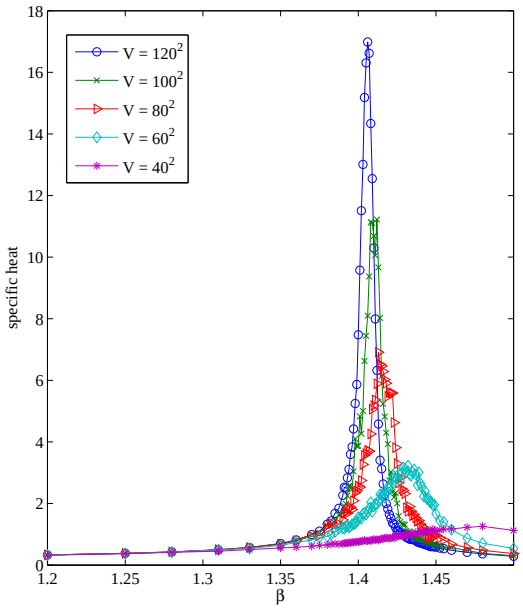

FIG. 11: The graph of specific heat vs. β at $\mu = 0.15$, for system volumes $V = 40^2$ through $V = 120^2$.

with probability p_i, a trial configuration $w(t)'$ which changes the length of $w(t)$ by ℓ_i. (The conditional probability of proposing the trial configuration w', given that w is the current configuration, is the same as that of proposing the trial configuration w, given that w' is the current configuration, as discussed in Section IV.) If $w(t)'$ is not self-avoiding then we take $w(t+1) = w(t)$; otherwise we set $w(t+1) = w(t)'$ with probability $q = \min(Q, 1)$, and $w(t+1) = w(t)$ with probability $1 - q$, where

$$Q = e^{\beta[\mu\ell_i + E(w(t)) - E(w(t)')]} \tag{17}$$

Here $p_1 = p_2 = 2/5$, $p_3 = 1/5$, $\ell_1 = -2$, $\ell_2 = 2$ and $\ell_3 = 0$. (The choices of the p_j were somewhat arbitrary.)

We computed mixing times for the simulation of each (β, μ) as described in section IV. We found that our simulations of each (β, μ) were, in the worst cases, at least 5 mixing

times long (on average), and we therefore believe our Monte Carlo runs are reasonably close to sampling the distributions $m_{\beta,\mu}$. (For μ between -0.05 and 0.06, mixing times, in units of Monte Carlo steps, are between 2×10^7 and 4×10^7, while mixing times increase to about 2×10^9 near the transition μ.)

We repeated each of our simulations 100 times, and obtained 95%-confidence intervals for the averages of particle density and energy per volume from Student's t-distribution with 99 degrees of freedom. The confidence interval widths were, for all (β, μ), less than 0.0009 for particle density and less than 0.004 for energy per volume; see [AR1] for details. (Measurements related to specific heat were calculated differently, and are discussed below.) A single simulation of the largest system ($V = 120^2$) contains 8×10^{11} basic Monte Carlo steps, with 10^{10} Monte Carlo steps in the simulation of each of 80 points (β, μ).

Along with average energy per volume $\langle E \rangle_{\beta,\mu}/V$ and average density $\langle \phi \rangle_{\beta,\mu}$, we measure order parameters *corr* and *lay*, which were introduced in [AR3] and are defined as follows. Given a polygon w, $corr(w)$ is the proportion of edges in w which have the same orientation (horizontal or vertical) as a randomly chosen edge in w. Given w, $lay(w)$ is the normalized volume u^2/V of the largest square sublattice $L' = (\mathbb{Z}/u\mathbb{Z})^2 \subset L$ such that the orientation of w (horizontal or vertical) at the origin agrees with the orientation of w at 80% or more of the sites in L'. (We choose an orientation for the polygon w so that each lattice site has a unique horizontal or vertical orientation. The number 80% is somewhat arbitrary; any value significantly above 50% should suffice.)

We compute specific heat $(1/V)\partial \langle E \rangle_{\beta,\mu}/\partial T$ from fluctuations, that is,

$$T^2 \frac{\partial \langle E \rangle_{\beta,\mu}}{\partial T} = \langle E \rangle_{\beta,\mu} \langle \mu N - E \rangle_{\beta,\mu} - \langle E \mu N - E^2 \rangle_{\beta,\mu} \tag{18}$$

To compute the values of $\langle \cdot \rangle_{\beta,\mu}$ in equation (18), we took averages of the relevant measurements over 100 independent simulations. Then for 95%-confidence intervals we repeated this process 4 times, and used the Student's t-distribution with 3 degrees of freedom. The widths of the confidence intervals for specific heat were all less than 2.8; see [AR1] for details. We checked that the curve computed from fluctuations agreed with the numerical derivative of

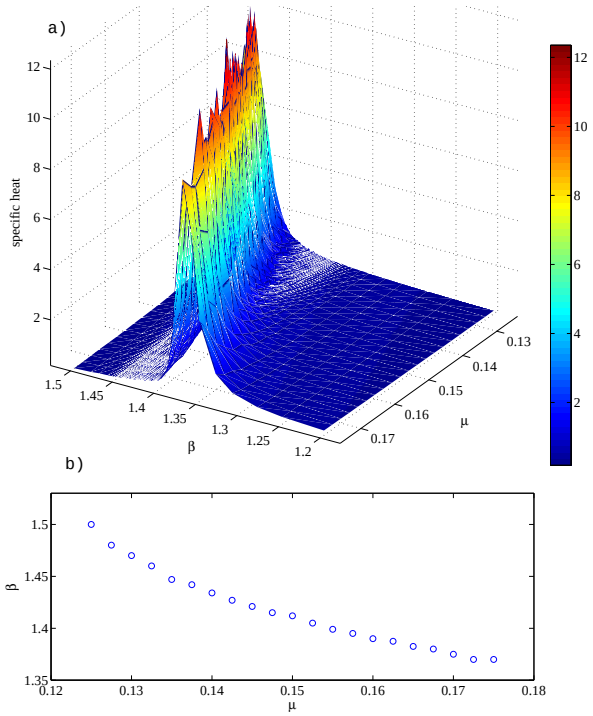

FIG. 12: a) The graph of specific heat vs. β and μ, for $V = 100^2$. b) Estimation of β values which maximize specific heat at fixed μ.

energy.

In contrast with [AR3] we simulate well into the ordered regime and find direct evidence of a first order phase transition. In particular the trends with increasing system size in the curves of Figs. 9 and 10 strongly suggest that the average density and average energy per volume both develop jump discontinuities at the transition, in the infinite volume limit. In confirmation, Fig. 11 shows the specific heat developing a delta function singularity at the transition.

We plot the specific heat surface as a function of β and μ, as well as the (β, μ)-coordinates of the maximum of specific heat, at various $0.125 \leq \mu \leq 0.175$, $1.35 \leq \beta \leq 1.5$ in Fig. 12. The latter gives an indication of the transition curve; note that as μ increases, the

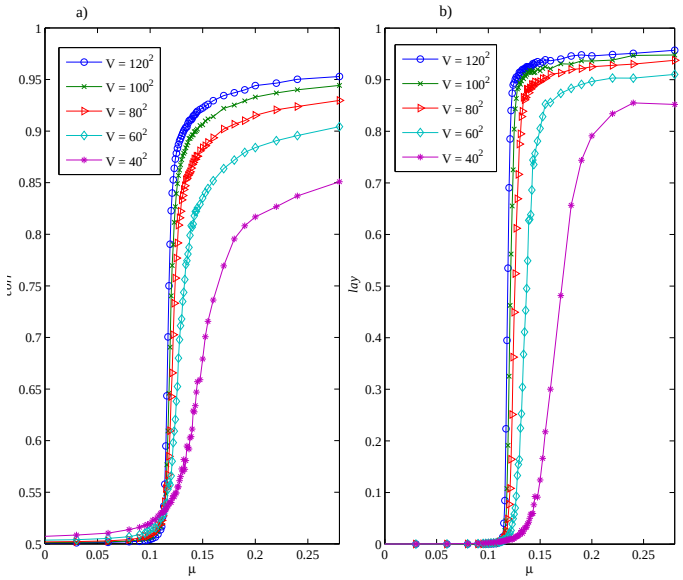

FIG. 13: a) The graph of *corr* vs. β at $\mu = 0.15$, for volumes $V = 40^2$ to $V = 120^2$. b) The graph of *lay* vs. β at $\mu = 0.15$, for volumes $V = 40^2$ to $V = 120^2$.

temperature at which the transition occurs increases.

As evidence of a nematic transition, the measurements *corr* and *lay* (see Figs. 13 and 14) exhibit a jump discontinuity at the transition from their disorder values of 1/2 and zero, respectively.

Our Monte Carlo simulations incorporate many moves which are "rejected". In fact the rejection rate ranges from about 95% to almost 99%, depending on (β, μ), with higher rejection rates at large β or μ. Simulations of a similar model using a rejectionless algorithm have been published [OFJK,Ja]. The rejectionless algorithm, however, applies only to random strings (with ends) and cannot be used with our model of random loops.

In summary, we have introduced a generalization of the Flory model of polymer melting which allows for a positive fraction of vacant lattice sites. Our model can also be thought of as a model of crumpled wire; in particular, as discussed above, energy can be considered an independent parameter in such (nonequilibrium) setting. We have shown by Monte Carlo

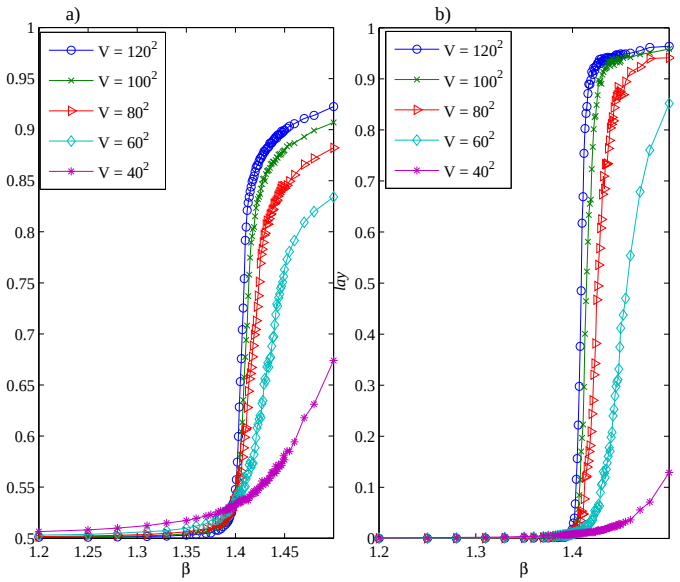

FIG. 14: a) The graph of *corr* vs. μ at $\beta = 1.5$, for volumes $V = 40^2$ to $V = 120^2$. b) The graph of *lay* vs. μ at $\beta = 1.5$, for volumes $V = 40^2$ to $V = 120^2$.

simulation that our model has a transition to a nematic phase at high density and low temperature. Whether real crumpled wire has such a phase transition is part of an ongoing experiment including the author.

The Flory model also has such a transition at low temperature. However, by contrast with the Flory model – which has one parameter and a second order phase transition [JK] – our model has two independent parameters, β and μ, and we find a first-order, discontinuous phase transition across the curve shown in Fig. 12 b). This is direct evidence supporting the suggestion in [JK] that the second order transition in the Flory model becomes first order at lower density when vacancies are included in the model. It still remains to reconcile this behavior with that found in the field-theoretic model of continuum loops in [BK].

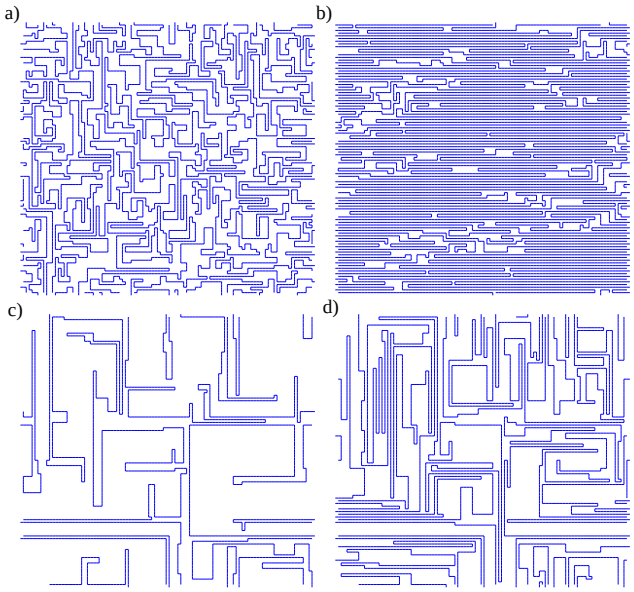

FIG. 15: Configurations with $V = 100^2$ in equilibrium at: a) $(\beta, \mu) = (1.5, 0.03)$ and density $\phi = 0.515$, b) $(\beta, \mu) = (1.5, 0.124)$ and density $\phi = 0.894$, c) $(\beta, \mu) = (2.5, 0.01)$ and density $\phi = 0.146$, d) $(\beta, \mu) = (2.5, 0.04)$ and density $\phi = 0.529$.

VII. DILATANCY TRANSITION IN A GRANULAR MODEL

Static granular matter, such as a sand pile, can exist in a range of densities. In its densely packed state it expands under shear, while when loosely packed it contracts under shear [RN]; the boundary between these regimes, 'dilatancy onset', was first popularized by Reynolds in 1885 [Re]. We introduce a model in which the transition between these different volume responses to shear appears to be singular, in the precise traditional sense of a second order phase transition, as discussed below. (For two dimensional treatments of the transition see [AS,PLR,TH], and for an interpretation as a glass transition see [CH].)

Such modeling can only apply to granular materials in states which are sufficiently reproducible to qualify for the term 'phase'; see [NKBJN, SNRS] for experimental efforts. To determine experimentally whether the response to shear corresponds to a change of phase, the states before and after shear should represent true phases. This necessitates that the shear be infinitesimal, so that it does not drive the material into a more complicated ('nonequilibrium') state. We are mainly concerned, therefore, with modeling the volume reaction to the infinitesimal shear of granular matter. Although, as noted above, the phenomenon of dilatancy onset has been known for over a hundred years, we know of no volume response measurements from which one may directly determine whether or not dilatancy onset is a phase transition. In large part this is due to the difficulty of working with granular samples, in the appropriate range of volume fractions, in states which are sufficiently reproducible [NKBJN, SNRS].

Our modeling follows in a long line of research, championed by Edwards [EO], de Gennes [dG1] and others, in which certain nonequilibrium materials, in particular granular matter, have been modeled probabilistically, using a simple variant of equilibrium statistical mechanics. For reviews on such modeling see for instance [BKLS, Ch, EG, He]. Markov chain Monte Carlo simulation of our model suggests that dilatancy onset can be understood as a second order phase transition, a discontinuity in a second derivative of the appropriate free energy.

The model

Our "granular hard cubes" model is a granular variant of the classical hard cubes model [HHB] of equilibrium statistical mechanics, the latter being a simplification of the classical hard sphere model in which the spheres are replaced by nonoverlapping, parallel cubes. So our model uses layered configurations of hard, parallel, unit cubic grains; see Fig. 16. To model the reaction to a change of strain we mimic the spherical caps that grains in one layer present to grains in neighboring layers by adding cubic "bumps" of width w to the top and bottom of our cubes; see Fig. 17b. We use $w = 0.3$, a choice discussed below; see Fig. 18. As we will see below when we discuss dilatancy, these bumps use the third dimension to add a significant resistance to shear. In our model each grain must sit on exactly four other grains (except grains on the boundary of the configuration), and grains cannot overlap. We do not allow any grain to sit on the bump of another grain; thus, the grains appear on discrete vertical layers, so the distance in the direction of gravity (or z-direction) between the centers of grains on adjacent layers is equal to 1; see Fig. 19. There are n^2 grains in each layer, and n total layers, so there are $N = n^3$ total grains.

For boundary conditions we require that in a given configuration the centers of the grains on the boundary in a single layer all lie on the edges of a rhombus with angle of strain α and area L^2, where $\alpha = 0$ represents a square (see Fig. 17a). Thus, our configurations have boundaries which are essentially cylinders on rhombic bases. The volume of a configuration is then defined as $V = nL^2$. To prevent grains from getting stuck between the boundary grains, we impose top-bottom periodic boundary conditions, and we remove the bumps from the grains nearest to the boundary and on the boundary. We restrict α to $\alpha \geq 0$ since the shapes of configurations corresponding to angles α of opposite sign are merely rotations of one another. (It is more complicated, and unnecessary, to model the effect of shear stress on the two representations of the same shape.) A configuration C is represented by the centers of all the grains in C, i.e. $C \in (\mathbb{R}^2 \times \mathbb{Z})^N$ (the grains are given an arbitrary fixed labeling, and the center of a grain is the center of the unit cube comprising the grain). A single grain g in C is represented by its center, $(x_g, y_g, z_g) \in \mathbb{R}^2 \times \mathbb{Z}$. For simplicity we

require one of the grain centers to be at the origin, and all of the grain centers to be in the octant $x \geq 0, y \geq 0, z \geq 0$.

We use the following "volume/strain" ensemble. (Related ensembles have been used previously in granular modeling – see for instance [BC, BE] – as well as modeling thermal systems – see for instance [PR, Ma].) Our ensemble, instead of fixing volume and strain, uses Lagrange multipliers p and f to control average volume and strain. The Lagrange multipliers enter into the maximization of entropy in the usual way. (In the literature $1/p$ and $1/f$ are sometimes called compactivity and angoricity.) In other words the states of the model, which, in the general approach of Edwards [EO] are probability densities of configurations of grains, optimize the free energy

$$F(p, f) := S - pV + f\alpha V, \tag{19}$$

where S is the entropy, V is the volume in physical space, and $\alpha \geq 0$ represents the angle of strain (see Fig. 17a). The ensemble partition function is

$$Z_{p,f} = \int_0^\infty \int_0^\infty \left(\int_{V,\alpha} dC \right) \exp(-pV + f\alpha V)\, dV\, d\alpha, \tag{20}$$

where $\int_{V,\alpha} dC$ represents integration over the space of allowed configurations at fixed α and V, and $\ln(\int_{V,\alpha} dC)$ is the entropy $S = S(V, \alpha)$. Consider the change of coordinates $\psi_{V,\alpha}$ which maps configurations C at fixed V and α into $\Omega = ([0,1]^2 \times \{0, 1/n, 2/n, ..., 1\})^N$ such that $\psi_{V,\alpha}$ maps each grain center (x, y, z) to $(L^{-1}(x - \tan(\alpha)y), L^{-1}y, n^{-1}z)$. It is easy to see that this map has Jacobian equal to V^{-N}. Thus, using the new coordinates one can rewrite the partition function as

$$Z_{p,f} = \int_0^\infty \int_0^\infty \int_\Omega \Phi(\psi_{V,\alpha}^{-1}(Q))\, V^N \exp(-pV + f\alpha V)\, dQ\, dV\, d\alpha, \tag{21}$$

where $\Phi(C) = 1$ if C corresponds to a configuration which satisfies the conditions of the model, and $\Phi(C) = 0$ otherwise. The probability density of a configuration with volume V

and strain angle α is therefore

$$m_{p,f}(C) = V^N \exp(-pV + f\alpha V)/Z_{p,f}. \tag{22}$$

Our model uses cubes instead of the more traditional spheres. Cubes are preferable here as they allow one to automatically maintain the contacts necessary to support grains 'under gravity' even while straining the system, a big advantage in the simulation.

Another natural question is whether we can correctly model the response in density to shear stress when we only consider (configurational) states which are regular in the sense that the network of contacts in the system forms the same graph structure as a face centered cubic crystal. It would be preferable to allow more general states, but this is very difficult in practice. And although such regular states may give misleading *quantitative* results for the response to shear, we expect to obtain the correct *qualitative* results, which is our only goal. In particular, the quantitative results we obtain are not meant to accurately represent real materials.

We show next why our model exhibits dilatancy onset: the separation of a high density regime of states, in which the material expands under infinitesimal shear, from a low density regime, in which it contracts under infinitesimal shear [RN]. (The more interesting question, however, and the main focus of this paper, is whether the model predicts that the transition through dilatancy onset is singular in the parameter p.)

From the probability density of (22) it follows that if $f = 0$ then the state of lowest possible particle density, called random loose packing, occurs at $p = 0$ [AR4] and some strain $\alpha = \alpha_0$. (For this argument the value of α_0 is irrelevent.) At sufficiently low p and infinitesimal increase of f from 0, which should correspond to an infinitesimal shear stress, the density has no way to change except to increase. So at sufficiently low density there is a regime in which the system contracts under infinitesimal shear stress.

On the other hand, at least since Reynolds [Re] one understands the expansion of (dense) granular matter under shear, which he termed dilatancy, in geometric terms, as the need for parallel layers of spheres to get out of each others' way under a strain deforming the layers, by separating and/or by thinning within the layers. For our grains, with bumps

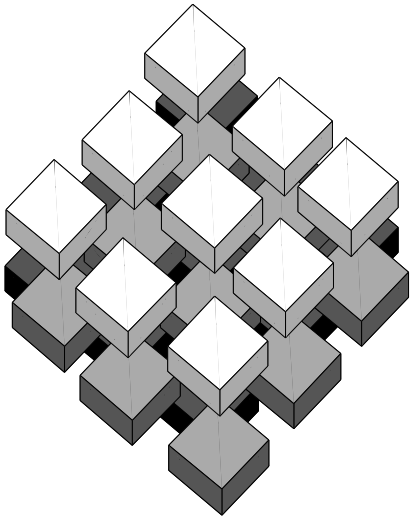

FIG. 16: Layers of parallel cubes.

mimicking spherical caps, this thinning phenomenon should still be present. That is, for a sufficiently dense configuration, neighboring layers should "feel" each others' bumps, so that under an infinitesimal shear stress the layers should then spread out, producing a dilatancy effect. Note that, among optimally symmetric configurations (where the particle centers on each layer form a square lattice), at particle density $\phi_d := (1+w)^{-2}$ the bumps on a given layer will touch the grains on the layer above. We interpret ϕ_d as a (rough) estimate of the minimal particle density required for dilatancy; see Fig. 18. In our simulations we use $w = 0.3$, and so $\phi_d \approx 0.59$. The qualitative dilatancy effect is not sensitive to the precise value of w, though the value ϕ_d is. To understand the choice of w consider the following. For cubes without bumps at zero pressure, a free volume estimate shows that the average particle density should be 9/16. At this density, neighboring cubes in perfectly regular configurations of cubes will be separated by a distance of 1/3, and so for such configurations adding a bump of width $w \leq 1/3$ will not create any overlap. We chose w slightly less than 1/3, so that the cubes would not feel the bumps at low pressure, and also so that very high pressures weren't necessary to see the dilatancy effect.

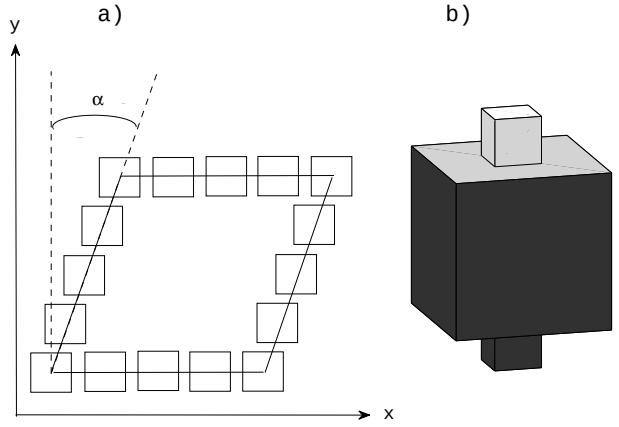

FIG. 17: a) A view from above of a layer in a configuration (only boundary grains, and without their bumps), with a definition of the strain angle α; b) A cubic grain, with bumps on top and bottom faces.

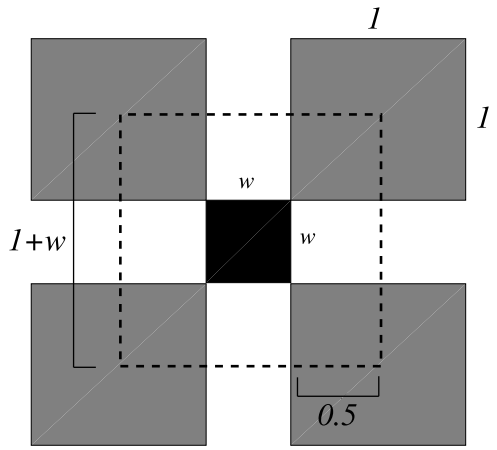

FIG. 18: A horizontal cross-section of the closest packing possible of maximally regular grains, with the small black square representing a bump. By partitioning along the dotted lines, one can calculate the particle density of the configuration, $\phi = (1+w)^{-2}$.

So the bumps, together with the universal behavior at low p or density, explain the existence of dilatancy onset. The main question then is: as density is varied, does the transition through the dilatancy onset proceed in a smooth or in a singular manner? We will show there is an unambiguous second order phase transition at dilatancy onset, at density near $\phi_d = 0.59$. This suggests, by analogy with matter in thermal equilibrium, that the material in the two regimes differs in other characteristics as well, for instance it would be expected that the yield force would behave differently in the two regimes. In [SNRS] the yield force is measured as a function of density, and a second order phase transition is found at a density roughly 0.598. Dilatancy onset was not carefully measured because of the experimental setup, but in other experiments has approximately coincided with the yield transition. Our result suggests the yield transition and dilatancy onset are simply different manifestations of the same phenomenon.

The Simulation, and Results.

Each simulation of N particles begins with $\alpha = 0$ and $V > N/\phi_d$. The basic Monte Carlo step is as follows. Let $C(k)$ be the configuration at the kth step of the Monte Carlo chain, where $C(k)$ has volume V and strain α. For each grain g in $C(k)$ let (x_g, y_g, z_g) be the coordinates of the center of g. We allow three types of move, each of which produces a trial configuration C'. In the first type a single particle moves locally, in the second type the configuration changes volume, and in the third type the configuration changes shape.

The first type of move is attempted with probability $1 - 1/N$. For this type of move we choose a random non-boundary grain g in $C(k)$, and obtain C' by replacing g with a grain centered at $(x_g + \beta\gamma, y_g + (1-\beta)\psi, z_g)$. Here β is a Bernoulli random variable, i.e. $\beta = 0$ or 1 each with probability $1/2$, and γ and ψ are random variables uniformly distributed in the largest intervals (a_1, a_2) and (b_1, b_2) containing zero such that, for all $a \in (a_1, a_2)$ and $b \in (b_1, b_2)$, replacing g with a grain centered at $(x_g + a, y_g, z_g)$ or $(x_g, y_g + b, z_g)$ does not create overlap of grains. Such moves will produce configurations satisfying the conditions of the model, and are accepted with probability 1.

The second and third types of move are each attempted with probability $1/(2N)$. Let η, ν be random variables distributed uniformly in $(-1, 1)$, and fix (small) positive real parameters ϵ and δ. For the second type of move, we obtain C' by replacing (x_g, y_g, z_g) by $(\lambda x_g, \lambda y_g, z_g)$ for each grain g in $C(k)$, where $\lambda = (V + \eta\epsilon)^{1/2}/V^{1/2}$. For the third type of move, we obtain C' by replacing (x_g, y_g, z_g) by $(x_g + \nu\delta y_g, y_g, z_g)$ for each grain g in $C(k)$.

By construction, the probability density of proposing a move $C \to C'$ is the same as the probability density of proposing a move $C' \to C$. To preserve detailed balance, the acceptance probability for the latter two types of moves is therefore

$$p = \min(1,\, \Phi(C')(V'/V)^N e^{-p(V'-V)+f(\alpha' V' - \alpha V)}), \tag{23}$$

with V' the volume of C' and α' the strain angle of C', and where, as above, $\Phi(C') = 1$ if C satisfies the conditions of the model and $\Phi(C') = 0$ otherwise. So for moves of the second and third type, we set $C(k+1) = C'$ with probability p, and $C(k+1) = C(k)$ with probability $1-p$. Thus, the Monte Carlo steps are chosen so that the stationary distribution of the Markov chain has the desired limiting probability distribution (22).

In our simulations, we want to measure how the average of the density $\phi = N/V$ changes as f varies near $f = 0$. (For convenience we do not include the bumps in the calculation of ϕ, but since particle number N is fixed in our simulation, the "true" volume fraction is just a constant multiple of ϕ.) That is, we want to estimate the derivative

$$D(p) := \left.\frac{\partial \langle\phi\rangle_{p,f}}{\partial f}\right|_{f=0} \tag{24}$$

of the average $\langle\phi\rangle_{p,f}$ of ϕ as a function of p. So $D(p) < 0$ (resp. $D(p) > 0$) represents volume expansion (resp. contraction) under infinitesimal strain, which is directly relevant to our study of dilatancy onset.

From the definition of $m_{p,f}$ in (22) we have

$$\langle\phi\rangle_{p,f} = \frac{1}{Z_{p,f}} \int_0^\infty \int_0^\infty \int_\Omega \frac{N}{V} \Phi(\psi_{V,\alpha}^{-1}(Q))\, V^N \exp(-pV + f\alpha V)\; dQ\, dV\, d\alpha, \tag{25}$$

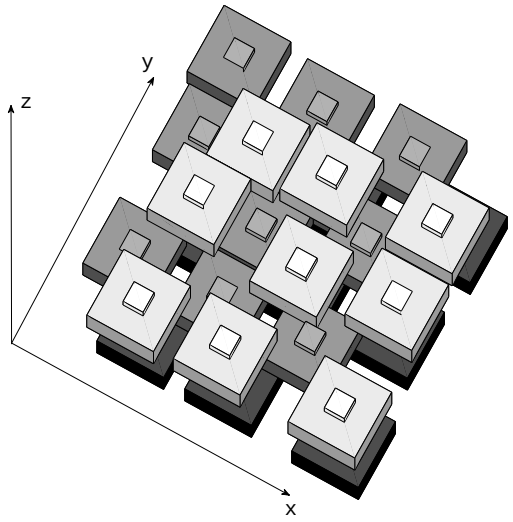

FIG. 19: An arrangement of grains, viewed from above.

from which it follows by differentiation that

$$D(p) = \frac{\partial \langle \phi \rangle_{p,f}}{\partial f}\bigg|_{f=0} = N\langle \alpha \rangle_{p,0} - \Big[\langle \phi \rangle_{p,0}\Big]\Big[\langle V\alpha \rangle_{p,0}\Big]. \tag{26}$$

Thus, to estimate $D(p)$ from our simulations we set $f = 0$ and calculate the sample averages of $N\alpha$, ϕ, and $V\alpha$. With the free energy $F(p, f) = S - pV + f\alpha V = \ln(Z_{p,f})$, which is the quantity minimized by the state $m_{p,f}$, one can see from (19), (21) and (25) that

$$\begin{aligned} &\frac{\langle \phi \rangle_{p,0}^2}{N} \frac{\partial}{\partial f}\left(\frac{\partial F(p,f)}{\partial p}\right)\bigg|_{f=0} \\ &\quad = \frac{\langle \phi \rangle_{p,0}^2}{N} \frac{\partial}{\partial f}\left(\frac{\partial \ln(Z_{p,f})}{\partial p}\right)\bigg|_{f=0} = D(p), \end{aligned} \tag{27}$$

and so the function $D(p)$, as a second derivative of the free energy, is a quantity for which a discontinuity might reasonably be described as a second order phase transition.

We investigate systems of $N = 8^3 = 512$, $10^3 = 1000$, $12^3 = 1728$, $14^3 = 2744$ and $16^3 =$

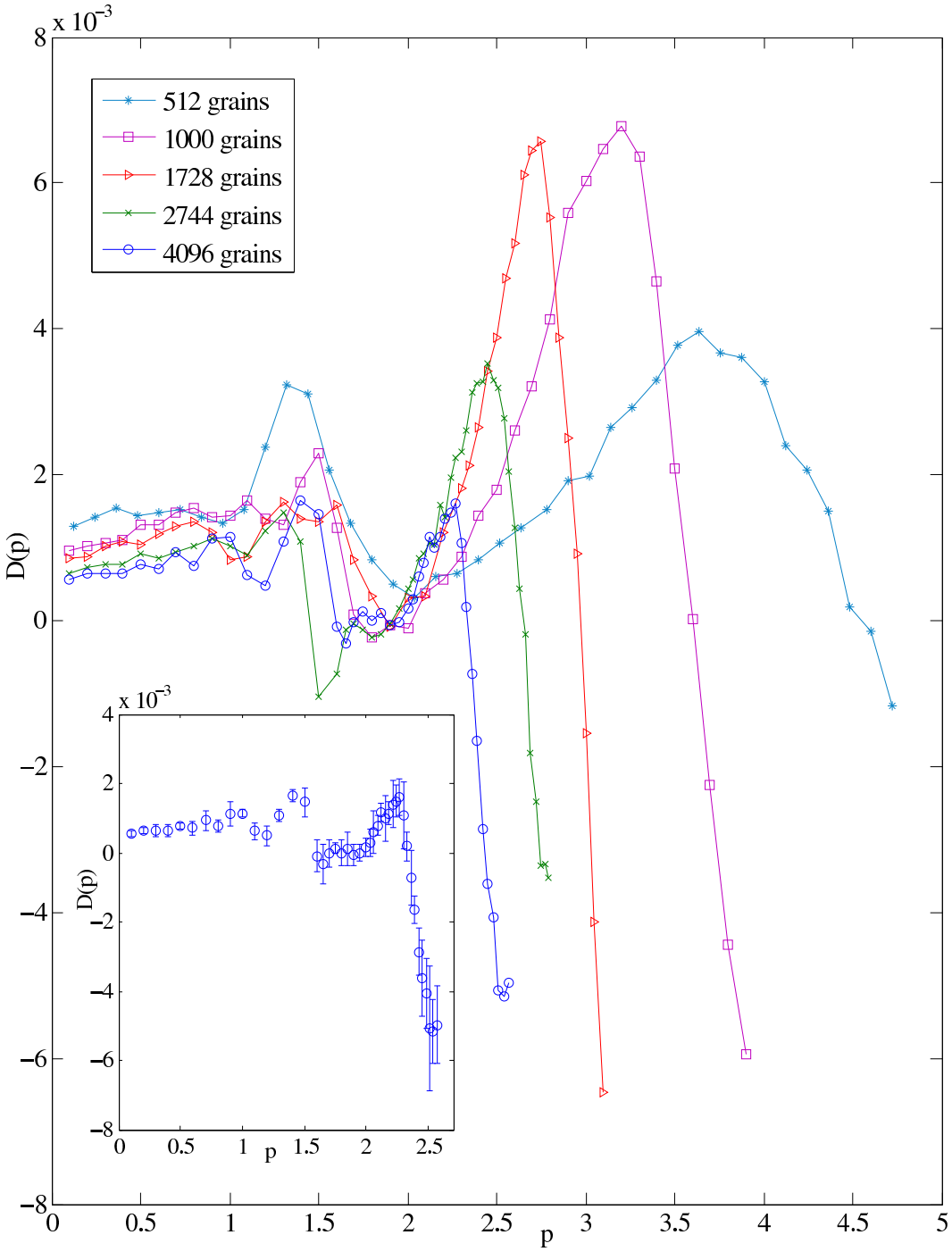

FIG. 20: The graph of $D(p) = \left.\frac{\partial \langle \phi \rangle_{p,f}}{\partial f}\right|_{f=0}$, which measures the response in average density, $\langle \phi \rangle_{p,f}$, to change of strain. The insert gives error bars on the system with 4096 grains.

4096 grains at $p_1 < ... < p_k$, where the p values chosen are different for each size system. In the simulations we begin at low p_1, and then slowly increase p until just after the derivative $D(p)$ falls sharply below zero, roughly corresponding to p_k. (For pressures significantly greater than p_k, the simulations become prohibitively slow.) The last configuration in the simulation of p_i is used as the starting configuration of the simulation of p_{i+1}. We use the standard biased autocorrelation function to determine a "mixing time", measured as the number of Monte Carlo steps required before the autocorrelation first crosses zero, and we run our simulations long enough so that the simulation of each p_i contains on average at least 20 mixing times. Then we run 200 independent copies of each simulation to obtain the averages $\langle\alpha\rangle_{p,0}$, $\langle\phi\rangle_{p,0}$, and $\langle V\alpha\rangle_{p,0}$. With these averages we compute $D(p)$ from (26). (We also ran some of our simulations much longer, with fewer copies and p values, and noted agreement with the already-obtained data on $D(p)$.) Then, for error bars on $D(p)$, we repeat the entire experiment 8 times and use the Student's t-distribution.

Our simulations suggest that $D(p)$ develops a discontinuity as the system size increases; see Fig. 20. Changing variables we find that D, as a function of $\langle\phi\rangle_{p,0}$, develops a discontinuity. We note that the ϕ-values where $D(p)$ drops sharply below zero are relatively close to the volume fraction $\phi_d \approx 0.59$ noted in the introduction. However because the sharp drop in $D(p)$ moves significantly with system size it is hard to pinpoint a precise transition point. We plot $\langle\phi\rangle_{p,0}$ against p in Fig. 21b and D against $\langle\phi\rangle_{p,0}$ in Fig. 21a.

Note that for $p \leq 1$, $D(p)$ exhibits regular behavior in which $D(p)$ is roughly constant, $D(p) = \eta \approx 0.001$. Then for $1 < p < 2$, $D(p)$ has some oscillation which is characteristic to the system size. Then for $p \geq 2$, $D(p)$ steadily increases to a peak, then sharply decreases through zero. We believe that $D(p)$ is discontinuous in the limit of infinite system size, but the rate of change of $D(p)$ is so large it is difficult to measure its variation with system size. Instead we consider two measures of the interval R in which the discontinuity is developing, and then note that R gets smaller and smaller as system size increases.

We expect that the oscillation observed in $D(p)$ in the interval $1 < p < 2$ is caused by finite-size effects, so that it disappears in the limit $N \to \infty$. Furthermore we expect the critical p_c to fall at either the end or the beginning of the oscillation region. These two

possibilities underlie, respectively, our measurements R_1 and R_2, defined below. Let η be the average value of $D(p)$ over $p \leq 1$. The left endpoint of R_1 is the smallest value of p where $p > 2$ and $D(p) \approx \eta$, and the right endpoint of R_1 is the value of p where $p > 2$ and $D(p) \approx 0$. The widths of R_1 are approximately 1.75 ± 0.05, 1.15 ± 0.05, 0.75 ± 0.05, 0.50 ± 0.05, and 0.30 ± 0.05 for systems of $N = 8^3$, 10^3, 12^3, 14^3 and 16^3 grains, respectively. On the other hand, the left endpoint of R_2 is defined as the smallest value of p such that $D(p)$ differs significantly from η, while the right endpoint of R_2 is the same as the right endpoint of R_1. We estimate that the widths of R_2 are approximately 3.55 ± 0.05, 1.55 ± 0.05, 1.25 ± 0.15, 1.15 ± 0.05, and 1.00 ± 0.05 for systems of $N = 8^3$, 10^3, 12^3, 14^3 and 16^3 grains, respectively.

In either case, based on the decreasing sizes of the intervals R_1 and R_2, we believe that the jump from $D(p) \approx \eta$ to $D(p) \ll 0$ occurs over an interval which is vanishing in the infinite volume limit, which, given the relation between $D(p)$ and the free energy $F(p, f)$ in (27), is reasonably termed a second order phase transition. And as noted in the introduction, there is experimental evidence for this interpretation in [SNRS].

Conclusion

We have analyzed a model of granular matter using an Edwards ensemble [AKLS, Ch, EG, He], the purpose being to understand the yield phase transition found in [SNRS]. The transition in [SNRS] occurs at approximately the same volume fraction, about 0.6, as dilatancy onset [RN], but corresponds to a different response of the material, a penetration force instead of a shear. Our granular model shows that shearing could produce a sharp phase transition at dilatancy onset, defined as the boundary between the volume fractions which expand under shear and those which contract under shear. As the two physical phenomena, the yield transition and dilatancy onset, both occur at volume fractions near 0.6, we argue that they coincide, in the sense that they simply represent responses of two phases of granular matter to different stimuli.

We also note that the behavior of granular matter at the random close packing density, about 0.64, has been interpreted in [Ra, AR2] as the freezing point of a first order phase

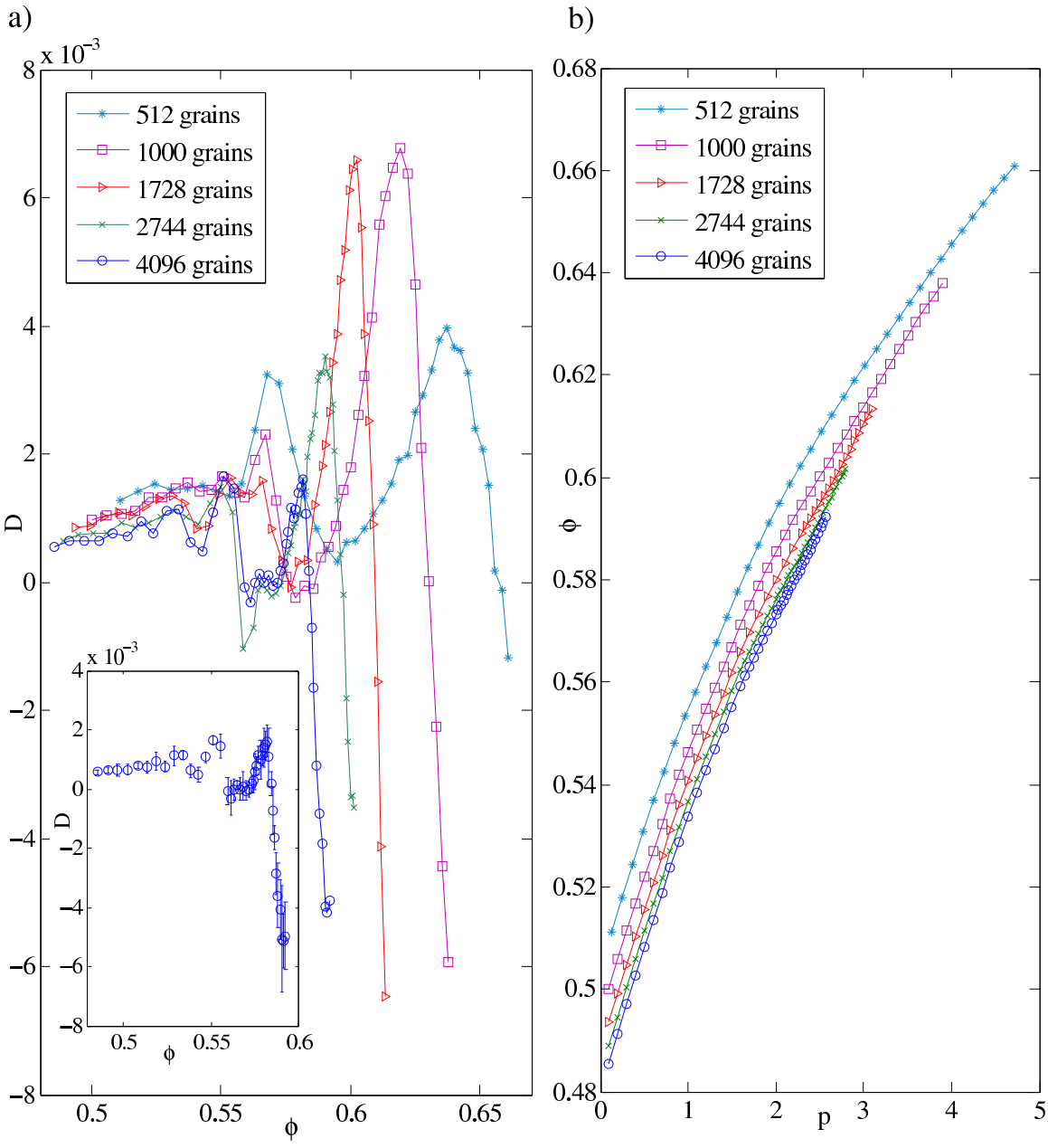

FIG. 21: a) $D(p)$, our measure of the response of density to change of strain, as a function of the average density, ϕ; b) The average density, ϕ, as a function of p.

transition in which the high density regime is an ordered phase. Together with our results here, this means that the usual freezing transition of equilibrium fluids, at which the material acquires the solid features of an ordered (typically crystalline) internal structure as well as a strong resistance to shear, seems to be split into two stages in granular materials, with significant resistance to shear occuring at dilatancy onset at density about 0.6 [RN] and the ordered internal structure occurring at the random close packing density of about 0.64 [SK].

A direct test of whether dilatancy onset defines a sharp phase transition poses some experimental difficulty. The statistical approach seems to require that repeated preparations of granular samples be able to sample the full granular phase space. This seems to be justified for the fluidization/sedimentation method of [SNRS], and the tapping method of [NKBJN]. A test would therefore require a way to combine shearing with one of these preparation protocols. It should be possible to perform a tapping protocol in a shear cell, but tapping does not ordinarily produce samples at volume fractions below 0.6, making it hard to see dilatancy onset. And while fluidization/sedimentation can prepare samples in the desired range of volume fractions, this protocol is hard to perform in a shear cell.

On the theoretical side, our result helps to firm up the phase diagram of granular matter. There was already experimental [SCM] and theoretical [Ra, AR2] support for a phase transition at random close packing, which is at volume fraction 0.64. Our result adds theoretical support to the experimental evidence of [SNRS] for a phase transition at volume fraction 0.6.

The statistical modeling of granular matter using ensembles of Edwards' type is, presumably, justifiable only for certain preparation protocols, such as the fluidization/sedimentation and tapping noted above. We hope that the growing evidence of interesting structure in the state space of granular matter will help motivate further experimental development to investigate these states, the analogue of the states of matter in thermal equilibrium.

VIII. FIRST ORDER PHASE TRANSITION IN A MODEL OF QUASICRYSTALS

Certain alloys have been shown to exhibit exotic structures in the sense that the structures produce sharp X-ray Bragg peaks with symmetries which cannot arise from any crystal [SBGC]. We model these materials with equilibrium statistical mechanics using a technique due to Levine and Steinhardt [LS] which employs an energy ground state associated with an "aperiodic tile set", that is, a set of several geometric shapes which only achieve their densest packings in nonperiodic ways, the best known two-dimensional example being the kite and dart shapes of Penrose [Ga]. There is very little direct evidence that any equilibrium statistical mechanics model would show a well-defined quasicrystalline phase at positive temperature; we know only one model for which there is (simulation) evidence [LP, KR] of such a phase. The theory of solid/fluid phase transitions often emphasizes the role of crystal symmetry, going back at least to Landau [LL, An], and it is of interest to understand how the quasicrystalline state, with its exotic form of symmetry [Ra2], fits into this picture. In this regard it is noteworthy that the simulations in [LP, KR] indicate a continuous (high order) transition between the fluid and quasicrystalline phases. We revisit this issue here with slightly more realistic models and find clear simulation evidence of a discontinuous (first order) transition. We contrast our results with related models of hard squares and of Widom-Rowlinson type.

The model

Our models are variants of that used in [LP, KR], which we describe first. The lattice model of [LP, KR] uses 16 types of particles, each corresponding to an element of a certain subset $\mathcal{S} \subset \{1,2,3,4,5,6\}^4$ of cardinality 16, associated with an aperiodic tiling set due to Ammann [GS]. The model consists of configurations of particles on the square lattice $\mathbb{Z}^2$. It is convenient to interpret each element of $\mathcal{S}$ as a unit-edge square *tile*, with its 4 edges colored using 6 possible colors $\{1,2,3,4,5,6\}$ in one of the 16 groups of 4 indicated by $\mathcal{S}$;

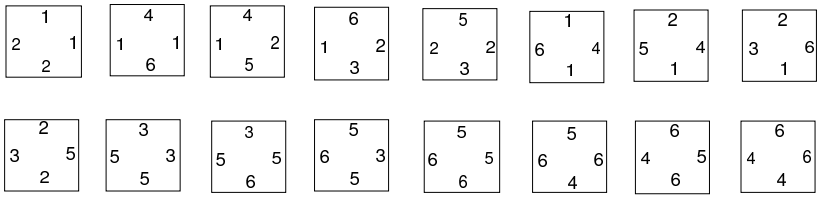

FIG. 22: Ammann's 16 Wang tiles.

see Fig. 22.

The model in [LP, KR] requires precisely one particle/tile centered at each lattice site, and each particle interacts with each of its 4 nearest neighbors only, with interaction energy 0 or -1, with the negative value when the edge colors match. A canonical ensemble is used, but with density fixed at 1. The model then exhibits a continuous phase transition at positive temperature [LP, KR], with the low temperature phase showing quasicrystalline structure, including the symmetry [Ra2] it inherits from Ammann's aperiodic tiling set.

We consider variants of the above model, investigating the consequences of two changes: extending the size of the square tiles to integer edge length $w \geq 1$ (they are still "hard" – no overlap of tiles is allowed); and allowing a full range from 0 to 1 of volume fraction for the particle configurations, in place of the fixed volume fraction of 1 used in [LP, KR]. Note that the latter adds a second thermodynamic variable to the model.

The description of the interaction is a bit more complicated than in the $w = 1$ model of [LP, KR], since tiles which are close but not touching may still interact, though with lower amplitude. To define the interaction we need some notation. A *tile-state* A is an element of $\mathbb{Z}^2 \times \mathcal{S}$, with the first coordinate of A representing its center on the lattice, and the second coordinate representing its edge colors. We define a pairwise interaction H between tiles as follows. For each tile-state A, consider the four "nearest neighbor" (empty) squares of the same size as A which surround A but do not overlap it, labelled N, S, W and E as in

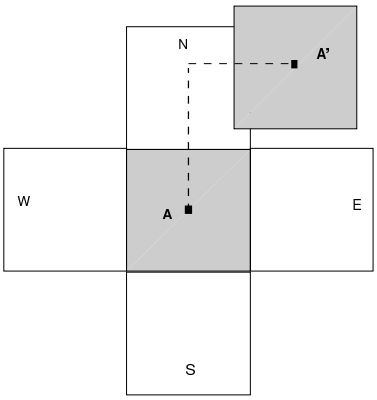

FIG. 23: The interaction energy depends on the ℓ^1 distance between particle centers (dashed line).

Fig. 23. If another tile-state A' is disjoint with A but overlaps one of these four squares – it cannot possibly overlap more than one – its energy of interaction with A, $H(A, A')$, is as follows. Assume without loss of generality that A' overlaps N. Then $H(A, A')$: is negative if and only if the north edge of A has the same color as the south edge of A', and positive otherwise; and has absolute value given by $|H(A, A')| = (3w - d)/(2w)$, where d is the ℓ^1 distance between the centers of A and A'. (The ℓ^1 distance between (x, y) and (x', y') is $|x - x'| + |y - y'|$.) If A' overlaps S, W, or E, then the energy H is defined similarly.

Given an inverse temperature β, a chemical potential μ (common to all tiles/particle types), and a finite volume $\mathcal{V} \subset \mathbb{Z}^2$, we consider the grand canonical ensemble: the probability $\mathcal{P}_{\beta,\mu}$ on configurations C of tile-states in $\mathcal{V}$ which is given by

$$\mathcal{P}_{\beta,\mu}(C) = \frac{\exp\left[-\beta(\mathcal{H}(C) - \mu\mathcal{N}(C))\right]}{Z,} \tag{28}$$

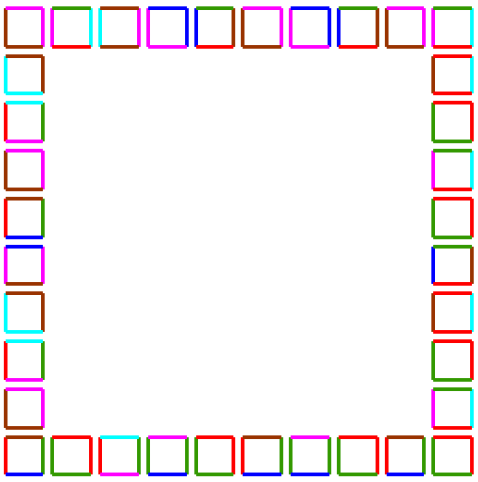

FIG. 24: A boundary shell (with edges colored instead of numbered).

where $\mathcal{N}(C)$ is the number of tiles-states in C, $\mathcal{H}(C) = \sum_{A \neq A' \in C} H(A, A')$ is the total energy of C, and $Z = Z(\mu, \beta)$ is the appropriate normalization. In our simulations we use "square" volumes $\mathcal{V} = \mathbb{Z}^2 \cap [-k, k]^2$ with k an integer multiple of w. We use boundary conditions as follows. Starting from a perfect tiling $\mathcal{T}$ by tile-states, that is, a configuration of tiles covering $\mathbb{Z}^2$ in which all edge colors match, we remove all the tiles except those just outside $\mathcal{V}$; this leaves a (fixed) boundary "shell"; see Fig. 24. (We use 10,000 different boundary shells arising from random translations of a single tiling.)

It remains to define the order parameter, χ. Each tile-state has a "long/short pattern" given by its 4 edge colors, where we call colors 1 and 2 "short" and colors 3, 4, 5 and 6 "long". Note that, for any tile, horizontal edges are either both short or both long, and vertical edges are either both short or both long, so there are 4 possible long/short patterns for a tile. Any tile-state A centered "near" the site $(wi, wj) \in \mathcal{V}$, namely centered in $[wi - w/2, wi + w/2) \times [wj - w/2, wj + w/2)$, will be said to *agree with* $\mathcal{T}$ if it has the same long/short pattern as the tile-state in $\mathcal{T}$ centered at (wi, wj). Now, consider the thick

"shells" $\mathcal{V}_j = \mathcal{V} - [-j, j]^2$. Given a configuration C in $\mathcal{V}$ and boundary from $\mathcal{T}$, let j^* be the largest integer such that at least 80% of sites (wi, wj) in $\mathcal{V}_{j^*}$ have a tile-state centered nearby (in the above sense) which agrees with $\mathcal{T}$. The order parameter χ is defined as the corresponding normalized volume, $\chi(C) = |\mathcal{V}_{j^*}|/|\mathcal{V}|$.

Simulations, and results

We ran Markov-chain Monte Carlo simulations of the model with tile widths $w = 1$, 2, and 3. For each tile width w we simulated volumes $|\mathcal{V}| = (20w)^2$, $(40w)^2$, $(60w)^2$, $(80w)^2$ and $(100w)^2$. (We will also use the notation $V = |\mathcal{V}|/w^2$, so V represents the maximum possible number of tile-states in a single configuration.) The Monte Carlo steps were designed to produce the target distribution of equation (28). The basic Monte Carlo step involves a choice between four types of moves: moving a particle (locally), changing a particle type, removing a particle, and adding a particle. As usual in grand canonical Monte Carlo simulation, given a configuration C a trial configuration C' is introduced, effecting one of the moves described above, and is accepted with probability determined by the desired limiting distribution, that is, equation (28).

More precisely, the basic Monte Carlo step is as follows. Let $C(n)$ be the configuration at the nth step of the Monte Carlo chain, and choose a random lattice site x. Select $k \in \{1, 2, 3, 4\}$ with probability p_k, where the p_k are the probabilities of attempting the four types of Monte Carlo moves, with the p_k summing to 1 and $p_3 = p_4$. (We choose the p_k somewhat arbitrarily.) Without loss of generality suppose $x \in R := [wi - w/2, wi + w/2) \times [wj - w/2, wj + w/2)$. First suppose $k \in \{1, 2\}$. If there is no tile-state centered in R, then $C(n + 1) = C(n)$; otherwise, let A be the (unique) tile-state centered in R, and produce a trial configuration $C(n)'$ by: if $k = 1$, moving the center of A to a site in R chosen uniformly at random; if $k = 2$, replacing A with a different tile-state centered at the same lattice site. Now suppose $k = 3$. If there is a tile-state A centered in R, then $C(n)'$ is obtained by removing A; otherwise $C(n + 1) = C(n)$. Finally suppose $k = 4$. If there is no tile-state centered in R, then let $C(n)'$ be the configuration obtained from $C(n)$ by adding

a tile-state chosen uniformly at random and centered at x; otherwise $C(n+1) = C(n)$. In cases where a trial configuration $C(n)'$ is introduced, we take $C(n+1) = C(n)'$ with probability $Q = \min(1, q)$; otherwise we take $C(n+1) = C(n)$. Here q is given by

$$q := \min\{1, e^{\beta[\mathcal{H}(C)-\mathcal{H}(C')+\mu^*(\mathcal{N}(C')-\mathcal{N}(C))]}\}, \tag{29}$$

where we have written C for $C(n)$ and C' for $C(n)'$, and take $\mathcal{H}(C') = \infty$ for trial configurations C' with overlapping tiles. Here $\mu^* = \mu + \beta^{-1}\ln(16s^2)$ is chosen so that the Monte Carlo configurations $C(n)$ have limiting probability distribution given by equation (28). (The value μ^* arises because of the following. Starting with a configuration C, the probability of proposing a trial configuration C' which removes tile-state A from C is $16s^2$ times the probability that, starting with the configuration C', a trial configuration $C'' = C$ is proposed which adds the tile-state A to C'.)

For $w = 2$ and $w = 3$ we find clear evidence of discontinuous (first order) phase transitions. At the transitions (at $\beta = 1.5$, near $\mu = 1.4$ for $w = 2$ and near $\mu = 2.0$ for $w = 3$) the average volume fraction ϕ and energy per volume $\mathcal{H}/V$ exhibit developing jump discontinuities as V increases; see Figs. 25-26. Furthermore the (volumetric) heat capacity, C_V (defined as the derivative of $\mathcal{H}/V$ with respect to $T = 1/\beta$), exhibits a developing delta function as V increases (see Figs. 25-26).

From our data in Fig. 27, for the $w = 1$ model, there appears to be a continuous transition (at $\beta = 1.5$ near $\mu = 0.8$), from a disordered fluid phase to a phase with quasicrystalline order, similar to the transition in [LP,KR] of the canonical ensemble at density 1.

To quantify the developing delta function in C_V noted above for $w = 2, 3$ we measure, from Figs. 25 and 26, the maximum value h of C_V divided by the "width" of the graph of C_V at $h/2$ (see Fig. 28). The order parameter χ also develops a discontinuity at the transition, signaling the onset of quasicrystalline symmetry: see Figs. 25-26.

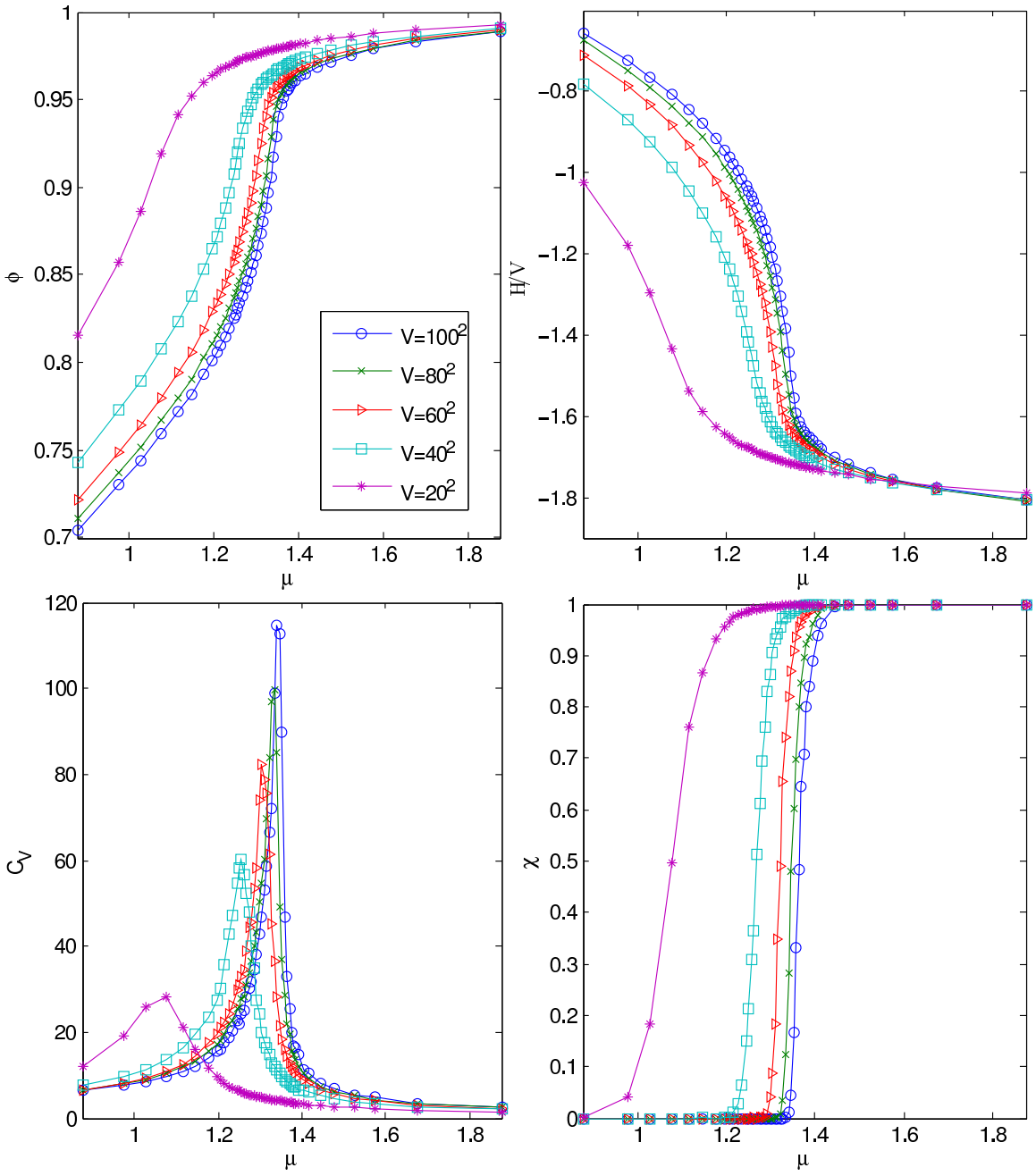

FIG. 25: Data for $w = 2$ and $\beta = 1.5$.

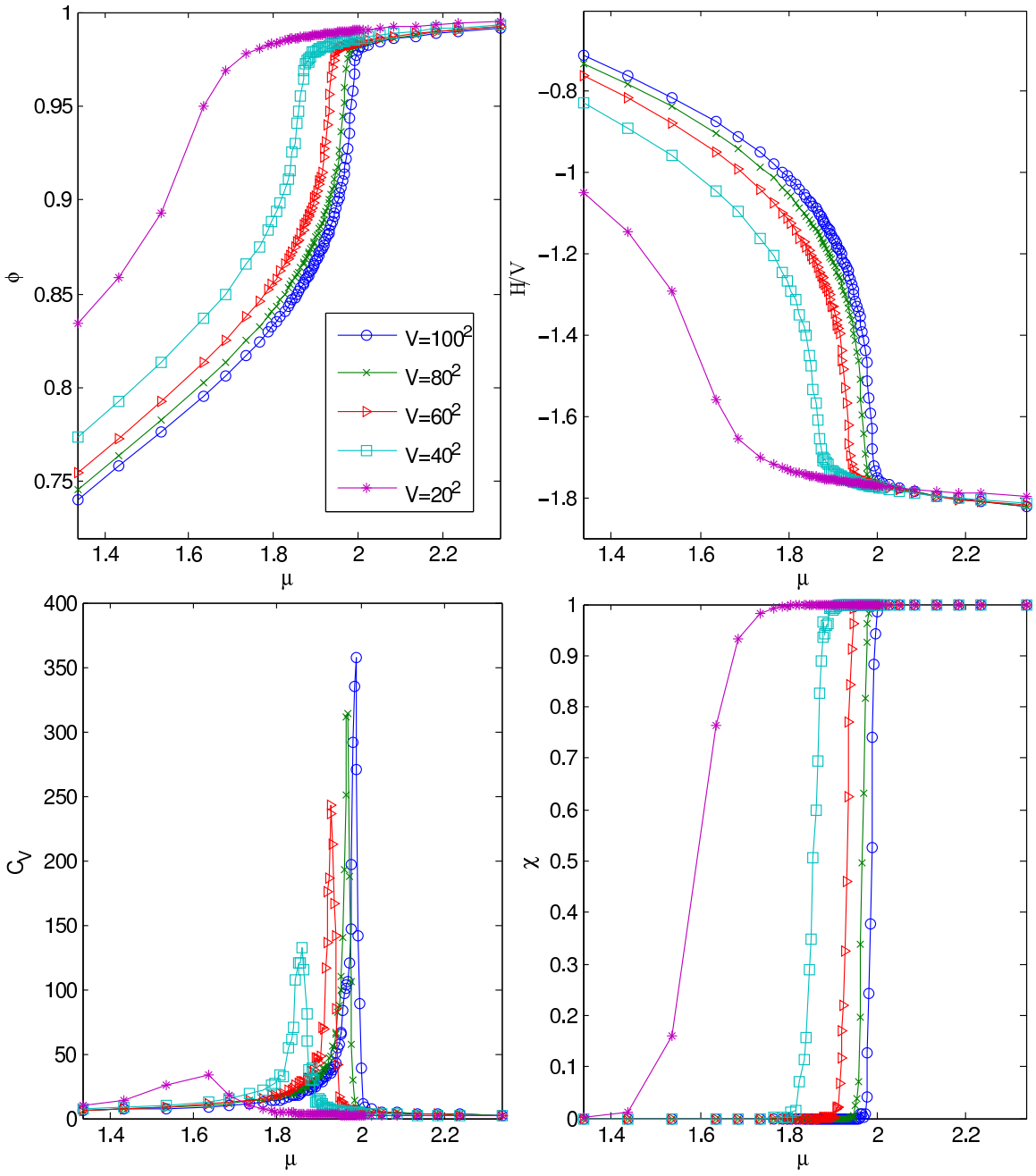

FIG. 26: Data for $w = 3$ and $\beta = 1.5$.

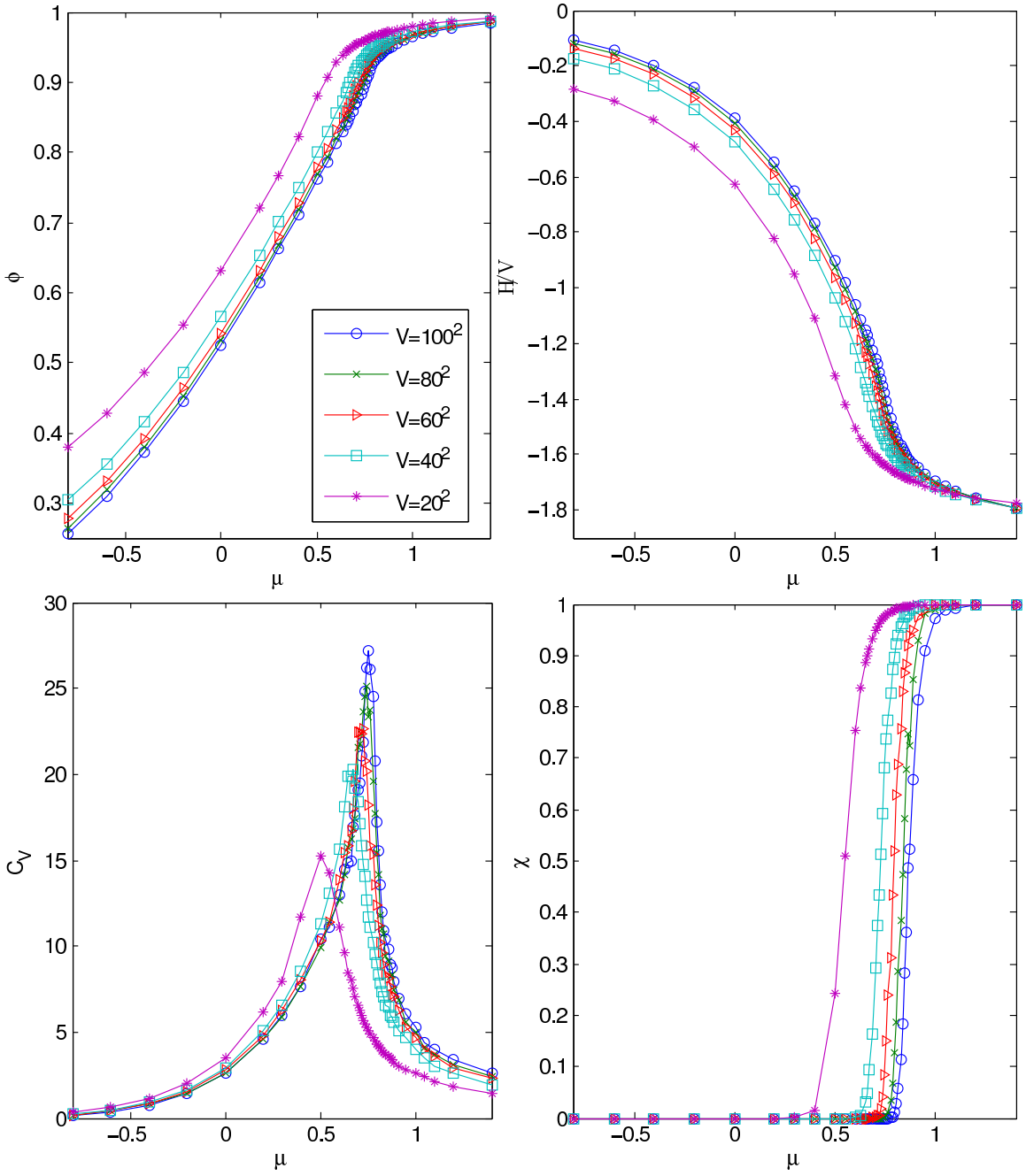

FIG. 27: Data for $w = 1$ and $\beta = 1.5$.

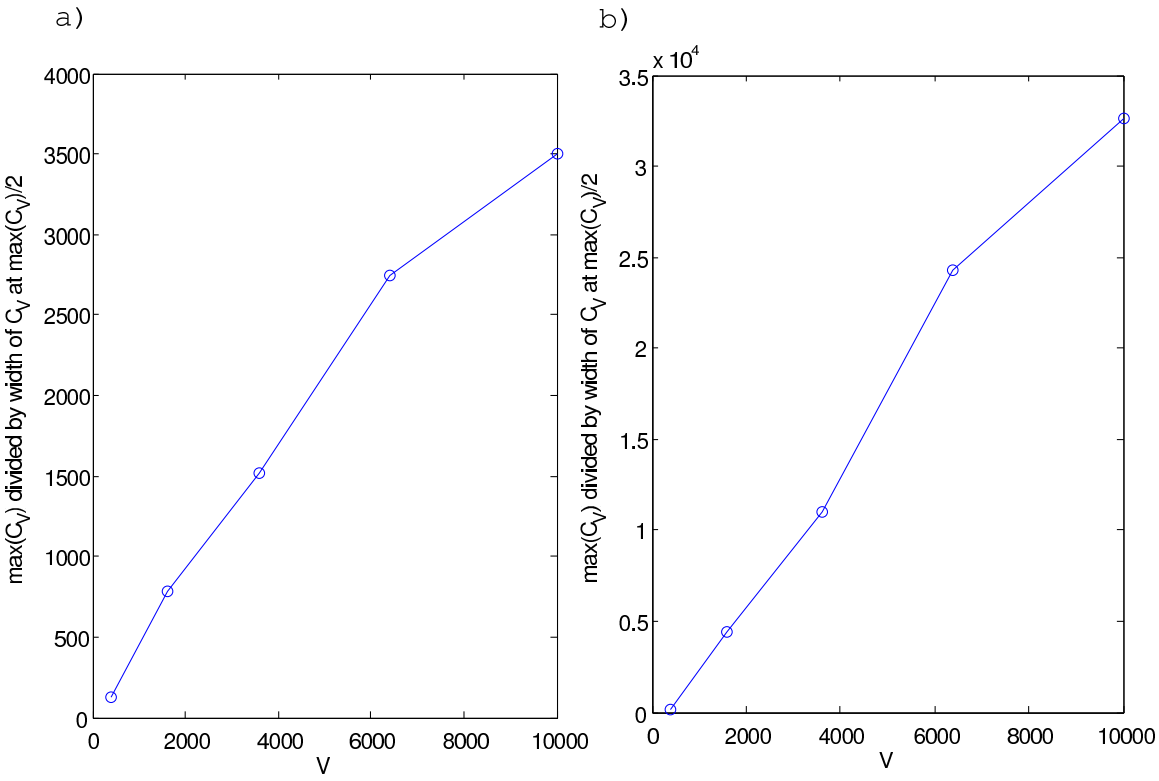

FIG. 28: Evidence of C_V developing into a delta function for a) $w = 2$, and b) $w = 3$.

Comparisons

We next compare our results with related models, in particular hard squares and Widom-Rowlinson models on $\mathbb{Z}^2$; see [FAL] for a review of, and earlier references to, the former and [LMNS] for a review of, and earlier references to, the latter.

At sufficiently high temperature the soft interaction between our particles must become negligible compared to the hard core so we first review what is known about hard square systems.

For hard squares on $\mathbb{Z}^2$ the energy is zero for all configurations so it is convenient to use a grand canonical ensemble with fixed temperature 1 and variable chemical potential μ. Hard

squares with edge size $w = 1$ ("point hard core") do not have a phase transition as μ is varied, since the variables at each site, 'occupied' or 'unoccupied', are independent. For fixed $w \geq 2$ the densest configurations, of volume fraction 1 and corresponding to $\mu \to \infty$, are degenerate, allowing parallel rows or columns of squares to slide independently in what is called a "columnar" phase. It is generally accepted from simulation [FAL] that the model with $w = 2$ has a continuous transition at volume fraction about 0.92. We only know of one paper on the model with $w = 3$ [FAL]; the authors claim a first order freezing transition beginning at a density above 0.91, but are unable to show developing discontinuities in any thermodynamic quantities.

We now compare our model to hard squares on $\mathbb{Z}^2$. Consider a version of our quasicrystal model with $w \geq 2$ but in a canonical ensemble with volume fraction fixed at 1. Based on the results of [LP,KR], we expect this model to have a columnar phase at high temperature, and a quasicrystalline phase at low temperature, with a transition between them at some unknown temperature T_c. Now considering the same model except at lower volume fraction or chemical potential, one expects the transition to the quasicrystalline phase to move to lower temperature since the soft interaction should have less effect as the density is lowered. We conclude that above temperature T_c our model should behave qualitatively like hard squares, with disordered and columnar phases, but without a phase with quasicrystalline order.

Absent from the above discussion is the effect on entropy, in our model, of the multiple types of particle. This effect is emphasized in Widom-Rowlinson models, which we now discuss. The multitype Widom-Rowlinson model with q colors, on $\mathbb{Z}^2$, is defined by the hard core condition that nearest neighbor sites cannot be occupied by different colors. The main conclusion of such work is the existence (for large enough q) of two types of high density phase transitions: one transition at which spatial symmetry is broken, producing different population densities for the two sublattices, but without breaking the symmetry between particle types, and a second (discontinuous) transition at higher density at which the symmetry between particle types is broken, so that one particle type dominates the density [LMNS]. These models, with diamond-shaped instead of square hard cores, are not

simply related to our models, but there are two interesting variants treated by Georgii and Zagrebnov [GZ] which are closely related. The first model has a square-shaped hard core, with square width $w = 2$, between particles of different color; the second model adds to this a smaller diamond-shaped hard core between nearest neighbor particles of the same color. One could think of these models as employing a hard core of size $w = 2$ between *all* particles, with a "cancelling" (or attractive) interaction between particles of like color on sites at separation $\sqrt{2}$ for the second model, and for sites at separation 1 and $\sqrt{2}$ for the first model. Thus the models can be thought of as hard squares with an added particle-type-dependent short range attraction, somewhat like our quasicrystal models. Both Widom-Rowlinson models show only one transition, which is discontinuous. For the first model the high density phase breaks particle type symmetry but not spatial symmetry, and for the second model the high density phase breaks the symmetry of both space and particle type. In particular the second model seems close to our ($w = 2$) quasicrystal model, and our results bear this out, with a discontinuous transition corresponding to broken spatial and particle-type symmetries. The correspondence might be closer if the attraction and repulsion in our model was a hard rather than soft interaction, as in [Ru2].

It would have been useful to simulate our model over a range of temperatures, but we found this prohibitively expensive in computation time. For this reason we investigated a technique noted in [RE], in which the initial state for the simulation is an energy ground state. However this technique proved to be unreliable here unless the runs were of comparable length to those starting from vacuum, thus yielding no advantage; see Fig. 29. (We suspect that simulations starting from an energy ground state get restricted to a narrow portion of phase space more easily than those starting from the vacuum.)

Conclusion

We have introduced an extension of a two dimensional lattice gas model of a quasicrystal [LP, KR]. That model was studied as a function of temperature at fixed density 1, with simulations showing a continuous phase transition between a disordered (fluid) phase and a

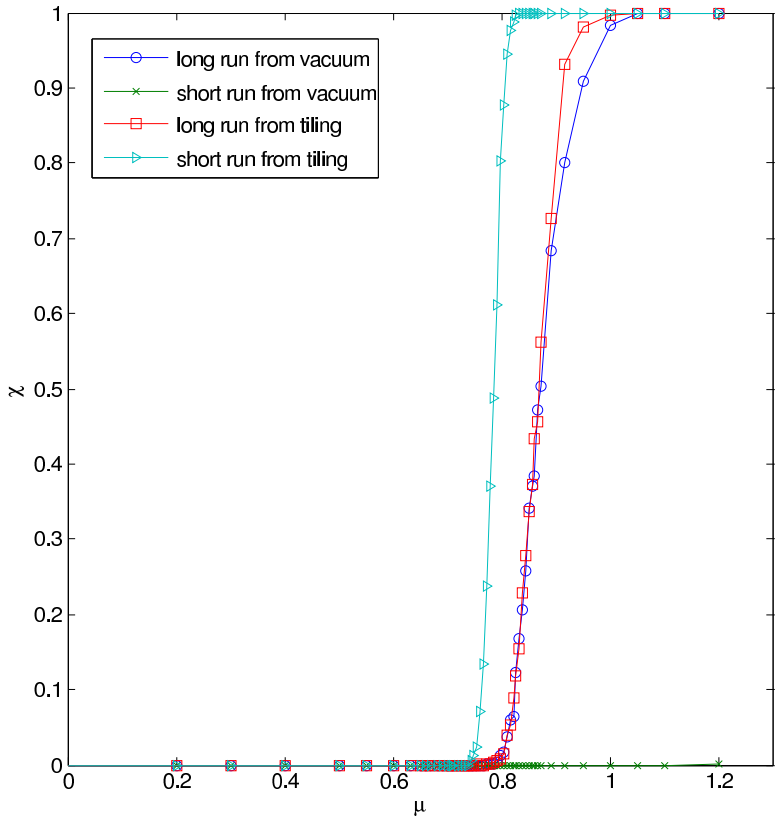

FIG. 29: Comparison of order parameter values of long and short runs starting from both vacuum and perfect tiling, for $w = 1$ and $V = 100^2$. (The long runs are 100 times longer than the short runs.)

phase with quasicrystalline order. When we introduce vacancies into the model we find that the basic character does not seem to change: there still appears to be only the two phases, disordered and quasicrystalline, with a continuous transition between them.

We then generalized the model by extending the range of the hard core as well as allowing variation in the density, and found, by simulation along a (low temperature) isotherm, that the model then exhibits a *discontinuous* transition between a low density disordered and high density quasicrystalline phase. The high density quasicrystalline phase breaks symmetries of space (a square sublattice is preferentially populated) and particle type (the particles inherit

the quasicrystalline boundary structure). Along an isotherm at sufficiently high temperature we expect the model to exhibit the transition of simple hard squares (continuous for $w = 2$ and possibly discontinuous for $w = 3$), between the low density disordered and high density columnar phases. At fixed high density or chemical potential we expect a transition from the quasicrystalline phase to a columnar phase as temperature is raised from zero.

This family of models with unusual symmetry adds a special flavor to the more traditional lattice gas models with hard core. Its complicated multiparticle structure seems at present to defy proof of a transition, and is also expensive to simulate. Further progress in filling out the phase structure of the model would be highly desirable.

IX. RANDOM LOOSE PACKING IN GRANULAR MATTER

We introduce and analyze a crude model for the random loose packings of granular matter. These packings, as well as random close packings, were carefully prepared by Scott et al in the 1960's [Sc,SK], mainly in samples of steel ball bearings. Gently pouring samples of 20,000 to 80,000 spheres into a container, the lowest possible volume fraction obtainable – the so-called random loose packing density – was determined to be 0.608 ± 0.006.

The above refers to monodisperse steel spheres immersed in air; they also worked with spheres of other materials immersed in other fluids; variations in the coefficient of friction and in the effective gravitational force lead to somewhat different values for the random loose packing density [SK].

Matter is generally described as "granular" if it is composed of a large number of non-cohesive subunits each of which is sufficiently massive that its gravitational energy is much larger than its thermal energy. A common example is a sand pile.

There are several classic phenomena characteristic of static granular matter, in particular dilatancy, random close packing, and random loose packing, none of which can yet be considered well-understood; see [dG2] for a good review. A basic question about these phenomena is whether they are sharply defined or inherently vague. Dilatancy has recently been associated with a phase transition measured by the response of the material to shear [SNRS], which answers the question for this phenomenon. The case of random close packing is controversial and awaits further experiment; see [TT,Ra1]. Our main goal here is to analyze this question with respect to random loose packing, to determine whether or not traditional theoretical approaches to granular matter predict a sharply defined random loose packing density. It is clear that any experimental determination of a random loose packing density will vary with physical conditions such as coefficient of friction, and we will take this variation into account in our analysis below.

We begin by contrasting two common approaches to modelling static granular matter. One, the more common, is the "protocol-dependent simulation," in which one studies properties of dense packings by exploring a variety of methods of preparation of the packings; see

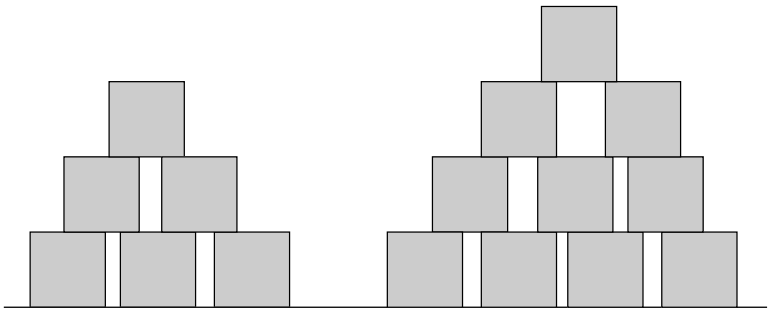

FIG. 30: An allowed configuration.

[GB], [TT] or [ZM] for examples. Another approach goes under the name of Edwards theory [EO], in which, basically, one adds the effects of friction and a strong gravitational force to the hard sphere model of equilibrium statistical mechanics. We note that appropriate specification of the added forces fully determines an Edwards model; there are no adjustable parameters beyond those familiar from statistical mechanics, such as density and pressure. (Of course one can always introduce further approximations or features, for instance mean field theory, soft core, attraction, etc.) In particular, in an Edwards model all Markov chain Monte Carlo simulations will, if done correctly, give the same result; there is no freedom in preparing the packings the way there is in protocol-dependent simulation.

These two approaches – the protocol-dependent simulations and the Edwards approach – have different strengths. There have been serious claims that the former approach has serious difficulty making sense of some granular phenomena, in particular random close packing [TT]. We have previously shown [Ra1] how Edwards theory allows a clean definition of random close packing, and in this paper we show, by a very different mechanism, how it allows for an understanding of random loose packing. In that sense our choice of using an Edwards-type model is central to our argument. (We do not claim that the Edwards approach has been proven the most accurate theory of static granular matter, but only that it is a serious contender.)

We briefly summarize our Edwards-style model as follows: We consider arrangements of hard-core parallel squares in a fixed rectangular box, where each square has to rest on either

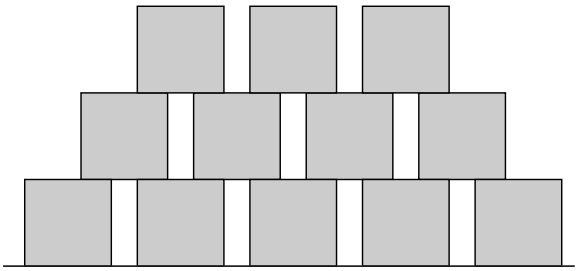

FIG. 31: A uniform configuration.

two squares below it or on the box's floor, and we put a uniform probability distribution on the set of all such arrangements. Then we run Markov chain Monte Carlo simulations and measure the packing fraction of the Markov chain configurations.

We begin more ambitiously by discussing a more realistic model. As is standard in Edwards theory we take as a starting point a variant of the hard sphere model of equilibrium statistical mechanics. Consider a model consisting of large collections of impenetrable, unit mass, unit diameter spheres in a large container, acted on by gravity and with infinite coefficient of friction between themselves and with the container. Put a probability density on the set of all mechanically stable packings of the spheres in their container, with the probability density of a packing c proportional to $\exp[-E(c)]$, where $E(c)$ is the sum of the heights, from the floor of the container, of the centers of the spheres in the packing c. We expect, but cannot show, that such an ensemble will exhibit a gradient in the volume fraction (with volume fraction decreasing with height) and that there is a well-defined random loose packing density as one approaches the top of the packing (where the analogue of hydrostatic pressure goes to zero). By a "well-defined random loose packing density" we mean that as one takes an infinite volume limit, the probability distribution for the volume fraction of the top layer of the packing becomes concentrated at a single nonzero value. We emphasize that we are focusing on a bulk property near the top of the configuration, not a surface phenomenon.

The above determines a well defined zero pressure probability distribution for packings c. One could imagine simulating the distribution with Monte Carlo or molecular dynamics,

but this is not practical at the high densities which are necessary in a granular model. (We emphasize that any such simulation should reproduce the above probability distribution; in this Edwards-style model the equilibrium probability distribution is completely determined, so there is no freedom available in deciding how packings are simulated.)

To make Monte Carlo simulations feasible, we make several simplifications in the way gravity and friction are incorporated in the above model. First we switch to an ensemble consisting of packings which are limits, as the gravitational constant goes to zero, of mechanically stable packings; we effect this by setting $E(c) = 0$ in the relative density $\exp[-E(c)]$. With this simplification configurations are now, in their entirety, representative of the top layer in the original model. Next we consider the two dimensional version of the above: congruent frictional unit disks in mechanically stable configurations under vanishingly small gravity. Note that each such disk must be in contact with either a pair of supporting disks below it or part of the container. (Here and elsewhere in this paper we neglect events of probability zero, such as one sphere perfectly balanced on another.) We simplify the role of gravity and friction in the model one last time by replacing the disks by congruent squares, with edges aligned with the sides of the (rectangular) container, each square in contact with either a pair of supporting squares below it or the floor of the container. This is now a granular version of the old model of "(equilibrium) hard squares" [Ho], which is a simplification of "hard disks" and "hard spheres" (see [AH] for a review), in which gravity and friction is neglected but kinetic energy plays a significant role. We emphasize that in our granular model there is no longer any need to concentrate on the "top layer"; in fact we will eventually be concerned with an infinite volume limit which, as usual, focuses on the middle of the collection of squares and lets the boundaries grow to infinity. (We note that the model is capable of handling higher densities by constraining the squares to lie in a tightly containing box. We also note recent work by Song et al [SWM,Za] which takes a different path, employing a mean field approximation instead of a simplified short range model which can be fully simulated, as we have done.)

We have run Markov chain Monte Carlo simulations on this model with the following results. We initialize the squares in an allowed configuration of some well-defined volume

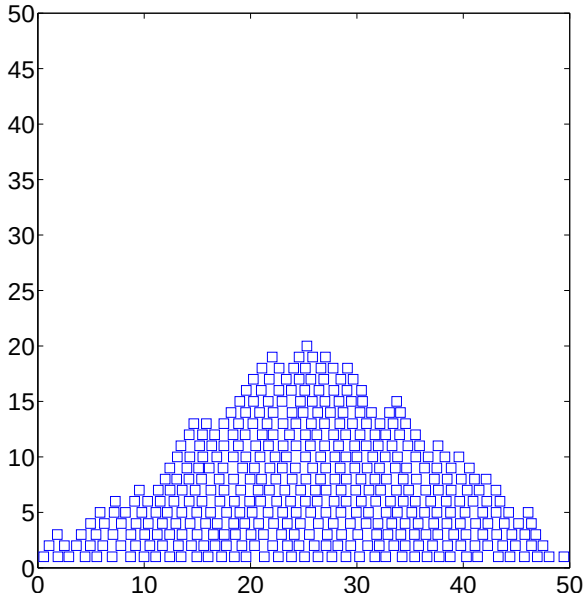

FIG. 32: 399 squares after 10^6 moves.

fraction anywhere between 0.5 and 1. If the initial volume fraction ϕ is not approximately 0.76, the simulation gradually expands or contracts the packings until the packing fraction reaches the range 0.76 ± 0.01; see Figs. 33 and 34. Furthermore, as the size of the packings increases, the standard deviation of the volume fraction tends towards zero.

The process is insensitive to the dimensions of the containing box except for extremes. We choose the height of the box to be large enough so that the configurations of squares cannot reach the ceiling (so the box height becomes irrelevant). We must choose the box width more carefully, since if the side walls of the containing box abut a closely-packed initial configuration, the simulation cannot significantly change the volume fraction; alternatively, if the width of the box is much larger than that of the initial configuration, the simulation will produce a monolayer on the floor. We ignore both extremes, however, and find that the equilibrium volume fraction is otherwise insensitive to the width of the box. More precisely, we found that the equilibrium volume fraction should be accurate if the box width is between

$2\sqrt{N}$ and $8\sqrt{N}$, where $N \geq 100$ is the number of squares. To understand these limits, first note that since we will be conjecturing the behavior of the model in the infinite volume limit, the equilibrium configuration should be a single bulk pile, so the box width should be on the order of $\sqrt{N}$. Regarding the lower bound, note that at any volume fraction a configuration occupies the least amount of floor space when the squares are arranged in a single full triangle. The bottom level of such a triangle has just under $\sqrt{2N}$ squares. Assume the containing box fits tightly around the triangle; if the triangle has volume fraction greater than 0.754 then the configuration will not be able to decrease to this equilibrium volume fraction. We avoid this by ensuring that the box width is at least $2\sqrt{N} > (0.754)^{-1}\sqrt{2N}$. To arrive at the upper bound we performed simulations on fixed particle number and let the box width vary. We found that the equilibrium volume fraction was reliable so long as the box width was less than about $8\sqrt{N}$, at least for $N \geq 100$.

We conclude that, for box widths in the aforementioned acceptable range, the equilibrium volume fraction depends only on the number of squares in the system. The main goal of our work is an analysis of the distribution of volume fraction – both the mean and standard deviation – as the number of particles increases. We conclude that the limiting standard deviation as particle number goes to infinity is zero, so the model exhibits a sharp value for the random loose packing density, which we estimate to be approximately 0.754.

The heart of our argument is the degree to which we can demonstrate that in this model there is a sharp value, approximately 0.754, for the equilibrium volume fraction of large systems, and we postpone analysis of error bars to later sections. But to understand the value 0.754, consider the following crude estimate of the volume in phase space of all allowable packings at fixed volume fraction ϕ. First notice that the conditions defining the model prevent the possibility of any "holes" in a configuration. Furthermore, if we consider any rectangle in the interior of a configuration, each horizontal row in the rectangle contains the same number of squares. (One consequence is that in the infinite volume limit each individual configuration must have a sharply defined volume fraction; of course this says nothing about the width of the distribution of volume fraction over all configurations.) Now consider a very symmetrical configuration of squares at any desired volume fraction ϕ, with

the squares in each horizontal row equally spaced, and gaps between squares each of size $(1-\phi)/\phi$ centered over squares in the next lower horizontal row; see Fig. 31. Consider these squares to represent average positions, fix all but one square in such a position, and consider the (horizontal) degree of motion allowed to the remaining square. There are two constraints on its movement: the gap size separating it from its two neighbors in its horizontal row, and the length to which its top edge and bottom edge intersects the squares in the horizontal rows above and below it. These two constraints are to opposite effect: increasing the gap size decreases the necessary support in the rows above and below. A simple calculation shows that the square has optimum allowed motion when the gap size is 1/3, corresponding to a volume fraction of 0.75, roughly as found in the simulations. In other words, this argument suggests that the volume in phase space (which for N squares we estimate to be L^N, where L is the allowed degree of motion of one square considered above) is maximized among allowed packings of fixed volume fraction by the packings of volume fraction about 0.75. Note that this is only a free volume-type estimate, so it is by no means a proof that a sharp entropy-maximizing volume fraction exists or is equal to or near 0.75.

To obtain accurate physical measurements a fluidization/sedimentation method has been developed to prepare samples of millions of grains in a controlled manner; see [OL,JS] and references therein for the current state of the experimental data. In these experiments a fluidized bed of monodisperse grains sediment in a fluid. The sediment is of uniform volume fraction, at or above 0.55 depending on various experimental parameters. Recall that the old experiments of Scott et al [Sc,SK] reported a value of 0.608 for ball bearings in air; to achieve the low value (0.55 ± 0.001 [JSSSSA]) the grains need to have a high friction coefficient and the fluid needs to have mass density only slightly lower than the grains to minimize the destabilizing effect of gravity. (In the absence of gravity one could still produce a granular bed by pressure; we do not know of experiments reporting a random loose packing value for such an environment.)

Given the dependence of the lowest achievable density on the characteristics of the experiment, we need to clarify the goal of this paper. From the physical perspective it is interesting that, for any fixed coefficient of friction and fixed relative density between the

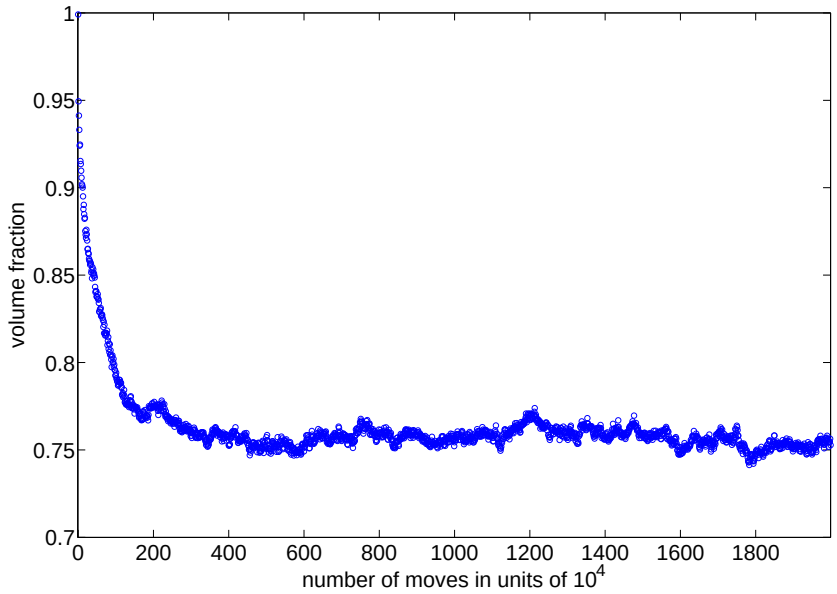

FIG. 33: Plot of volume fraction versus number of moves, from an initial volume fraction of 0.9991, for 970 squares.

grains and background fluid, there seems to be a sharply defined lowest volume fraction achievable by bulk manipulation. It is possible furthermore that by suitably varying the coefficient of friction and relative density there is a single lowest possible volume fraction (currently believed to be about 0.55 [JSSSSA]); we expect that this is the case, and that this has a simple geometrical interpretation in terms of ensembles of frictional hard spheres under gravity, as discussed above. This was the motivation of this work, and it is supported by simulations of our model. Our results suggest that whatever the initial local volume fraction of the fluidized granular bed, on sedimentation (in low effective gravity) most samples would have a well-defined volume fraction, the random loose packing density, with *no intrinsic lower bound* on the standard deviation of the distribution of volume fraction.

There have been previous probabilistic interpretations of the random loose packing density, for instance [MP,PC], as well as the recent mean field model of Song et al [SWM, Za]. A distinguishing feature of our results is our analysis of the degree of sharpness of the basic

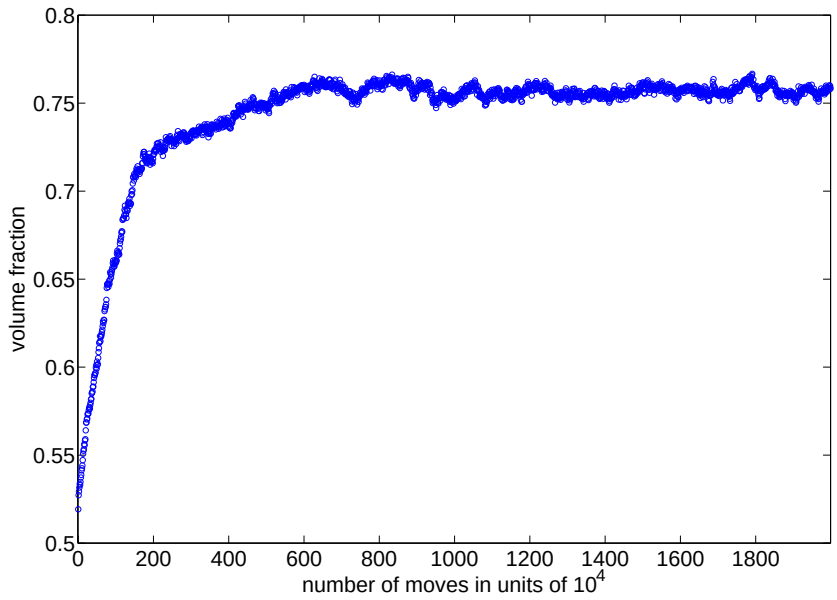

FIG. 34: Plot of volume fraction versus number of moves, from an initial volume fraction of 0.5192, for 994 squares.

notion, which, as we shall see below, requires unusual care in the treatment of error analysis.

In summary, we have performed Markov chain Monte Carlo simulations on a two dimensional model of low pressure granular matter of the general Edwards probabilistic type [EO]. Our main result, superficially summarized in Fig. 40, is that in this model the standard deviation of the volume fraction decays to zero as the particle number increases, which indicates a well-defined random loose packing density for the model. This suggests that real granular matter exhibits sharply defined random loose packing; this could be verified by repeating sedimentation experiments [JSSSSA] at a range of physical dimensions. Our argument is only convincing to the extent that the confidence intervals in Fig. 40 are small and justified, which required a statistical treatment of the data unusual in the physics literature. We hope that our detailed error analysis may be useful in other contexts.

Analysis of simulations

We performed Markov chain Monte Carlo simulations on our granular model, which we now describe more precisely. We begin with a fixed number of unit edge squares contained in a large rectangular box B. A collection of squares is "allowed" if they do not overlap with positive area, their edges are parallel to those of the box B, and the lower edge of each square intersects either the floor of the box B or the upper edge of each of two other squares; see Fig. 30. Note that although the squares have continuous translational degrees of freedom in the horizontal direction, this is not in evidence in the vertical direction because of the stability condition: the squares inevitably appear at discrete horizontal "levels".

Markov chain simulations were performed as follows. In the rectangular container B a fixed number of squares are introduced in a simple "crystalline" configuration: squares are arranged equally spaced in horizontal rows, the spacing determined by a preassigned volume fraction ϕ, and with squares centered above the centers of the gaps in the row below it; see Fig. 31. The basic step in the simulation is the following. A square is chosen at random from the current configuration and all possible positions are determined to which it may be relocated and produce an allowed configuration. Note that if the chosen square supports a square above it then it can only be allowed a relatively small horizontal motion; otherwise it may be placed atop some pair of squares, or the floor. So the boundary of the configuration plays a crucial role in the ability of the chain to change the volume fraction. In any case the positions to which the chosen square may be moved constitute a union of intervals. A random point is selected from this union of intervals and the square is moved. The random movement of a random square is the basic element of the Markov chain. It is easy to see that this protocol is transitive and satisfies detailed balance, so the chain has the desired uniform probability distribution as its asymptotic state [NB]. See Fig. 32 for a configuration of 399 squares after 10^6 moves. Our interest is in random loose packing, which occurs in the top (bulk) layer of a granular pile, and we assume that the entirety of each of our configurations represents this top layer. We emphasize that our protocol is not particularly appropriate for studying other questions such as the statistical shape of the boundary of a granular pile,

or properties associated with high volume fraction, such as random close packing.

After a prescribed number of moves, a volume fraction is computed for the collection of squares as follows. Within horizontal level L_j, where $j = 0$ corresponds to the squares resting on the floor, the distances between the centers of neighboring squares is computed. (Such a distance is $1 + g$ where g is the gap between the squares.) Suppose that n_j of these neighboring distances are each less than 2, and that the sum of these distances in the level is s_j. At this point our procedure will be complicated by the desire to obtain information during the simulation about inhomogeneities in the collection, for later use in analyzing the approach to equilibrium. For this purpose we introduce a new parameter, p. For fixed $0 < p < 1$ we consider those levels, beginning from $j = 0$, for which n_j is at least $0.75p$ times the length of the box's floor. Suppose $L_{J(p)}$ is the highest level such that it, and all levels below it, satisfy the condition. We then assign the volume fraction

$$\phi(p) = \frac{\sum_{j=0}^{J(p)} n_j}{\sum_{j=0}^{J(p)} s_j} \tag{30}$$

to the assembly of squares. (The factor 0.75 represents the volume fraction we expect the box's floor to reach in equilibrium. Note that any two such calculations of volume fraction of the same configuration may only differ by a term proportional to the length of the boundary of the configuration, so any inhomogeneity is limited to this size.) Such a calculation of volume fraction was performed regularly, after approximately 10^6 moves, producing a time series of volume fractions ϕ_t for the given number of squares. (We suppress reference to the variable p for ease of reading. As will be seen later all our results correspond to the choice $p = 0.4$, so one can, without much loss, ignore other possibile values.) Variables ϕ_t and ϕ_{t+1} are highly dependent, but we can be guaranteed that if the series is long enough then the sample mean:

$$\frac{1}{N} \sum_{t=1}^{N} \phi_t \tag{31}$$

will be a good approximation to the true mean of the target (uniform) probability distribu-

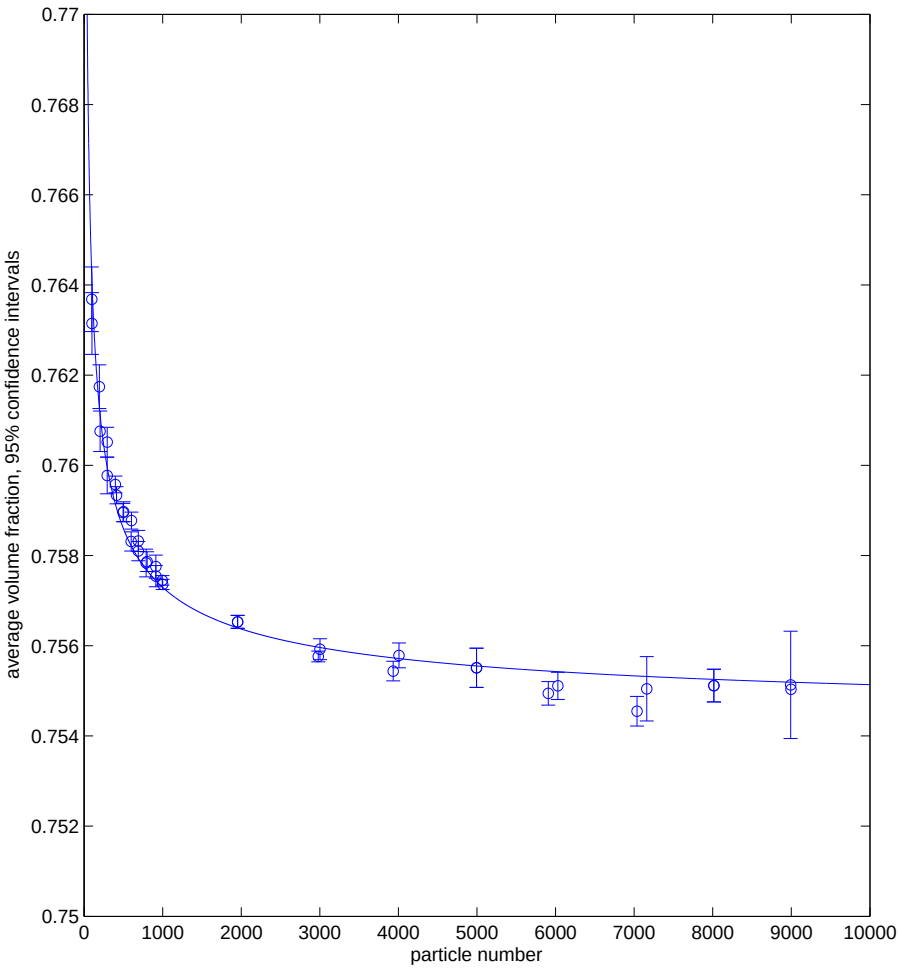

FIG. 35: Plot of the mean of the volume fraction versus number of squares, using f_2 for confidence intervals. The curve is $y = 0.7541 + 0.0998\, x^{-1/2}$.

tion for the given number of squares [KV].

We created such time series ϕ_t, each of about 10^4 terms (roughly 10^{10} elementary moves), using values $p = 0.2, 0.4, 0.6, 0.8$, on systems for the following numbers of squares: $100m$, and $1000m$, for $m = 1, 2, \ldots, 9$, with varying initial volume fractions. For each system we needed

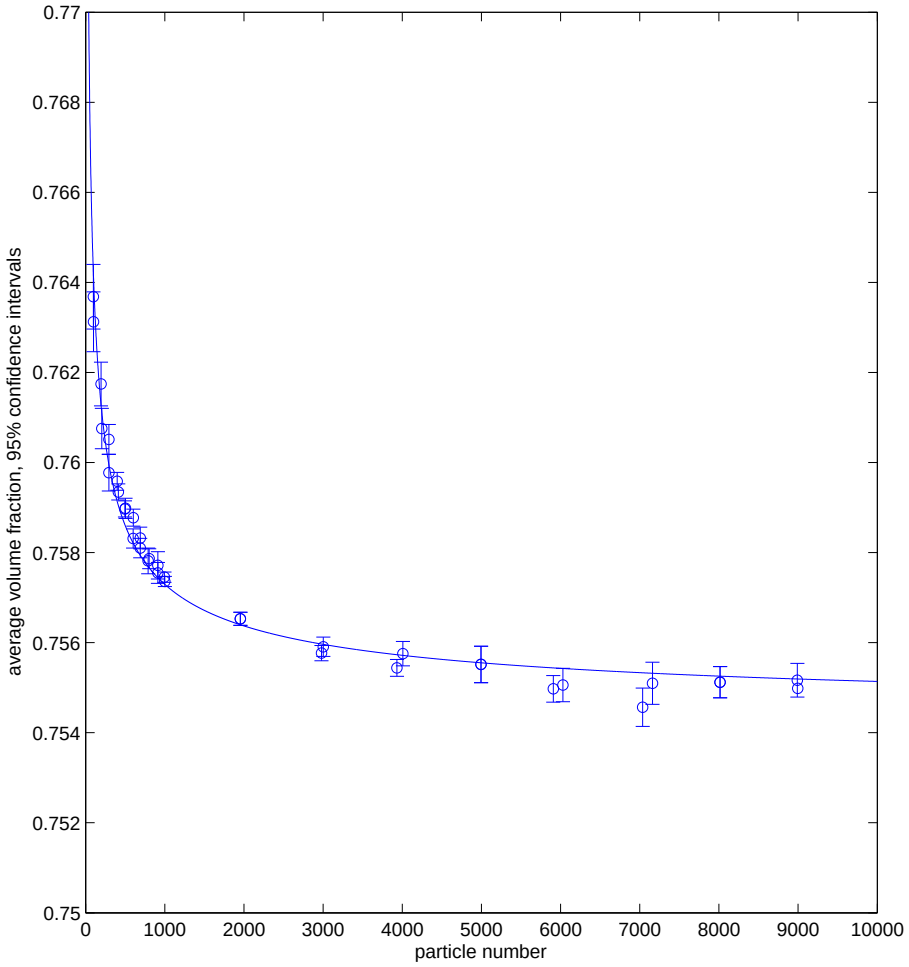

FIG. 36: Figure 12. Plot of the mean of the volume fraction versus number of squares, using f_1 for confidence intervals. The curve is $y = 0.7541 + 0.0998\,x^{-1/2}$.

to determine the initialization period – the number of moves necessary to reach equilibrium – and then the total number of moves to be performed. Both of these determinations were made based on variants of the (sample) autocorrelation function $f(k)$ of the time series

$\{\phi_t \mid 1 \le t \le T\}$ of volume fractions, defined for $1 \le k \le T$ by:

$$f(k) = \frac{1}{T-k+1} \sum_{t=1}^{T-k+1} (\phi_t - \bar{\phi})(\phi_{t+k} - \bar{\phi}), \tag{32}$$

where $\bar{\phi}$ is the mean of the series. This function is easily seen to give less reliable results as k increases, because of limited data, so it is usual to work with functions made from it as follows. One way to avoid difficulties is to restrict the domain of f; we define the "unbiased" autocorrelation $f_1(k)$ by $f_1(k) = f(k)$ for $k \le T/10$. Another variant we consider is the "biased" autocorrelation f_2, defined for all $1 \le k \le T$ by:

$$f_2(k) = \frac{1}{T} \sum_{t=1}^{T-k+1} (\phi_t - \bar{\phi})(\phi_{t+k} - \bar{\phi}), \tag{33}$$

which reduces the value of $f(k)$ for large k. (See pages 321-324 of Priestley [Pr] for a discussion of this biased variant.) We consider both variants of autocorrelation; to refer to either we use the term f_j.

With these autocorrelations we determined the smallest $k = k_z$ such that $f_j(k) = 0$. We then computed the sample standard deviation σ_{f_j} away from zero of f_j restricted to $k \ge k_z$, and defined k_I to be the smallest k such that $|f_j(k)| \le \sigma_{f_j}$; see Figs. 37-38. (For ease of reading we sometimes do not add reference to j to quantities derived using f_j.) This defined the initialization period. Then starting from ϕ_{k_I} we recomputed the autocorrelation $\tilde{f}_j$ and $\sigma_{\tilde{f}_j}$ and determined the mixing time, the smallest $k = k_M$ such that $|\tilde{f}_j(k)| \le \sigma_{\tilde{f}_j}$. k_M was interpreted as the separation k needed such that the random variables ϕ_t and ϕ_{t+k} are roughly independent for all $t \ge k$. (We performed the above using the different definitions of volume fraction corresponding to different values of p, allowing us to analyze different geometrical regions of the samples. For each system of squares we selected, for initialization and mixing times, the largest obtained as above corresponding to the various values of p, which was always that for $p = 0.2$, corresponding to the lowest layers of the configuration.)

Once we determined k_I and k_M we ran the series to ϕ_F, where $F = k_I + Tk_M$ for some $T \ge 20$. The values of k_I and k_M are given in Tables 1 and 2; the empirical means and

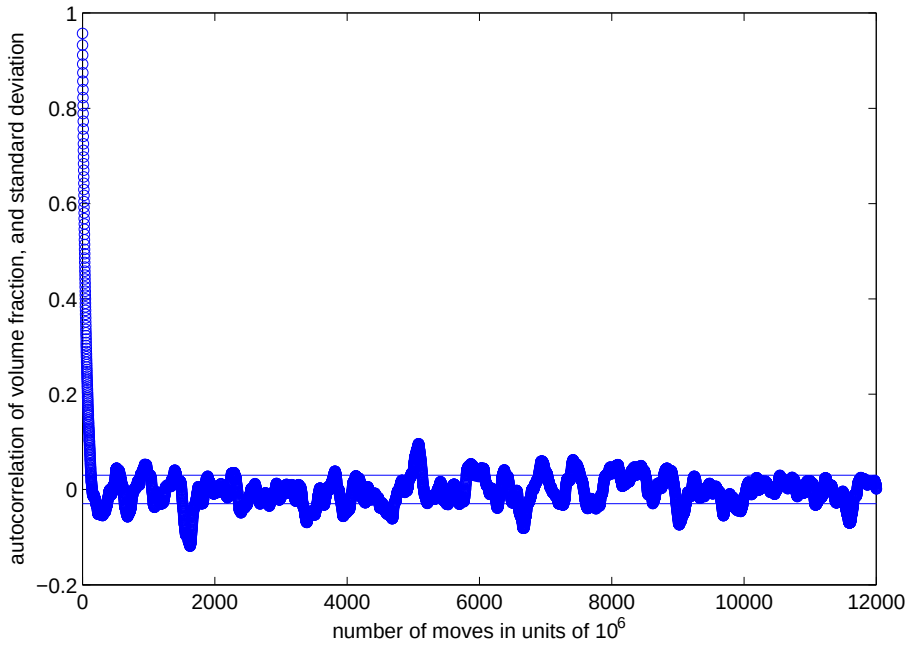

FIG. 37: Plot of biased autocorrelation (for 8000 particles) versus number of moves, with horizontal lines denoting one standard deviation away from zero.

standard deviations of volume fraction are given in Tables 3 and 4.

In all our results we use $p = 0.4$ to minimize the boundary effects presumably associated with small or large p. (With large p the lowest level may have undue influence on the volume fraction; with small p, the surface levels could have undue influence. Note that the arrangements of squares on the lowest level and the surface levels are not restricted by the arrangements of squares below and above them, respectively, and so the corresponding volume fractions are not bound to the logic, discussed above, which suggested that each level should equilibrate at a volume fraction of about .75. In spite of this, we found that using any series corresponding to p in the range $0.2 \leq p \leq 0.8$ generated a similar result.) For all systems the volume fraction quickly settles to the range 0.76 ± 0.01 and we can easily see from Table 4 that the empirical standard deviations decrease with increase of particle

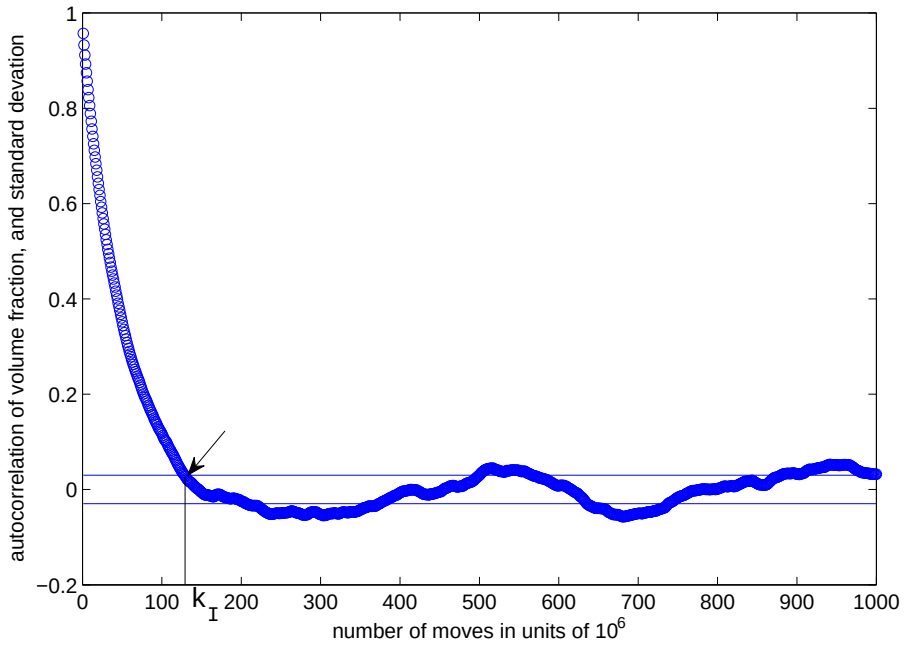

FIG. 38: Close-up of Fig. 37, with initialization time.

number. In Fig. 39 we plot the empirical standard deviations against particle number, and in Fig. 40 the data is replotted using logarithmic scales. In Fig. 40 we include the best least-squares fit to a straight line $y = ax + b$, obtaining $a = -0.5004$ and $b = -0.8052$. The corresponding curve is included in Fig. 39. Also included in both graphs are 90% confidence intervals for the true standard deviations, obtained as described in the next section, using f_2. (There was not enough data to obtain a confidence interval by this method for the system with 8995 squares.) The same data is reanalyzed in Figs. 41 and 42 with confidence intervals derived using f_1.

We use the close fit to the line in Figs. 40 or 42, corresponding to 33 data points in a range of particle number varying from 100 to 9000, to extend the agreement to arbitrarily large particle number, and therefore to claim that the standard deviation is zero in the infinite volume limit, or that there is a sharp value for the random loose packing density. The

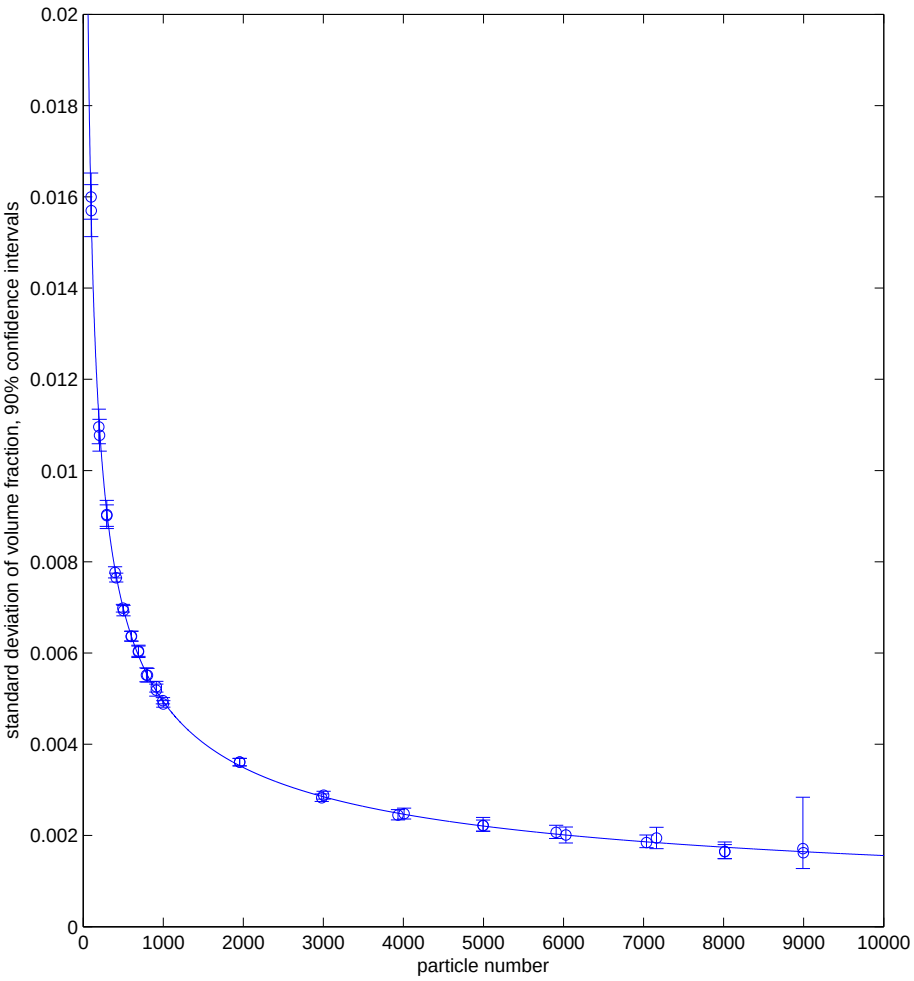

FIG. 39: Plot of the standard deviation of the volume fraction versus number of squares, using f_2 for confidence intervals.

argument is supported from the theoretical side by noting the closeness of the slopes in Figs. 40 and 42 to $-1/2$. A slope of $-1/2$ would be expected if it were true that an equilibrium configuration of N squares could be partitioned into similar subblocks which are roughly independent – a proposition which would not be surprising given a phase interpretation of

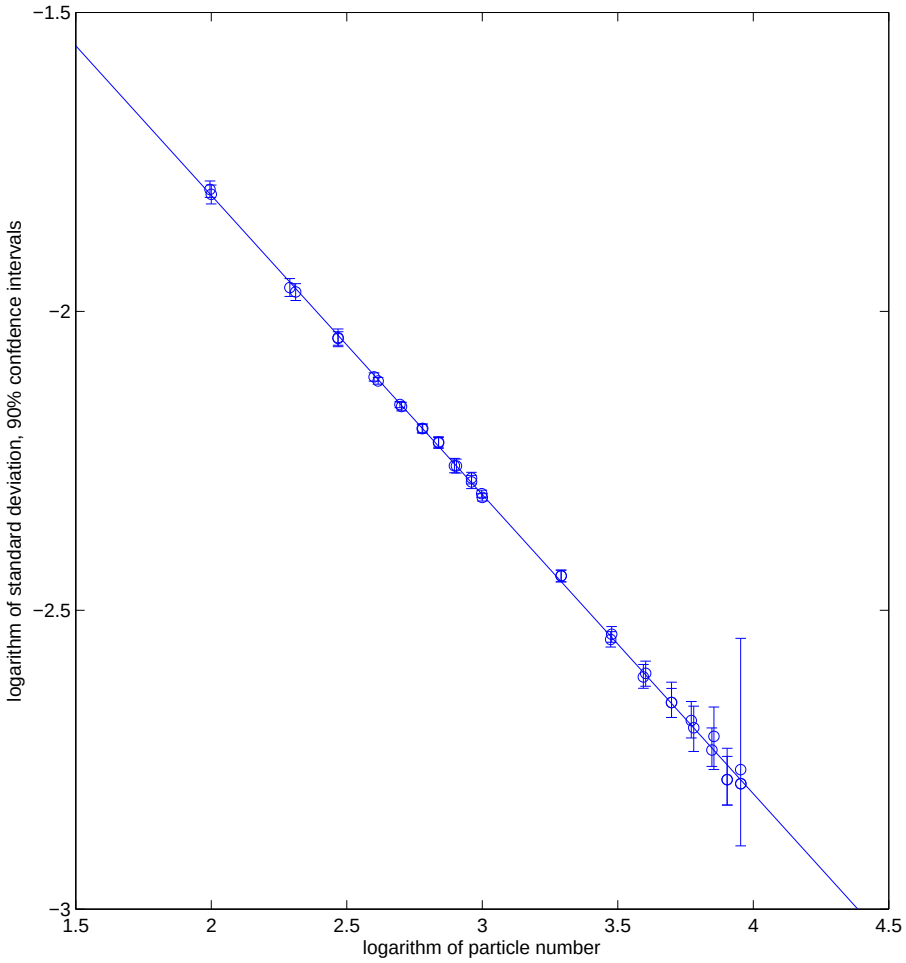

FIG. 40: Plot of the standard deviation of the volume fraction versus number of squares, using log scales and f_2 for confidence intervals. The line is $y = -0.5004\,x - 0.8052$.

granular media [Ra1]. Verifying such independence might be of some independent interest but would require much more data and much longer running times.

This is our main result, since it shows how to make sense of a perfectly well-defined random loose packing density within a granular model of the standard Edwards' form.

As to the actual asymptotic value of the volume fraction in the limit of large systems, we assume that our simulations suffer from a surface error proportional to $\sqrt{N}$ for a system of N squares. The least-squares fit of a function of form $A + B/\sqrt{N}$ to the data (see Figs. 35 and 36) yields $A = 0.7541$, and the good fit suggests an (asymptotic) random loose packing density in our granular model of about 0.754.

Our argument concerning asymptotically large systems depends on the fit of our standard deviation data to a curve, and the degree to which this fit is convincing depends on the confidence intervals associated with our simulations. In the next section we explain how we arrived at our confidence intervals.

Data analysis

A good source for common ways to analyze the data in Markov chain Monte Carlo simulation is chapter 3 in Newman and Barkema [NB]. We will give a more detailed analysis, following the paper by Geyer [Ge] in the series put together for this purpose by the statistics community [GR]. As will be seen, our argument is based on the precision of estimates of various statistical quantities, and necessitates a delicate treatment.

Our simulations produce a time series c_j of (dependent) random configurations of squares. From this we produce other series $g(c_j)$ using functions g on the space of possible configurations c, in particular the volume fraction $g_1(c) = \phi$ and $g_2(c) = (\phi - K)^2$ for constant K.

We use the common method of batch means. As described in the previous section, we first determine an initialization time k_I and a mixing time k_M for our series c_j from autocorrelations. After removing the initialization portion of the series, we break up the remaining W terms of the series into $w \geq 2$ equal size consecutive batches (subintervals), each of the same length W/w, discarding the last few terms from the series if w does not divide W evenly.

It should be emphasized that rarely, if ever, are conclusions drawn from a finite number of Monte Carlo simulations a literal proof of anything interesting. We are going to obtain confidence intervals (using the Student's t-test [St]) for the mean and standard deviation

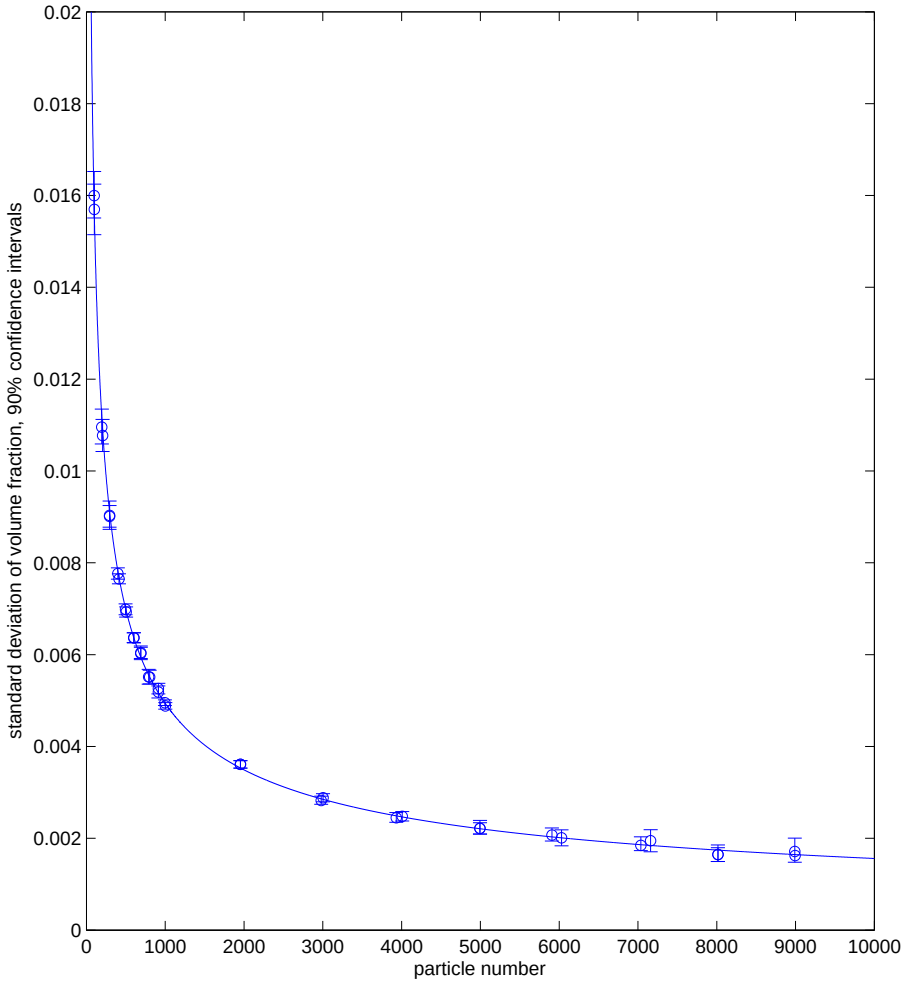

FIG. 41: Plot of the standard deviation of the volume fraction versus number of squares, using f_1 for confidence intervals.

of the volume fraction of our systems of fixed particle number. The t-test's results would be mathematically rigorous if in our simulations we had performed infinitely many moves; of course this is impossible, so we will try to make a convincing case that we have enough data to give reliable results. Ultimately, this is the most sensitive point in our argument.

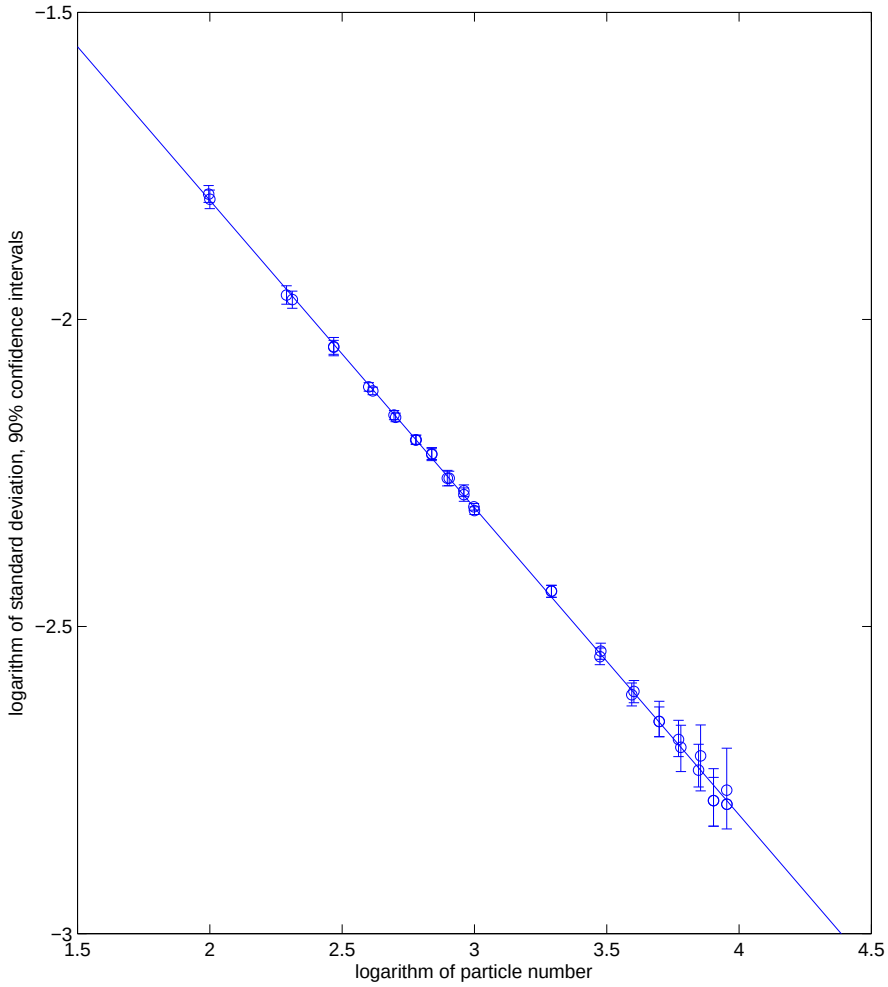

FIG. 42: Plot of the standard deviation of the volume fraction versus number of squares, using log scales and f_1 for confidence intervals. The line is $y = -0.5003\,x - 0.8055$.

Assume fixed some function g, and denote the true mean of $g(c)$ by μ_g. Assume, temporarily, that enough moves have been taken for the t-test to be reliable. (We will come back to this assumption below.) With the notation $\overline{g(c)}$ for the empirical average $(1/w)\sum_k \langle g(c)\rangle_k$

of $g(c)$, where $\langle g(c)\rangle_k$ is the empirical average of the k^{th} batch, the random variable:

$$\frac{\overline{g(c)} - \mu_g}{\sqrt{\frac{1}{w(w-1)}\sum_k (\langle g(c)\rangle_k - \overline{g(c)})^2}} \tag{34}$$

approximates a t-distribution, allowing one to compute confidence intervals for μ_g.

The above outline explains how (given the validity of the t-test) we could compute confidence intervals for the mean value of the volume fraction for the time series associated with our simulations for fixed numbers of squares. A small variation allows us to give confidence intervals for the standard deviations of these variables, as follows.

Denote the true standard deviation of $g(c)$ by σ_g. Using conditioning,

$$\begin{aligned} \Pr(\mu_g \in I \cap \sigma_g \in J) &= \Pr(\mu_g \in I)\Pr(\sigma_g \in J \mid \mu_g \in I) \\ &= \Pr(\mu_g \in I)\sum_i \Pr(\sigma_g \in J \mid \mu_g \in I_i)\Pr(\mu_g \in I_i \mid \mu_g \in I), \end{aligned} \tag{35}$$

where $\{I_i\}$ is a partition of I. We have discussed how to obtain I so that the factor $\Pr(\mu_g \in I)$ is at least 0.95. We now want to obtain J so that the factor $\Pr(\sigma_g \in J \mid \mu_g \in I)$ is also at least 0.95, and therefore $\Pr(\mu_g \in I \cap \sigma_g \in J)$ is at least $(0.95)(0.95) > 0.90$.

Consider, for each constant K, the random variable

$$\Sigma_K = \sqrt{(1/w)\sum_j [\langle g(c)\rangle_j - K]^2}. \tag{36}$$

Using (34) with $(g(c)-K)^2$ playing the role of $g(c)$, we can obtain a 95% confidence interval for the mean of Σ_K^2, which we translate into a 95% confidence interval J_K for the mean of Σ_K. Assume the partition so fine that within the desired precision $J_K = J_i$ only depends on i, where $K \in I_i$. Note that if $K = \mu_g$, then the random variable Σ_K has as its mean the standard deviation σ_g. So if we let $J = \cup_i J_i$, then $\Pr(\sigma_g \in J \mid \mu_g \in I_i) > 0.95$ for all i, and therefore $\Pr(\sigma_g \in J \mid \mu_g \in I) > 0.95$. In practice the union $J = \cup_i J_i$ is easy to compute.

In the above arguments we have assumed that enough moves have been taken to justify the t-test, which has independence and normality assumptions which are not strictly satisfied in

our situation. We now consider how to deal with this situation. Some guidance concerning independence can be obtained from the following toy model.

Assume that for the time series of the simulation one can determine some number k_M, perhaps but not necessarily derived as above from the autocorrelation $f(k)$, such that variables ϕ_i and ϕ_{i+k} in the time series are roughly independent if $k \geq k_M$. We model this transition between independent random variables as follows.

Let T and M be nonnegative (integer) constants. For $0 \leq t \leq T$ and $1 \leq m \leq M-1$ we first define independent, identically distributed random variables X_{tM} and from these define:

$$X_{tM+m} = \Big(1 - \frac{m}{M}\Big) X_{tM} + \frac{m}{M} X_{(t+1)M}, \tag{37}$$

together defining X_t for $0 \leq t \leq TM-1$. Note that variables X_t and X_{t+m} are independent for $m \geq 2M-1$.

A simple calculation shows that:

$$\sum_{m=0}^{M-1} X_{tM+m} = \Big(\frac{M+1}{2}\Big) X_{tM} + \Big(\frac{M-1}{2}\Big) X_{(t+1)M}. \tag{38}$$

Then another simple calculation shows that:

$$S_T \equiv \frac{1}{TM} \sum_{m=0}^{TM-1} X_m = \frac{1}{T}\Big[\sum_{t=1}^{T-1} X_{tM} + \frac{1}{2}(X_0 + X_{TM}) + \frac{1}{2M}(X_0 - X_{TM})\Big]. \tag{39}$$

In other words S_T is the mean of roughly K *independent* variables.

Returning to the question of the assumptions in the t-test, the toy model suggests that the independence assumption is easily satisfied. The normality assumption is usually taken as the more serious [Ge]. But we note from [DL] that the t-test is quite robust with respect to the normality assumption. Although the robustness of the t-test is well known and is generally relied on, in practice one still has to pick specific batch partitions in a reliable way. This is not covered in [Ge]. We arrived at a standard for batches of length 10 times

mixing time for our series as follows. In outline, we use mixing times as computed above to standardize comparison between our systems with different particle number. Those for which our runs constituted at least 800 mixing times are assumed to give accurate values for the mean volume fraction. Various initial segments of these runs are then used, with various choices of batch partitions, to see which choices (if any) give reliable results for confidence intervals. Batches of size 10 mixing times proved reliable even for initial segments in the range of 20-100 mixing times, so this choice was then used for all systems. We emphasize that we are using this method to determine a minimum reliable batch size on the sequence of configurations, and then we apply this to the time series ϕ_t as well the time series $[\phi_t - K]^2$. We now give more details.

For most of the systems of particle numbers 100-900 we have over 500 mixing times worth of data, yet for some of the systems of particle numbers 1000-9000 we have, for practical reasons, less than one tenth that depth of data. We want to choose a fixed multiple of mixing time as batch length for all of our batches. To decide what range of mixing times will be reliable we used various portions of the data from those of our longest runs, and then applied the conclusions we drew to the other 3/4 of the runs.

More specifically, we treat as "reliable" the empirical volume fraction of the longest runs, those of length at least 800 times mixing time. We then consider a range of batch partitions of these systems to see which ones give accurate t-test results. We are looking for 95% confidence intervals, so we expect such intervals to contain the true volume fraction 95% of the time; since the true volume fraction is unknown we instead check how frequently the intervals contain the empirical volume fraction, which for the longer runs we have assumed is reliable. We do this for each of the runs of length 800 or more times mixing time. The results on these systems are the following.

For each of our longer runs (of at least 800 mixing times), we considered various initial portions of the run in each of six ranges of mixing times: 20-100, 100-200, 300-400, 400-500, and 500-600. For each of these truncated runs we considered batch partitions of the data into equal size batches of a variety of multiples of mixing time: 1-5, 6-10, 11-15, 16-20, 21-30, 31-40 and 41-50. For each size run and for each batch size we computed a 95%

confidence interval for the true mean of the volume fraction, and determined whether or not the confidence interval covers the sample mean for the full run (which we are assuming is interchangeable with the true mean). The fraction of the more than 200 cases in each category for which the sample mean lies within the confidence interval is recorded in Table 5. From this it appears that using batches of size 1-5 mixing times would be unreliable, but that size 10 times mixing times would be reliable. (Table 5 is based on mixing times obtained using the autocorrelation f_2. Table 6 is similar, using the autocorrelation f_1, and again justifies the use of batches of size 10 times mixing time.)

We then used batches of size 10 times mixing times to obtain 95% confidence intervals for the true mean of all the systems, obtaining the results tabulated in Table 3 and included in Figs. 35 and 36.

Finally, we applied the above batch criterion to obtain 90% confidence intervals for the true standard deviation of all our systems, using the method described earlier in this section. The results are in Table 4 and in Figs. 39 – 42.

Table 1

Basics

(using unbiased autocorrelation f_1)

number of squares in packing	number of moves in units of 10^9	step size in units of 10^6 moves	k_I (init. time) in units of step size using f_1	k_M (mixing time) in units of step size using f_1	run length in units of mixing time using f_1
99	0.4	0.2	1	1	1998
100	0.4	0.2	1	1	1998
195	0.4	0.2	1	1	1998
205	0.4	0.2	1	1	1998
294	0.4	0.2	5	5	398
294	0.4	0.2	4	4	498
399	2	0.2	10	10	998
413	2	0.2	9	9	1110
497	2	0.2	17	17	587
504	2	0.2	17	17	587
600	2	0.2	12	12	832
603	2	0.2	23	23	433
690	2	0.2	14	14	713
690	2	0.2	20	20	498
790	2	0.2	43	43	231
803	2	0.2	14	14	713
913	2	0.2	34	34	293
913	2	0.2	75	73	135
996	12	1	13	13	953
1001	12	1	16	16	755
1955	12	1	38	38	318
2980	12	1	44	44	277
3003	12	1	51	53	234
3933	12	1	64	63	193
4008	12	1	99	75	158
4995	12	1	193	174	68
5908	12	1	163	96	125
6030	12	1	143	143	84
7037	12	1	223	261	46
7161	12	1	222	181	48
8015	12	1	132	120	100
8991	12	1	283	287	41
8995	12	1	632	631	18

Table 2

Basics

(using biased autocorrelation f_2)

number of squares in packing	number of moves in units of 10^9	step size in units of 10^6 moves	k_I (init. time) in units of step size using f_2	k_M (mixing time) in units of step size using f_2	run length in units of mixing time using f_2
99	0.4	0.2	1	1	1998
100	0.4	0.2	3	2	998
195	0.4	0.2	1	1	1998
205	0.4	0.2	1	1	1998
294	0.4	0.2	5	5	398
294	0.4	0.2	4	4	498
399	2	0.2	12	12	832
413	2	0.2	11	11	908
497	2	0.2	20	20	498
504	2	0.2	19	19	525
600	2	0.2	12	12	832
603	2	0.2	23	23	433
690	2	0.2	14	15	665
690	2	0.2	25	20	498
790	2	0.2	43	44	226
803	2	0.2	15	14	713
913	2	0.2	36	38	262
913	2	0.2	77	75	132
996	12	1	18	18	687
1001	12	1	16	16	755
1955	12	1	38	38	318
2980	12	1	56	56	218
3003	12	1	51	54	230
3933	12	1	76	78	156
4008	12	1	101	88	135
4995	12	1	191	177	67
5908	12	1	179	100	120
6030	12	1	139	151	80
7037	12	1	220	290	41
7161	12	1	199	186	47
8015	12	1	131	126	95
8991	12	1	282	355	33
8995	12	1	565	609	19

Table 3

Volume Fraction

number of squares in packing	sample value	end points of 95% confidence interval for true value, using f_1	end points of 95% confidence interval for true value, using f_2
99	0.7637	0.7637±0.0007	0.7637±0.0007
100	0.7631	0.7631±0.0007	0.7631±0.0007
195	0.7617	0.7617±0.0005	0.7617±0.0005
205	0.7608	0.7608±0.0005	0.7608±0.0005
294	0.7605	0.7605±0.0004	0.7605±0.0004
294	0.7598	0.7598±0.0004	0.7598±0.0004
399	0.7596	0.7596±0.0002	0.7596±0.0002
413	0.7593	0.7593±0.0002	0.7593±0.0002
497	0.7590	0.7590±0.0002	0.7590±0.0002
504	0.7590	0.7590±0.0003	0.7590±0.0002
600	0.7583	0.7583±0.0002	0.7583±0.0002
603	0.7588	0.7588±0.0002	0.7588±0.0002
690	0.7581	0.7581±0.0002	0.7581±0.0002
690	0.7583	0.7583±0.0003	0.7583±0.0003
790	0.7578	0.7578±0.0003	0.7578±0.0003
803	0.7579	0.7579±0.0002	0.7579±0.0002
913	0.7575	0.7575±0.0002	0.7575±0.0003
913	0.7578	0.7578±0.0003	0.7578±0.0003
996	0.7575	0.7575±0.0001	0.7575±0.0001
1001	0.7574	0.7574±0.0001	0.7574±0.0001
1955	0.7565	0.7565±0.0002	0.7565±0.0002
2980	0.7558	0.7558±0.0002	0.7558±0.0001
3003	0.7559	0.7559±0.0002	0.7559±0.0003
3933	0.7554	0.7554±0.0002	0.7554±0.0002
4008	0.7558	0.7558±0.0003	0.7558±0.0003
4995	0.7555	0.7555±0.0004	0.7555±0.0005
5908	0.7549	0.7549±0.0003	0.7549±0.0003
6030	0.7551	0.7551±0.0004	0.7551±0.0003
7037	0.7545	0.7545±0.0005	0.7545±0.0004
7161	0.7550	0.7550±0.0005	0.7550±0.0007
8015	0.7551	0.7551±0.0004	0.7551±0.0004
8991	0.7551	0.7551±0.0004	0.7551±0.0012
8995	0.7550	none	none

Table 4

Standard deviation of volume fraction

number of squares in packing	sample value	end points of 90% confidence interval for true value, using f_1	end points of 90% confidence interval for true value, using f_2
99	0.0160	0.0160±0.0005	0.0160±0.0005
100	0.0157	0.0157±0.0006	0.0157±0.0006
195	0.0110	0.0110±0.0004	0.0110±0.0004
205	0.0108	0.0108±0.0004	0.0108±0.0004
294	0.0090	0.0090±0.0003	0.0090±0.0003
294	0.0090	0.0090±0.0003	0.0090±0.0003
399	0.0078	0.0078±0.0001	0.0078±0.0002
413	0.0076	0.0077±0.0001	0.0077±0.0001
497	0.0070	0.0070±0.0001	0.0070±0.0001
504	0.0069	0.0069±0.0001	0.0069±0.0001
600	0.0064	0.0064±0.0001	0.0064±0.0001
603	0.0064	0.0064±0.0001	0.0064±0.0001
690	0.0060	0.0061±0.0002	0.0060±0.0001
690	0.0060	0.0060±0.0002	0.0060±0.0001
790	0.0055	0.0055±0.0002	0.0055±0.0002
803	0.0055	0.0055±0.0002	0.0055±0.0002
913	0.0052	0.0052±0.0002	0.0052±0.0002
913	0.0053	0.0053±0.0001	0.0053±0.0001
996	0.0050	0.0050±0.0001	0.0050±0.0001
1001	0.0049	0.0049±0.0001	0.0049±0.0001
1955	0.0036	0.0036±0.0001	0.0036±0.0001
2980	0.0028	0.0028±0.0001	0.0028±0.0001
3003	0.0029	0.0029±0.0001	0.0029±0.0001
3933	0.0024	0.0025±0.0001	0.0025±0.0001
4008	0.0025	0.0025±0.0001	0.0025±0.0002
4995	0.0022	0.0022±0.0002	0.0022±0.0002
5908	0.0021	0.0021±0.0002	0.0021±0.0002
6030	0.0020	0.0020±0.0002	0.0020±0.0002
7037	0.0018	0.0019±0.0002	0.0019±0.0002
7161	0.0019	0.0020±0.0003	0.0021±0.0004
8015	0.0016	0.0017±0.0002	0.0017±0.0002
8991	0.0017	0.0017±0.0003	0.0021±0.0008
8995	0.0016	none	none

Table 5

Fraction of times the given batch size gives acceptable confidence interval for given segment of total data of long runs, using unbiased autocorrelation f_1

		20-100 mixing times of total data	100-200 mixing times of total data	200-300 mixing times of total data	300-400 mixing times of total data	400-500 mixing times of total data	500-600 mixing times of total data
	1-5	0.0849	0.0867	0.1119	0.1191	0.1938	0.2082
number of	6-10	0.9410	0.9394	0.9830	1.0000	1.0000	1.0000
mixing	11-15	0.9648	0.9231	0.9656	1.0000	1.0000	1.0000
times	16-20	0.9524	0.9095	0.9777	0.9879	1.0000	1.0000
per batch	21-31	0.9650	0.9177	0.9673	1.0000	1.0000	1.0000
	31-40	0.9712	0.9042	0.9643	1.0000	1.0000	0.9957
	41-51	0.9375	0.8869	0.9402	0.9511	0.9783	0.9402

Table 6

Fraction of times the given batch size gives acceptable confidence interval for given segment of total data of long runs, using biased autocorrelation f_2

		20-100 mixing times of total data	100-200 mixing times of total data	200-300 mixing times of total data	300-400 mixing times of total data	400-500 mixing times of total data	500-600 mixing times of total data
	1-5	0.0833	0.0924	0.1182	0.1259	0.2006	0.2326
number of	6-10	0.9245	0.9784	0.9805	0.9552	0.9762	1.0000
mixing	11-15	0.9107	0.9451	0.9607	0.9524	0.9707	1.0000
times	16-20	0.9728	0.9212	0.9745	0.9493	0.9655	1.0000
per batch	21-31	0.9486	0.9059	0.9592	0.9547	0.9744	1.0000
	31-40	0.9780	0.9190	0.9592	0.9704	0.9852	1.0000
	41-51	0.9000	0.8639	0.9441	0.9565	0.9814	1.0000

X. CONCLUSION

We have examined in detail four models of nonequilibrium (soft) matter, as well as an equilibrium model of quasicrystals; in all these models we find abrupt changes in behavior arising at certain densities. In the granular model of sections III and V, we find a phase transition at high density corresponding to the onset of crystalline structure. We associate this transition with the physical phenomenon of random close packing [Ra1], which has been shown in experiments to correspond to the appearance of bulk-sized crystals [ND, SCM]. (There are ongoing experiments to determine whether random close packing is a phase transition in a precise sense.) The model of polymers/crumpled wires of section VI exhibits a similar transition at high density, this time to a nematically ordered phase. For crumpled wires we do not know of experimental evidence of such a transition. (The author is involved in an ongoing experiment to determine whether such a transition exists.)

The granular model of section VII exhibits a phase transition to a phase which is "solid" in the sense that it resists shear. More precisely, the linear volume response to an infinitesimal shear has a change in character at a certain density ϕ_c, such that for densities below ϕ_c a small shear causes an increase in density, while for densities above ϕ_c produces the opposite effect. The transition through these regimes in the model is sharp, in the precise sense of a second order phase transition. Dilatancy onset, represented in the model by ϕ_c, has been experimentally associated with a phase transition in [SNRS, MSRSS]. Thus granular matter may exhibit two distinct phase transitions: one in which there is a sharp change in response to shearing (at dilatancy onset), and one in which bulk-size crystals start to appear (at random close packing). In contrast with the models discussed in the previous paragraph, the transition at dilatancy onset does not seem to be associated with any obvious geometric ordering.

The model of quasicrystals of section VIII, unlike the other models in this paper, is a true "equilibrium" model. (The model is a more realistic generalization of the models of [LP, KR].) While the equilibrium theory of fluid-solid phase transitions often emphasizes the crystalline symmetry of solids, our model shows a transition to a solid phase with an

unusual "quasicrystalline" structure. The transition, like the fluid-solid transition of typical equilibrium solids, is first order. The solid phase has crystalline spatial order (evidenced by the particles preferentially populating a certain sublattice), and quasicrystalline particle-type order. In particular, as with true quasicrystals, the model (at high density) does not have translational particle type symmetry.

The granular model of section IX, unlike the rest of the models of this paper, is not meant to show a phase transition in the traditional sense. However, the model does show an abrupt change at a certain density – in the sense that bulk random configurations do not exist below this density. We associate this abrupt change with the physical phenomenon of random loose packing [SK]. In particular we show that there is no intrinsic lower bound on the variance of the lowest possible density achievable by bulk random samples in the model. Thus the model shows how Edwards modeling [EO] allows for a precise definition of random loose packing. (Such modeling is only appropriate for carefully prepared granular samples [SNRS].)

In sum, following the lead of de Gennes [dG1, dG2] and Edwards [EO], we have employed ideas from equilibrium statistical mechanics to try to understand nonequilibrium (soft) matter. Our models provide theoretical support for understanding certain physical phenomena in soft matter (like random close packing and dilatancy onset) as phase transitions, in the traditional sense of equilibrium statistical mechanics. It would be very desireable to expand on this understanding – for example to see if random loose packing can be understood as a phase transition, or if crumpled wires really exhibit a phase transition to a "layered" state at high density.

Bibliography

[AF] L. Angelani and G. Foffi, Configurational entropy of hard spheres, J. Phys.: Condens. Matter 19 256207 (2007)

[AH] B.J. Alder and W.G. Hoover, Numerical Statistical Mechanics, in Physics of Simple Liquids, edited by H.N.V. Temperley, J.S. Rowlinson and G.S. Rushbrooke, (John Wiley, New York, 1968) 79-113

[An] P. W. Anderson, Basic Notions of Condensed Matter Physics, Benjamin/Cummings, Menlo Park, 1984, chapter 2

[AR1] D. Aristoff and C. Radin, First order phase transition of a long polymer chain, J. Phys. A: Math. Theor. 44 (2011) 065004

[AR2] D. Aristoff and C. Radin, Random close packing in a granular model, J. Math. Phys. 51, 113302 (2010)

[AR3] D. Aristoff and C. Radin, Layering in crumpled sheets, Europhys. Lett. 91 (2010) 56003

[AR4] D. Aristoff and C. Radin, Random loose packing in granular matter, J. Stat. Phys. (2009) 135: 1-23

[AR5] D. Aristoff and C. Radin, Dilatancy transition in a granular model, J. Stat. Phys. (to appear) arXiv:1005.1907

[AR6] D. Aristoff and C. Radin, First order phase transition in a model of quasicrystals, arXiv:1102.1982

[AS] E. Aharonov and D. Sparks, Rigidity phase transition in granular packings, Phys. Rev. E 60, 6890 (1999)

[Bar] Barker, J.A., Lattice Theories of the Liquid State, Macmillan, New York, 1963

[Bax] R. J. Baxter, "Exactly Solved Models in Statistical Mechanics" Academic Press, 1982

[BC] D. Bi and B. Chakraborty, Rheology of granular materials: dynamics in a stress

landscape, Phil. Trans. R. Soc. 367, 5073 (2009)

[BE] R. Blumenfeld and S.F. Edwards, On granular stress statistics: compactivity, angoricity, and some open issues, J. Phys. Chem. B 113, 3981 (2009)

[BK] L. Boué and E. Katzav, Folding of flexible rods confined in 2D space, Europhysics Lett. 80, (2007) 54002

[BKLS] A. Barrat, J. Kurchan, V. Loreto and M. Sellitto, Edwards' Measures for Powders and Glasses, Phys. Rev. Lett. 85, 5034 (2000)

[CD] S. Chatterjee and P. Diaconis, Estimating and understanding exponential random graph models, arXiv:1102.2650

[Ch] B. Chakraborty, Statistical ensemble approach to stress transmission in granular packings, Soft Matter 6, 2884 (2010)

[CH] A. Coniglio and H.J. Herrmann, Phase transitions in granular packings, Physica A 225, 1 (1996)

[dG1] P.G. de Gennes, Scaling Concepts in Polymer Physics (Cornell University Press, Ithaca) 1979

[dG2] P.G. de Gennes, Granular matter: a tentative view, Rev. Mod. Phys. 71 (1999) S374-S382

[dGP] de Gennes, P.G. and Prost, J., The Physics of Liquid Crystals, Oxford: Clarendon Press, 1993

[DL] P. Diaconis and E. Lehmann, Journal of the American Statistical Association, March 1, 2008, 103 (481): 16-19.

[EG] S.F. Edwards and D.V. Grinev, Granular materials: towards a statistical mechanics of jammed configurations, Adv. Phys. 51, 1669 (2002)

[EO] S.F. Edwards and R.B.S. Oakeshott, Physica A, 157 (1989) 1080

[FAL] H.C.M. Fernandes, J.J. Arenson and Y. Levin, Monte Carlo simulations of two-dimensional hard core lattice gases, J. Chem. Phys. 126 (2007) 114508

[Fl] P.J. Flory, Statistical Mechanics of Chain Molecules (Hanser Publishers, Munich) 1989

[Fr] D. Frenkel, Computer simulation of hard-core models for liquid crystals, Mol. Phys. 60 (1): 1-20 (1987)

[Ga] M. Gardner, Extraordinary nonperiodic tiling that enriches the theory of tiles, Sci. Am. (USA) 236 (1977) 110-119.

[GBH] G-J. Gao, J. Blawzdziewicz and C.S. O'Hern, Frequency distribution of mechanically stable disk packings, Phys. Rev. E 74 (2006) 061304

[Ge] C.J. Geyer, Practical Markov chain Monte Carlo., Stat. Sci. 7, 473483 (1992)

[Gr] R.B. Griffiths, Rigorous Results and Theorems, from Phase Transitions and Critical Phenomena, vol. 1, ed. C. Domb and M.S. Green (Academic Press, New York, 1972)

[GR] A. Gelman and D.B. Rubin, Inference from iterative simulation using multiple sequences, Stat. Sci. 7 (1992) 457-511

[GS] B. Grünbaum and G.C. Shephard, Tilings and Patterns, Freeman, New York, 1986, page 593

[GZ] H.-O. Georgii and V. Zagrebnov, Entropy-driven phase transition in multitype lattice gas models, J. Stat. Phys. 102 (2001) 35-67

[Ha] T. C. Hales, A proof of the Kepler conjecture, Annals of Mathematics, Second Series 162 (3): 10651185 (2005)

[He] H.J. Herrmann, Statistical models for granular materials, Physica A **263**, 51 (1999)

[HHB] W.G. Hoover, C.G. Hoover and M.N. Bannerman, Single-Speed Molecular Dynamics of Hard Parallel Squares and Cubes, J. Stat. Phys. 136, 715 (2009)

[Ho] W.G. Hoover, Bounds on the configurational integral for hard parallel squares and cubes, J. Chem. Phys. 43 (1965) 371-374

[HR] Hoover, W.G and Ree, F.H., Melting transition and communal entropy for hard spheres, J. Chem. Phys. 49, 3609 - 3617 (1968)

[Ja] J.L. Jacobsen, Unbiased sampling of globular lattice proteins in three dimensions, Phys. Rev. Lett. 100, 118102 (2008)

[JK] J.L. Jacobsen and J. Kondev, Conformal field theory of the Flory model of polymer melting, Phys. Rev. E 69, 066108 (2004)

[JSSSSA] M. Jerkins, M. Schröter, H.L. Swinney, T.J. Senden, M. Saadatfar and T. Aste, Onset of mechanical stability in random packings of frictional particles, Phys. Rev. Lett. 101 (2008) 018301

[KR] H. Koch and C. Radin, Modelling quasicrystals at positive temperature, J. Stat. Phys., 138 (2010), 465-475

[KV] C. Kipnis and S.R.S. Varadhan, Central limit theorem for additive functionals of reversible Markov processes and applications to simple exclusions, Comm. Math. Phys. 104, 1-19 (1986)

[LL] L.D. Landau and E.M. Lifshitz, Statistical Physics, Pergamon Press, London 1958, trans. E. Peierls and R.F. Peierls, Chapter XIV

[LMNS] J.L. Lebowitz, A. Mazel, P. Nielaba and L. Samaj, Ordering and demixing transition in multicomponent Widom-Rowlinson models, Phys. Rev. E 52 (1995) 5985-5996

[Lo] H. Löwen, Fun with hard spheres, pages 295-331 in Statistical physics and spatial statistics: the art of analyzing and modeling spatial structures and pattern formation, ed. K.R. Mecke and D. Stoyen, Lecture notes in physics No. 554, Springer-Verlag, Berlin, 2000

[LP] L. Leuzzi, G. Parisi, Thermodynamics of a tiling model, J. Phys. A 33 (2000) 4215-4225

[LS] D. Levine and P.J. Steinhardt, Quasicrystals: a new class of ordered structures, Phys. Rev. Lett. 53 (1984) 2477-2480

[Ma] I.R. MacDonald, NpT-ensemble Monte Carlo calculations for binary liquid mixtures, Molecular Physics Vol. 100, 95 (2002)

[MP] R. Monasson and O. Pouliquen, Entropy of particle packings: an illustration on a toy model, Physica A 236 (1997) 395-410

[MRRTT] N. Metropolis, A.W. Rosenbluth, M.N. Rosenbluth, A.H. Teller, E. Teller, Equations of state calculations by fast computing machines, J. Chem. Phys. 21 (1953): 10871092

[MSRSS] J.-F. Mtayer, D.J. Suntrup III, C. Radin, H.L. Swinney and M. Schrter, Shearing of frictional sphere packings, Europhys. Lett. 93, 6 (2011) 64003

[NB] M.E.J. Newman and G.T. Barkema, Monte Carlo methods in statistical physics, (Oxford University Press, 1999)

[ND] M. Nicolas, P. Duru and O. Pouliquen, Compaction of a granular material under cyclic shear, Eur. Phys. J. E 3 (2000) 309-314

[NKBJN] E.R. Nowak, J.B. Knight, E. Ben-Naim, H.M. Jaeger and S.R. Nagel, Density fluctuations in vibrated granular materials, Phys. Rev. E 57, 1971 (1998)

[OFJK] R. Oberdorf, A. Ferguson, J.L. Jacobsen, and J. Kondev, Secondary structures in long compact polymers, Phys. Rev. E 74 (2006) 051801

[OL] G.Y. Onoda and E.G. Liniger, Random loose packings of uniform spheres and the dilatancy onset Phys. Rev. Lett. 64 (1990) 2727-2730

[On] L. Onsager, The effects of shape on the interaction of colloidal particles, Ann. N.Y. Acad. Sci. 51 (4): 627 (1949)

[PC] M. Pica Ciamarra, A. Coniglio, Random very loose packings, Phys. Rev. Lett. 101, 128001 (2008)

[PLR] M. Piccioni, V. Loreto, and S. Roux, Criticality of the "critical state" of granular media: Dilatancy angle in the Tetris model, Phys. Rev. E 61, 2813 (2000)

[PN] J. Park and M.E.J. Newman, Statistical mechanics of networks, Phys. Rev. E 70, 066117 (2004)

[Pr] M.B. Priestley, Spectral analysis and time series, vol.1, (Academic Press, New York, 1981)

[PR] M. Parrinello and A. Rahman, Strain fluctuations and elastic constants, J. Chem. Phys. 76, 2662 (1982)

[Ra1] C. Radin, Random close packing of granular matter, J. Stat. Phys. 131 (2008), 567-573

[Ra2] C. Radin, Symmetries of quasicrystals, J. Stat. Phys. 95 (1999), 827-833.

[RDXRC] M.A. Rutgers, J.H. Dunsmuir, J.-Z. Xue, W.B. Russel, P.M. Chaikin, Measurement of the hard-sphere equation of state using screened charged polystyrene colloids, Phys. Rev. B 53 9 (1996), 5043-5046

[Re] O. Reynolds, On the dilatancy of media composed of rigid particles in contact, with experimental illustrations, Phil. Mag. Series 5 20 (1885) 469-481

[RE] Z. Rotman and E. Eisenberg, A finite-temperature liquid-quasicrystal transition in a lattice model, Phys. Rev. E, 83, 1 (2011) 011123

[RH] H. Reiss and A.D. Hammerich, Hard spheres: scaled particle theory and exact relations on the existence and structure of the fluid/solid phase transition., J. Chem. Phys. 90, 6252-6260 (1986)

[RN] K.K. Rao and P.R. Nott, An Introduction to Granular Flow, Cambridge University Press, Cambridge, 2008

[Ru1] D. Ruelle, Statistical Mechanics: Rigorous Results, W.A. Benjamin, Inc., New York, New York (1969)

[Ru2] D. Ruelle, Thermodynamic Formalism, Addison-Wesley, New York, 1978, section 4.15

[SB] E. Sultan and A. Boudaoud, Statistics of Crumpled Paper, Phys. Rev. Lett., 96 (2006) 136103

[SBGC] D. Shechtman, I. Blech, D. Gratias and J.W. Cahn, Metallic phase with long-ranged orientational order and notranlational symmetry, Phys. Rev. Lett. 53 (1984) 1951-53

[Sc] G.D. Scott, Packing of spheres, Nature (London) 188 (1960) 908-909

[SCM] G.D. Scott, A.M. Charlesworth and M.K. Mak, On the random packing of spheres, J. Chem. Phys. 40, 611 (1964)

[SK] G.D. Scott and D.M. Kilgour, The density of random close packing of spheres, Brit. J. Appl. Phys. (J. Phys. D) 2, 863 (1969)

[SNRS] M. Schröter, S. Nägle, C. Radin and H.L. Swinney, Phase transition in a static granular system, Europhys. Lett. 78 (2007), 44004

[Sp] R. Speedy, The hard sphere glass transition, Mol. Phys. 95 (1998), 169-178

[St] Student [William Sealy Gosset], The probable error of a mean, Biometrika 6 (1): 125

[SWM] C. Song, P. Wang and H.A. Makse, A phase diagram for jammed matter, Nature 453 (2008) 629-632

[TH] H.-J. Tillemans and . J. Herrmann, Simulating deformations of granular solids under shear, Physica A **217**, 261 (1995)

[TR] Temperley, H.N.V., Rowlinson, J.S. and Rushbrooke, G.S., Physics of Simple Liquids, Wiley, New York, 1968

[TT] S. Torquato, T.M. Truskett and P.G. Debenedetti, Is random close packing of spheres well defined?, Phys. Rev. Lett. 84 (2000) 2064-2067

[vR] E.J. Janse van Rensburg, Monte Carlo Methods for the Self-Avoiding Walk, J. Phys. A 42 (2009) 323001

[Za] F. Zamponi, Packings close and loose, Nature 453 (2008) 606-607

[ZHB] T. Zykova-Timan, J. Horbach, and K. Binder, Monte Carlo simulations of the solid-liquid transition in hard spheres and colloid-polymer mixtures, J. Chem. Phys. 133, 014705 (2010)

[ZM] H.P. Zhang and H.A. Makse, Jamming transition in emulsions and granular materials, Phys. Rev. E 72 (2005) 011301